An ab-initio study of bilayer graphene using higher order quantum chemical methods

im Fachbereich Physik
der Freien Universität Berlin eingereichte
Dissertation zur Erlangung des Akademischen Grades
DOKTOR RERUM NATURALIUM

von
M. Sc.
Andrea G. Sanfilippo

Berlin 2010

Erster Gutachter (Betreuer): Prof. Dr. Karsten Reuter

Zweiter Gutachter: Prof. Dr. E.K.U. Gross

Disputationsdatum: 25.06.2010

... trying to find the simple in the complex

Abstract

Graphite and carbon-based structures represent important test case systems for the validation of novel computational methodologies aimed at accurately describing van der Waals interactions at the nanoscale. In this context, Density Functional Theory (DFT)[71,90] has played a key role when describing the ground-state properties of a wide variety of molecular systems, under local and semi-local approximations[150,152] to the exchange-correlation (XC) potential. Nevertheless, non-covalent systems, such as bilayer graphene, cannot yet be accurately described under these DFT functionals due to the lack of long range correlation. In addition, they suffer from spurious self-interaction as well as the absence of discontinuity in the chemical potential[58,93,140]. In this sense, exchange-correlation functionals have been specifically developed to account for van der Waals interactions[34,35,57,145], commonly as a post-processing correction to an initial calculation based on local or semi-local XC functionals. One successful example is the PBE+vdW functional, by A. Tkatchenko and M. Scheffler[184]. On the other hand highly accurate wavefunction-based methods represent an alternative, even though they come at a high-computational expense. Such methods mainly involve Møller-Plesset perturbation theory and the Random Phase Approximation (RPA) and Coupled Cluster (CC). In this work we focus mainly on the former two methods, which represent a good compromise between accuracy and computing time and are considered as the cheapest alternative to DFT. Indeed they scale as the N^5 and N^4 power of the number of wave functions N respectively, against the N^3 scaling of local and semi-local DFT functionals. Furthermore, a representative $\pi - \pi$ system, like the benzene dimer, shows excessive binding in the MP2 method while underbinding in the RPA method compared to accurate coupled cluster calculations[84]. It is expected that in an infinite system like bilayer graphene, the binding would be between the two. Moreover, RPA theory describes the dispersion interactions correctly in the infinite limit of electron densities and interlayer distances[42,47,122] (i.e. the distances between two subsystems taken apart), and for such a reason the binding in a bulk material like graphite, where dispersion effects are larger due to a larger number of neighbouring atoms, is expected to be described more accurately. In our study we implemented, for such a purpose, the Møller-Plesset perturbation theory at the second order (MP2) in our in-house code FHI-AIMS[19], based on numerical atomic orbitals (NAO)[19], and we have applied it along with PBE+vdW and RPA/RPA+ techniques to the study of mono and bilayer graphene with the aim of understanding in particular the role of dispersion in such a bilayer graphene system.

Andrea Sanfilippo

Berlin, 2010

Zusammenfassung

Graphit und andere auf Kohlenstoff basierende Strukturen sind wichtige Testsysteme für die Überprüfung neuartiger Computermethoden zur akkuraten Beschreibung von van der Waals Wechselwirkungen im Nanometerbereich. Die Dichtefunktionaltheorie (DFT)[71,90] unter Verwendung lokaler und semilokaler Näherungen für das Austauschkorrelationspotential[150,152] spielt eine Schlüsselrolle in der Berechnung der Grundzustandsobservablen einer Vielzahl molekularer Systeme. Dennoch können nicht-kovalent gebundene Systeme, wie zweilagiges Graphen, durch diese DFT Funktionale nicht akkurat beschrieben werden, da langreichweitige Korrelations-Wechselwirkung vernachlässigt wird. Weitere Probleme dieser Funktionale sind die artifizielle Selbstwechselwirkung und ein fälschlicherweise kontinuierliches chemisches Potential[58,93,140]. Aus diesem Grund wurden spezielle Austauschkorrelations - Funktionale entwickelt, um van der Waals Wechselwirkungen besser beschreiben zu können[34,35,57,145] Dies geschieht üblicherweise in Form einer nachträglichen Korrektur von Rechnungen, die auf üblichen lokalen oder semilokalen Austauschkorrelations-Funktionalen basieren. Ein erfolgreiches Beispiel hierfür ist das PBE+vdW Funktional von A. Tkatchenko und M. Scheffler[184]. Einen alternativen Ansatz stellen äußerst genaue wellenfunktionsbasierte Methoden dar. Speziell vom Interesse sind Møller-Plesset Störungsrechung, die Random Phase Approximation (RPA) oder die Coupled Cluster Methode (CC), deren Anwendung jedoch durchweg mit einem sehr hohen rechnerischem Aufwand verbunden ist. In dieser Arbeit konzentriere ich mich vor allem auf die ersten beiden Methoden, da sie einen guten Kompromiss zwischen Genauigkeit und rechnerischem Aufwand darstellen und im Allgemein als die günstigste Alternative zu DFT betrachtet werden können. In der Tat skalieren die Rechenzeiten wie N^5 beziehungsweise N^4, wobei N die Anzahl der Wellenfunktionen ist. Im Vergleich dazu skalieren Methoden die auf lokalen oder semilokalen DFT Funktionalen basieren, mit N^3. Bindungsenergien eines repräsentativen π-π Systems wie dem Benzen-Dimer werden im Vergleich zu hochgenauen Coupled Cluster Rechnungen von MP2 überschätzt, wohingegen RPA sie unterschätzt[84]. Es wird erwartet, dass für ein unendlich ausgedehntes System, wie zweilagiges Graphen, die Bindungsenergie dazwischen liegt. Ausserdem beschreibt RPA die Dispersionswechselwirkung im Limes unbeschränkter Elektronendichte und grossem Abstand zwischen zwei Schichten exakt[42,47,122]. Daher ist zu erwarten, dass in einem Volumenmaterial wie Graphit, wo Dispersioneffekte aufgrund der höheren Koordinierung größer sind, die Bindungsenergien von RPA genauer beschrieben werden. Im Rahmen dieser Arbeit wurde daher Møller-Plesset-Störungstheorie bis zur zweiten Ordnung für den FHI-AIMS Programmcode[19], der auf numerischen Atomorbitalen (NAO) basiert implementiert[19]. Diese wurde zusammen mit PBE+vdW und RPA/RPA+ Techniken zur Untersuchung von ein- und zweilagigem Graphen eingesetzt. Ziel war es die Rolle von Dispersion in zweilagigem Graphen zu verstehen.

Andrea Sanfilippo
Berlin, 2010

Contents

1 Introduction

Carbon, which takes its name in different languages from charcoal or burnt wood, is, after hydrogen, helium and oxygen, the most abundant element in the universe[11] and it is considered fundamental for the presence of life. Most of the surrounding everyday objects and all life forms are made of carbon. The large variety of carbon-based configurations is attributed to the capacity of carbon atoms to bind or hybridize in different manners, providing thus finely tuned properties which are essential for such systems. Examples range from the well-known strength of diamond to the weak interaction between layers of graphite and the elasticity of carbon nanotubes[26] among others.
Even though carbon has been known to mankind since the earliest civilizations, it was not until the 18th century when Lavoisier suggested carbon to be an "oxidizable and acidifiable nonmetallic element" in his "Traité Élémentaire de Chemie", published in Paris in 1789. Lavoisier also showed that diamond is another form of carbon. Graphite was thought to be a form of lead until 1779, when C.W. Scheele demonstrated the opposite by burning a piece of it, weighing it and then comparing it to the same initial amount of lead. It then took two hundreds years to find another form of carbon, or allotrope, when H. Kroto, R. Curl and R. Smalley discovered buckminsterfullerene in 1985[8,91], which has very important properties in catalysis, in drugs and as a lubricant, and its discovery earned them the Nobel Price in Chemistry in 1996. In the same years carbon nanotubes, which can be considered geometrically as a 2D honeycomb carbon lattice, or graphene, folded in different manners, were discovered[20,74].
The term graphene first appeared in 1987[134] to describe single layers of graphite, but not until 2004 was a layer of graphene pulled out by graphite and deposited on a Silicon substrate[142]. According to the Mermin-Wagner theorem[126] 2D crystals cannot exist because of long-wavelength oscillations which would eventually break the 2D symmetry. However such modes can be largely suppressed [45] by anharmonic interactions or the presence of a substrate. Since its discovery graphene and derivates have attracted plenty of scientific interest due to their materials properties[52,88,140], their electronic band structure[33,60,123–125,192], and the relatively weak interactions with many substrates. Applications appear unlimited, including steel production, hydrogen storage in fuel cells[180], electronics, optics, spintronics and detectors of organic molecules[56] among many others. The interested reader is referred to ref.[140] and references therein, for a wider and more detailed description of graphite applications. Some properties like the band structure of mono or multilayer graphene can be accurately described by tight-binding models or model pseudo-relativistic Hamiltonians, but the correct description of van der Waals (vdW) interactions in different environments, in particular in bilayer graphene and graphite itself, still represents a major challenge to the scientific community.
Van der Waals forces are a pure quantum mechanical effect: they are due to the zero-

point oscillations between two parts of a system, and they decay at most as the sixth power of distance[25,41,113,118]. However, it is fundamental to understand such interactions and to provide suitable methodologies for their accurate description. For such a reason the role of dispersion has not been clear, while short range interactions and the role of electrostatics in graphene and graphite, are generally considered very weak[86,158,190]. In the last century computational power has seen major improvements, allowing to calculate more complex systems with more and more sophisticated theories. Density Functional Theory (DFT) local and semilocal functionals by construction fail to describe dispersion forces, so higher order theories are needed. To achieve high accuracy it is vital to make use of an efficient code, such as FHI-AIMS [19,161], which employs the resolution of identities technique and efficient numerical atomic orbitals basis sets (NAO). Such orbitals have been successfully implemented in the past for DFT approximations[19], and, now we have implemented such a technique for wavefunction methods, ranging from Hartree-Fock (X. Ren) to MP2 (A. Sanfilippo) to GW approximations (X. Ren)[161] along with the essential basis set superposition error counterpoise correction (BSSE-CP)[22] (A. Sanfilippo).
Regarding graphitic systems, it has been shown that RPA is expected a priori to give good agreement with experiments since the adimensional parameter r_s, often used to describe the electron density in diagrammatic theories, is very low for graphene, about $r_s \sim 0,5$, and RPA is known to recover the exact correlation in the limit $r_s \to 0$[47,122,139]. RPA provides at the same time the correct description of correlation in the long range of distances separating the graphitic layers. MP2 perturbation theory on the other side fails, generally overbinding[84] small aromatic systems, although it can provide upper bonding limits. Within the present work we aim to describe the cohesive energy of a layer of graphene and subsequently the interaction between two layers of graphene by using higher order quantum chemical methods, like PBE+vdW[184], MP2[112] and RPA[42] and RPA+ [94]. We will extrapolate from small systems to the infinite limit with a proper mathematical formalism. Moreover, with such a scheme we wish to understand the interbinding between layered $\pi - \pi$ structures and the role of van der Waals interactions via *ab-initio* treatments.

2 Theory and Methodologies

2.1 The Schrödinger Equation

Every particle system is characterized, according to the most widespread interpretation of quantum mechanics [154], by a state, which can be expressed as a generalized vector in a Hilbert or Fock space[4,6,37,47,127,139,154,165]. The measure of the position of such an entity provides the so-called wave function, related to the density probability of finding a particle in a certain position and its momentum as well. The linear operators, which are defined on the domain of Hilbert (Fock) space of states, dictate their evolution throughout space-time and can *measure* observables [6,154]. All such notions appear in standard quantum mechanics courses and we will move rapidly through all these concepts. A propagator is an entity which describes how a state propagates through space-time. The fundamental properties of the system are hence deeply linked to such an entity, since it describes the system response to external perturbations and the measures themselves. The propagation for an isolated system, by physical intuition, should satisfy some properties like hermitianicity and completeness of the fermionic Hilbert (Fock) space[6,9,98,139]. If we consider the propagation along the time direction, we can introduce a time evolution operator $\hat{U}$, *

$$\hat{U}(t_0 + dt, t_0)|\psi(t_0)\rangle = (1 + i\hat{H}dt)|\psi(t_0)\rangle, \tag{2.1}$$

where $|\psi\rangle$ is a state, in the Dirac notation[37], which evolves from time t_0 to $t_0 + dt$. $\hat{H}$ is an Hermitian operator for isolated systems, and it is regarded as a generator of time evolution, which in classical mechanics is shown to be equal to the energy by symmetry reasons[53,96,99,100,127]. $\hat{H}$ is hence defined as the Hamiltonian of our quantum system. Such an expression for infinitely small transformations, or rotations, in the Hilbert space, brings us to the following differential equation, also known as the Schrödinger equation

$$\hat{H}|\psi(t)\rangle = E|\psi(t)\rangle, \tag{2.2}$$

where the $\hat{H}$ operator is Hermitian, and identified as the classical energy provided by the principle of correspondence, E is an observable and it corresponds to the internal energy of our isolated system. Such an Hamiltonian can be written, in the adiabatic Born-Oppenheimer (ABO) approximation, i.e. adiabatic coupling between the motion of electrons and nuclei, as[53,76,96,97,99,100,127]

*Throughout this thesis we will apply atomic units in mathematical expressions in order to simplify the notation. Physical constants are taken from references[1,132].

$$\hat{H} = \hat{K}_{\mathrm{N+e}} + \hat{U}_N - \sum_{ij}^{N_{\mathrm{nuclei}},N_{\mathrm{el}}} Z_i \hat{V}_{ij} + \sum_{ij}^{N_{\mathrm{el}}} \hat{V}_{ij} =$$
$$= \sum_i^{N_{\mathrm{el}}} \frac{\hat{\mathbf{p}}_\mathbf{i}^2}{2} + \sum_i^{N_{\mathrm{nuclei}}} \frac{\hat{\mathbf{P}}_\mathbf{i}^2}{2} + \sum_{ij}^{N_{\mathrm{nuclei}}} \frac{Z_i Z_j}{|R_i - R_j|} - \sum_{ij}^{N_{\mathrm{nuclei}},N_{\mathrm{el}}} \frac{Z_i}{|r_i - R_j|} + \sum_{ij}^{N_{\mathrm{el}}} \frac{1}{|r_i - r_j|}, \quad (2.3)$$

where N_{el} is the number of electrons with momentum $\hat{\mathbf{p}}$, N_{nuclei} is the number of nuclei, Z the number of protons of each nucleus with coordinate $\mathbf{R}$ and momentum $\hat{\mathbf{P}}$. If we neglect the electron-electron interaction, this system of equations can be easily solved[99,127], and for such a reason, it appears a natural choice to put the Coulomb interaction as a perturbation. Such an expression is at the basis of all perturbative theories in zero and non-zero temperature formalism. In such treatment the system is assumed to be moved to a perturbed state which can be expressed as a superposition of unperturbed states. The beauty of such methodologies is that they simplify notably in mathematical series, in particular when we wish to express all our formalism in a single-particle picture, i.e. to rewrite our equations in a formalism of a particle in a potential. This is possible only when the kinetic energy prevails over the potential energy[4,47,122,139]. The major issue is then to find a proper way to take into account the proper terms in such series[47,75,122,139]. The **zero temperature Green function** is defined as[47,139,165] (the non-zero temperature formalism can be derived straightforwardly, and it does not concern us in our study)

$$iG_{\alpha\beta}(\mathbf{x},t,\mathbf{x}',t') = \frac{\langle\psi_0|T[\hat{\psi}_{\mathrm{H}\alpha}(\mathbf{x},t),\hat{\psi}_{\mathrm{H}\beta}(\mathbf{x}',t')]|\psi_0\rangle}{\langle\psi_0|\psi_0,\rangle} \quad (2.4)$$

where $|\psi_0\rangle$ is the ground state, $\hat{\psi}_{\mathrm{H}\beta}(\mathbf{x},\mathbf{t})$ is the field operator in the Heisenberg representation, and T is the time ordering operator. All fundamental properties like the expectation values of single-particle operators, ground state energy and excitation spectrum, can be represented in terms of this function. A fundamental quantity like the electron density is e.g. simply derived as[47]

$$\rho(\mathbf{x}) = iTr[G_{\alpha\beta}(\mathbf{x},t,\mathbf{x},t^+)], \quad (2.5)$$

where the + superscript denotes the limit along the positive direction of the time axis and the trace is over the real space.

2.2 Perturbation Theory

Let us partition our Hermitian operator in an unperturbed part H_0, of which we know the solutions already, and an additional "perturbative" term H_1. The equation (2.4) for a perturbation $\hat{H}_1$, can thus be written as a series expansion, as follows[47]

$$iG_{\alpha\beta}(x,y) \equiv iG^0_{\alpha\beta}(x,y) - \frac{i}{2}\sum_{\lambda\lambda'\mu\mu'}\int \hat{H}_{1\ \lambda\lambda'\mu\mu'}(x',x'')\langle\psi_0|T[\hat{\psi}_\lambda(x')\hat{\psi}_{\lambda'}(x'')\hat{\psi}_\mu(x')$$
$$\hat{\psi}_{\mu'}(x'')\hat{\psi}_\alpha(x)\hat{\psi}_\beta(y)]|\psi_0\rangle + ... \quad , \quad (2.6)$$

where we defined ($x \equiv \mathbf{x}, t$), greek letters represent spin-states and $G^0_{\alpha\beta}(\mathbf{x}, t, \mathbf{x}', t)$ is the unperturbed Green function. All integrals are done over space and time.
The Wick-Theorem[47,139] allows us to write the perturbed Green function as a Dyson equation for the inter-particle interactions under a $\hat{H}_1$ perturbation,

$$\begin{aligned} iG_{\alpha\beta}(x,y) = iG^0_{\alpha\beta}(x,y) + iG^1_{\alpha\beta}(x,y) + ... = iG^0_{\alpha\beta}(x,y) - \frac{1}{2}i \sum_{\lambda\lambda'\mu\mu'} \int_{\mathcal{V}',\mathcal{V}''} \hat{H}_{1\ \lambda\lambda'\mu\mu'}(x',x'') \\ \{iG^0_{\alpha\beta}(x,y)[iG^0_{\mu\mu'}(x''x'')iG^0_{\lambda'\lambda}(x',x') - iG^0_{\mu'\lambda}(x'',x')iG^0_{\lambda'\mu}(x',x'')] + \\ +iG^0_{\alpha\lambda}(x,x')[iG^0_{\lambda'\mu}(x',x'')iG^0_{\mu'\beta}(x',x') - iG^0_{\lambda'\beta}(x',x)iG^0_{\mu'\mu}(x'',x'')] + \\ +iG^0_{\alpha\mu}(x,x')[iG^0_{\mu'\lambda}(x'',x')iG^0_{\lambda'\beta}(x',y) - iG^0_{\mu'\beta}(x'',y)iG^0_{\lambda'\lambda}(x'x')\} + ..., \end{aligned} \tag{2.7}$$

where $G^1_{\alpha\beta}$ is the first-order perturbation, and $\mathcal{V}', \mathcal{V}''$ are volumes in phase space.
Such an equation can be written in a more compact form as follows [47,139]

$$\begin{aligned} G_{\alpha\beta}(x,y) = G^0_{\alpha\beta}(x,y) + \int_{\mathcal{V}'} G^0_{\alpha\lambda}(x,x')\Sigma_{\lambda\mu}(x',x'')G^0_{\mu\beta}(x'',y) = \\ G^0_{\alpha\beta}(x,y) + \int_{\mathcal{V}'} G^0_{\alpha\lambda}(x,x')\Sigma^*_{\lambda\mu}(x',x'')G_{\mu\beta}(x'',y), \end{aligned} \tag{2.8}$$

where the Einstein sum rule has been applied and Σ is called **self-energy**, and Σ^* is also known as **proper self-energy**[47], which allows to write a Dyson equation in terms of $G_{\alpha\beta}$. The latter form leads to a self consistent equation and we can first replace the perturbed Green function G with the unperturbed Green function G^0. Such a formalism is very general and can be applied to a large variety of physical systems, such as retarded fields and relativistic quantum electrodynamics. Since there are many terms in such equations, graph theories have been applied to simplify the formalism, the so-called **Feynman** or **Stueckelberg diagrams**. What is truly important, is that for each class of retained diagrams in a certain approximation, such an approximation should be **conserving**, i.e. the continuity equation and physical conservation laws must be satisfied[29].
The objective of the physicist is to find suitable approximations to such a formalism, depending on the system and the feasibility of the mathematical treatments and their eventual implementation in a computer code. There are many ways to approximate equation (2.8), among them the best known in the history of quantum mechanics are the Epstein-Nesbet, Hartree, Hartree-Fock, RPA and Coupled Cluster approximations and Møller-Plesset perturbation theory[12]. Even though such theories have been initially derived by different formalisms, they can be unified in one unique formalism using Green function methods. In our study we will focus specifically on Møller-Plesset perturbation theory at the second order (MP2)[112], based on the Hartree-Fock approximation, and RPA[47,122,139].

2.3 Hartree-Fock Approximation

In the Hartree-Fock approximation[12,47,122,139], we assume a mean-field, where *each particle moves in a single-particle potential that comes from its average interaction with all the other particles*[47]. In such a case, for an unperturbed hamiltonian $\hat{H}^0 = \hat{K} + \hat{U}$ ($\hat{K}$ stands for the kinetic energy, $\hat{U}$ for the nuclear potential), in an instantaneous single particle Coulomb potential[76,127] $\hat{H}_1(x, x') \equiv V(\mathbf{x}, \mathbf{x}')\delta(t - t')$, we obtain at first order in perturbation theory the well-known self-consistent **Hartree-Fock equation** for the ground state

$$[-\frac{1}{2}\triangle + U(\mathbf{x})]\phi_j(\mathbf{x}) + \int_{\mathcal{V}''} \Sigma^*_{\mathrm{HF}}(\mathbf{x}, \mathbf{x}'')\phi_j(\mathbf{x}'') = \epsilon_j\phi_j(\mathbf{x}), \tag{2.9}$$

where $\phi_j(\mathbf{x}) \equiv \langle \mathbf{x}|\phi_j\rangle$ is an eigenstate of the system with energy ϵ_j, U is the nuclear potential, while the proper mean-field self-energy Σ^* depends only on the coordinates, not on the energy

$$\begin{aligned}\Sigma^*_{\mathrm{HF}}(\mathbf{x}, \mathbf{x}'') = \delta(\mathbf{x} - \mathbf{x}'') \int_{\mathcal{V}'''} V(\mathbf{x} - \mathbf{x}''') \sum_j \phi_j(\mathbf{x}''')\phi^*_j(\mathbf{x}''')\theta(\epsilon_F - \epsilon_j) + \\ -V(\mathbf{x} - \mathbf{x}'') \sum_j \phi_j(\mathbf{x})\phi^*_j(\mathbf{x}'')\theta(\epsilon_F - \epsilon_j),\end{aligned} \tag{2.10}$$

where ϵ_F is the Fermi level, θ the Heaviside function and $\sum_j \phi_j(\mathbf{x}''')\phi^*_j(\mathbf{x}''')\theta(\epsilon_F - \epsilon_j)$ simply corresponds to the electron density. We can notice how the proper self-energy consists of a local term which depends on the electron density, the **direct term**[47,122] E_{H}, and a non-local term, called **exchange**, E_{x}. The exchange term is zero for all states of pairs with different spin, so electrons with different spin do not repel each other. The total energy is then the summation over occupied orbitals[98]

$$E_{HF} = \sum_{i=0}^{\infty} \epsilon_i\theta(\epsilon_F - \epsilon_i) - E_{\mathrm{H}} - E_{\mathrm{x}}. \tag{2.11}$$

2.4 Beyond Hartree-Fock and Dispersion Forces

2.4.1 Møller-Plesset Perturbation Theory

Historically all contributions to the ground state energy beyond the Hartree-Fock approximation were defined as **correlation**. Correlation contributions are dominant over exchange at large separation (the range of distances where the wave functions are negligibly overlapping). In such a distance range the exchange term is almost zero, since it decays exponentially[86]. Therefore, if we want to describe dispersion forces at large distances from the nuclei, we need to accurately evaluate the correlation contributions. Such contributions can be evaluated via perturbative expansions at higher order terms.

If we go further in perturbation theory, it is possible to show, through the Goldstone theorem[47], that the second-order self-energy (excluding the case of the degeneracy of wave functions) is simply given by

$$\Sigma^*_{\mathrm{MP2\ ij}}(E) = \frac{1}{2}\sum_{ars}^{N_{\mathrm{occ}},\ N_{\mathrm{virt}}} \frac{((ir|as)-(is|ar))((jr|as)-(js|ar))}{|E+\epsilon_a-\epsilon_r-\epsilon_s|} + \\ +\frac{1}{2}\sum_{abr}^{N_{\mathrm{occ}},\ N_{\mathrm{virt}}} \frac{((ia|rb)-(ib|ra))((ja|rb)-(jb|ra))}{|E+\epsilon_r-\epsilon_a-\epsilon_b|}, \tag{2.12}$$

where E is the energy variable, the indices i, j represent the projection on the unperturbed states, r, s are indices over occupied orbitals and a, b are indices over the so-called virtual excitations, i.e. *empty* states, simplifying

$$(ia|jb) \equiv \int_{\mathcal{V},\mathcal{V}'} \frac{\phi_i(\mathbf{x})\phi_j(\mathbf{x}')\phi_a(\mathbf{x})\phi_b(\mathbf{x}')}{|r_i-r_j|}, \tag{2.13}$$

so that the total energy at the second order of the perturbation expansion is

$$E^{(2)} \equiv E_{MP2} = -\frac{1}{4}\sum_{ijab}^{N_{\mathrm{occ}},\ N_{\mathrm{virt}}} \frac{|(ia|jb)-(ja|bi)|^2}{\epsilon_a+\epsilon_b-\epsilon_i-\epsilon_j}, \tag{2.14}$$

where, i, j are occupied states, and the total ground state energy can be approximated as

$$E \approx E_{HF} + E_{MP2}, \tag{2.15}$$

The numerator in Eq. (2.14) involves now a summation over direct terms and an exchange term over excited levels, called **second order exchange**. Such a term provides a positive contribution to the total energy, hence a repulsive contribution to the ground state energy.
We can see how the denominator in Eq. (2.14) becomes larger the higher the number of excited states involved in the summation. However the numerator of Eq. (2.14) is equally important, since the superposition of certain occupied and virtual states can be relatively high even at high excitation energies, thus determining a relatively slow convergence behaviour of the summation in Eq. (2.14) with respect to a, b excited levels. This observation is fundamental for the implementation of such a theory in a numerical code[67,80] and for the choice of the basis set, as we will see in the next sections.

An equally important derivation, with plenty of physical insight, follows from the definition of the response function[47]

$$n_{\mathrm{ind}}(\mathbf{x}, i\omega) = \int_{\mathcal{V}'} \chi(\mathbf{x}, \mathbf{x}', i\omega) V_{\mathrm{ext}}(\mathbf{x}', i\omega), \tag{2.16}$$

or

$$\chi(\mathbf{x},\mathbf{x}') = \frac{\delta n_{\rm ind}(\mathbf{x},i\omega)}{\delta V_{\rm ext}(\mathbf{x}',i\omega)}, \tag{2.17}$$

where $n_{\rm ind}$ is the change of electron density, or induced density, caused by an external time dependent (or, equally, frequency dependent) perturbation $V_{\rm ext}$, acting like an external potential. Let us consider two separate fragments, or subsystems, each one characterized by a response function χ_1 and χ_2 respectively, then we obtain the second order perturbation energy as a Longuet-Higgins expression[114,119]

$$E'^{(2)} = -\frac{1}{2\pi}\int_{\mathcal{V},\mathcal{V}',\mathcal{V}'',\mathcal{V}'''} V(\mathbf{x}-\mathbf{x}'')V(\mathbf{x}'-\mathbf{x}''')\int_0^\infty \chi_1(\mathbf{x},\mathbf{x}',i\omega)\chi_2(\mathbf{x}'',\mathbf{x}''',i\omega), \tag{2.18}$$

where the response functions are the *bare* ones, obtained by the Hartree-Fock calculation. However, such an expression for the second-order expansion of the correlation energy differs from Eq. (2.14) -even though they converge to the same result at large distances- because it involves the Hartree-Fock responses of each isolated fragment, rather then Hartree-Fock interactions[61] in the whole system, as in Eq. (2.14). In fact, a theory which takes into account the perturbation expansion of the interaction between two fragments, or subsystems, is the so-called Symmetry Adapted Perturbation Theory (SAPT)[31,32,86,164,195], which allows to partition as well the contributions to the total energy coming from van der Waals (dispersion) interactions, exchange and electrostatics[23,86]. We remember the reader that such quantities cannot be partitioned by simple energy difference between MP2 calculations for the total system and the energy of its subsystems, because of the *relaxation* of the orbitals, and the different dimension of the Hilbert Space[86].
As we are interested in bilayer graphene equilibrium distances as well as in long range we applied the MP2 methodology of Eq. (2.14). However, via the response function formalism, it can be also easily shown that for large separations such an expression, for a given response function, decays as the sixth power of the separation distance[86,119], i.e. $E^{(2)} \sim O(R^{-6})$, as it is expected for the correct -at least in the asymptotic decay- description of van der Waals interactions[113]. The proportionality coefficients can thus be calculated from Eq. (2.18)[119] and they will be encountered again in section 2.5.3, in a different context.

2.4.2 Random Phase Approximation (RPA)

In the previous section we have considered only the first two orders in perturbation theory. If we neglect the second and higher orders in the exchange, and we sum over all orders of the direct terms, we obtain a geometric series, such that the ground state correlation energy can be written as follows[4,42,47,122,139]

$$E_c^{RPA} = \frac{1}{4\pi}\int_0^\infty d\omega Tr[ln(1-V\chi^0(i\omega)) + V\chi^0(i\omega))], \tag{2.19}$$

where V is the Coulomb potential, and the previously employed response function χ, is nothing other than the Kubo formula[47,119,119]

$$\chi(\mathbf{x},\mathbf{x}',i\omega) = G^0_{\alpha\beta}(x,y,i\omega)G^0_{\beta\alpha}(y,x,i\omega)|_R, \tag{2.20}$$

The term Π, multiplies the Coulombic part in Eq. (2.19), and it provides the so-called **screening** of the *bare* Coulomb potential, due to the interaction of one electron with all other electrons. We are still in a single-particle framework, that means we are mapping the electrodynamics of an electron in a sea of electrons as the dynamics of a *quasi-particle* represented by the electron and its perturbation itself as a unique entity[122]. It can be shown that for large separation between two subsystems, the exchange terms go to zero at all orders, such that RPA correlation correctly approximates the van der Waals interaction[119], and the second order perturbation of the correlation itself can be written as

$$E'^{(2)} = -\frac{1}{2\pi}\int_{\mathcal{V},\mathcal{V}',\mathcal{V}'',\mathcal{V}'''} V(\mathbf{x}-\mathbf{x}'')V(\mathbf{x}'-\mathbf{x}''')\int_0^\infty \chi_1^{RPA}(\mathbf{x},\mathbf{x}',i\omega)\chi_2^{RPA}(\mathbf{x}'',\mathbf{x}''',i\omega), \tag{2.21}$$

which decays as $E^{(2)} \sim O(R^{-6})$ for large separations R between two subsystems, and where χ^{RPA} is the RPA response function.

2.5 Density Functional theory (DFT)

We derived all our formalism in the previous sections starting from the concept of a state and we move for mathematical simplicity to the notion of Green's functions. An important observation is that all these equations can be rewritten in terms of an observable quantity which depends only on the coordinates (or time in principle), the density. In fact, we define the **N-particle density matrix** as

$$\hat{\gamma} = |\psi\rangle\langle\psi|, \tag{2.22}$$

and the so-called **i-reduced** density matrices, as the traces, or integrals, all over the $N-i$ coordinates. In particular integrals over $N-1$ and $N-2$ coordinates and spin states, provide the electron density in real space ρ and the two-particle non-local density ρ_2 respectively. The expectation value of a single particle operator[47,139] $\hat{O}$ is easily obtained as $\langle\hat{O}\rangle = Tr[\hat{\gamma}\hat{O}]$ so that the generalization of the Schrödinger equation in this formalism is straightforward, but too long to be discussed here[58]. It can be shown that the ground state energy will depend on -or more precisely it is a functional of[162]- the electron density $\rho(\mathbf{x}) \equiv \rho_1(\mathbf{x},\mathbf{x}')_{\mathbf{x}=\mathbf{x}'}$, as well as on the two-particle non local-density[58,146] $\rho_2(\mathbf{x},\mathbf{x}')$

$$\begin{aligned} E = E[\rho_1(\mathbf{x},\mathbf{x}'),\rho_2(\mathbf{x},\mathbf{x}'')] = -\frac{1}{2}\int_{\mathcal{V}}[\triangle\rho_1(\mathbf{x},\mathbf{x}')]_{\mathbf{x}=\mathbf{x}'} + \int_{\mathcal{V}} V_{\mathrm{N}}(\mathbf{x})\rho(\mathbf{x}) + \\ +\frac{1}{2}\int_{\mathcal{V}} V(\mathbf{x},\mathbf{x}')\rho(\mathbf{x})\rho(\mathbf{x}') + \frac{1}{2}\int_{\mathcal{V}} V(\mathbf{x},\mathbf{x}')\rho(\mathbf{x}')\rho_{\mathrm{xc}}(\mathbf{x},\mathbf{x}'), \end{aligned} \tag{2.23}$$

where ρ represents the electron density and ρ_{xc} a correction to the single particle density ρ, known also as the **exchange-correlation hole**, V_{N} the nuclear potential and V the Coulomb potential. Such a description involves the treatment of a non-local functional, and this problem is not yet practical to solve. In particular we need an approximate expression for the two-particle ρ_{xc} term.
Ideas on how to treat such an equation in a relatively simple and feasible manner, although in a slightly different formalism, go back to Thomas, Fermi and Dirac[36,46,183]. A major step forward was given by the theorems of Hohenberg, Kohn[71] and by the Kohn-Sham ansatz[90] (and further extended by the works of Lieb[109] and Levy[106,107]) and it allowed to reduce the problem of the ground state of a see of interacting electrons to the ground state of a free particle moving in an effective potential[82]

$$E[n] = K'[n] + V_{\mathrm{N}}[n] + V_{\mathrm{H}}[n] + E_{\mathrm{xc}}[n], \tag{2.24}$$

where K' is the kinetic energy of the non-interacting system, V_{N} is the external potential represented by nuclei or other additional fields, V_{H} is the classical Coulomb, or Hartree, potential between two charge densities, and E_{xc} is the so-called **exchange-correlation** term, which includes all the differences between the real and the fictitious system, and its exact form is not known yet. There is no perturbative, or **diagrammatic expansion**, of the exchange-correlation energy, but Schlüter and Sham devised a scheme to obtain the exchange-correlation potential from the self-energy[29,170].
Kohn and Sham in their seminal paper pointed out the simplest form of the exchange-correlation functional, a local density approximation (LDA) (or more generally LSDA, when spin degrees of freedom are included). As the name suggests, the energy functional depends only on the density in every point in space.

$$E_{\mathrm{xc}}^{\mathrm{LDA}}[n] \equiv \int_{\mathcal{V}} n(\mathbf{x}) \epsilon_{\mathrm{xc}}^{\mathrm{heg}}(n(\mathbf{x})), \tag{2.25}$$

where $\epsilon_{\mathrm{xc}}^{\mathrm{heg}}$ is the exchange-correlation energy per electron in a homogeneous electron gas. A well known form of such an exchange-correlation functional, that we will use in this work, is known as the Perdew-Wang-LDA (PW-LDA)[152]. Such an approximation has been obtained fitting correlation energies to analytical or accurate Monte-Carlo computations for the degenerate electron gas.
An extension of the LDA approximation involves naturally the gradients of the density, hence it is addressed as *semi-local functionals*, even though it is not a simple series expansion. It is named generalized gradient approximation (GGA), and in our study we will apply the parameters optimized by Perdew, Burke and Ernzerhof (PBE-GGA)[150],

$$E_{\mathrm{xc}}^{\mathrm{GGA}}[n] \equiv \int_{\mathcal{V}} n(\mathbf{x}) \epsilon_{\mathrm{xc}}(n(\mathbf{x}), \nabla n(\mathbf{x})). \tag{2.26}$$

While the PBE-GGA approximation is fitted to reproduce well jellium properties and the exchange energy in atoms, a variant of such a functional has been elaborated to fit better jellium bulk and surface energies, the so-called *PBEsol* functional[151]. This *flavour* tends to worsen cohesive energies, but it will improve the equilibrium geometries

and lattice constants, in particular for closed packed structures[151].
Such local and semi-local functionals are easily tractable from a computational point of view, since they involve the density and only few degrees of freedom (space coordinates and possibly spin). By construction they can approximate with a relatively good accuracy, short-range properties, like bond lengths in chemical bonding and the electrostatic interaction, a classical property which depends on the density itself. A plethora of functionals, or *flavours*[5,54,69,77,104,153,181,182,200], have been formulated in the last forty years, but only few of them have been largely tested and are now widely used by the scientific community.
When it comes to the long range, where non-local properties of the correlation are important and densities are negligibly overlapping, i.e. van der Waals interaction, such functionals fail or, in certain cases, recover relatively good energies and geometries due to the fortuitous error cancellations[44,121,133,147]. A review of details and limitations of such functionals is found in textbooks and reviews[58,82,93,121,146].

2.5.1 Linear Response

The fact that density functional theory maps the interacting electron problem on the problem of a non-interacting electron in an effective potential, has brought considerable success to such a theory. However, when it comes to response properties and excited states, the current approximations cannot be applied successfully[121]. Furthermore there is no Koopman's theorem for DFT. For this purpose a Green functions approach, as we wrote about in last sections, is a natural choice. Another approach, but inherently different, is time-dependent density functional theory (TDDFT)[119,155,163,198]. Green functions involve the effect of the perturbation in the system caused by addition or removal of electrons, while TDDFT involves excitations conserving the number of particles. Notwithstanding response properties of the collective mode of the system can be determined for both methods, since it can be shown that, through the **adiabatic connection fluctuation dissipation theorem** (ACFDT)[101,102], the response function for a Coulomb potential V is

$$\begin{aligned}\chi(\mathbf{x},\mathbf{x}',i\omega) &\equiv \frac{\delta n_{\mathrm{ind}}(\mathbf{x},i\omega)}{\delta V_{\mathrm{ext}}(\mathbf{x}',i\omega)} = \\ &\quad \chi^0(\mathbf{x},\mathbf{x}',i\omega) + \\ &+ \int_{\mathcal{V}'',\mathcal{V}'''} \chi^0(\mathbf{x},\mathbf{x}'',i\omega)(V(\mathbf{x}'',\mathbf{x}'') + f_{xc}(\mathbf{x}'',\mathbf{x}''',i\omega))\chi(\mathbf{x}''',\mathbf{x}',i\omega),\end{aligned} \tag{2.27}$$

where $G^{KS}_{\alpha\beta}$ are the Green functions obtained from the Kohn-Sham orbitals, f_{xc} is the so-called **exchange-correlation function**, which contains the dynamical exchange and correlation effects, i.e.

$$f_{xc}(\mathbf{x},\mathbf{x}',i\omega) \equiv \frac{\delta V_{xc}[n(\mathbf{x},i\omega)]}{\delta n(\mathbf{x}',i\omega)}, \tag{2.28}$$

where V_{xc} is the exchange-correlation potential.
If we apply the Longuet-Higgins response function formalism[114,119], we can rewrite the second-order perturbation and RPA equations using Kohn-Sham orbitals [38,119], rather than Hartree-Fock ones. Moreover the RPA approximation can be shown as resulting by putting $f_{xc} = 0$ in equation (2.27) [119]. RPA can be regarded, in the TDDFT formalism, as the lowest order of approximation, where f_{xc} is set to 0. This shows how all methods, even though they appear radically different, are intertwined when we consider fundamental properties like the response function. Such properties are easily defined via Green's functions, and are as well a collective property of the system which can be calculated via DFT, TDDFT and in general, linear response theory[141]. RPA in the TDDFT formalism, i.e. based on Kohn-Sham orbitals, received recently considerable success for atomic, molecular and infinite systems[10,51,63] as well in the Green function formalism[130]. Since the Hartree-Fock approximation does not include the correlation, polarizabilities (response functions are simply their gradients[119]) are relatively poor, while in the DFT case, they have been shown to be better[179]. On the other side, a DFT perturbation theory has been well formulated by Görling and Levy (GL), but it is beyond the scope of our study[54].
In the present study we therefore focus on the RPA approximation based on the TDDFT formalism.

2.5.2 RPA+

We showed how the random phase approximation (RPA) gives the correct dispersion decay and correlation energy in the asymptotic limit of infinite distances between two sub-systems. However, when it comes to short range interactions, such as around equilibrium distances, *short range correlation* is expected to play an important role, competing with the exchange interaction. For such a reason S. Kurth and J.P. Perdew proposed a correction to RPA which includes DFT short range correlation, called RPA+[94]. Such a short range part can be tackled in principle by local and semi-local functionals, and we can thus write

$$E_{\mathrm{c\ sr}}^{\mathrm{LDA/PBE}} = E_{\mathrm{c}}^{\mathrm{LDA/PBE}} - E_{\mathrm{c}}^{\mathrm{RPA}}, \tag{2.29}$$

where the subscript c means correlation, sr means short range, and $E_{\mathrm{c}}^{\mathrm{RPA}}$ is obtained from the RPA expression for a uniform electron gas[94].

2.5.3 PBE+vdW

In the last section we introduced DFT and we briefly discussed about its limitations for long range distances, i.e. where densities or wave functions overlap are essentially negligible. There have been many attempts[34,35,55,57,145] to overcome this issue, and a promising scheme has been recently elaborated by A. Tkatchenko and M. Scheffler: the PBE+vdW method[184].

The non-relativistic interaction between two spherically symmetric atoms decays asymptotically as the sixth power of the distance[113]. Such *asymptotes* are in practise assumed at distances not further than ~ 100Å, as can happen in suspensions, otherwise relativistic corrections must be included, which lower the asymptotic power law to the seventh power of the distance[75,86,135].
The dispersion interaction among atoms in molecules or in bulk can be generally approximated by a pairwise summation, noting that second-order perturbation theory -as shown in section 2.4.1- is additive[38,86,119],

$$E^{(2)} = \sum_{l=3}^{\infty} \frac{C_{2l\mathrm{AB}}}{r_{\mathrm{AB}}^{2l}}, \tag{2.30}$$

where r_{AB} is the separation between two sub-systems. The first non-vanishing coefficients of such a series are the so-called dispersion coefficients C_6 and they are usually expressed as functionals of the polarizabilities, i.e. using the Casimir-Polder integral

$$C_{6\mathrm{AB}} = \frac{3}{\pi} \int_0^{\infty} \alpha_{\mathrm{A}}(i\omega)\alpha_{\mathrm{B}}(i\omega), \tag{2.31}$$

where ω are real frequencies. The difficult task is to express such coefficients in terms of the atomic contributions, taking into account that atoms in molecules have different hybridizations.
Following the treatments described in ref.[81,184,185], one can define a weight over the C_6 coefficients of isolated species in order to obtain effective C_6 coefficients for atoms in molecules, which take into account the depletion or increase of the electron density compared to the isolated, or free, species. Such weight can be based for example on a Hirshfeld partitioning of the charge densities [70].
The $C_{6\mathrm{AB}}$ hetero coefficients are determined by the equation, [185]

$$C_{6\mathrm{AB}} = \frac{2C_{6\mathrm{AA}}C_{6\mathrm{BB}}}{\frac{\alpha_B^0}{\alpha_A^0}C_{6\mathrm{AA}} + \frac{\alpha_{\mathrm{A}}^0}{\alpha_{\mathrm{B}}^0}C_{6\mathrm{BB}}}, \tag{2.32}$$

where α^0 represent static polarizabilities of atoms in molecules (taken from the database in ref.[28]), so that the effective coefficients are approximated by the following formula

$$C_{6\mathrm{AA}} \sim \left(\frac{V_{\mathrm{A}}^{\mathrm{eff}}}{V_{\mathrm{A}}^{\mathrm{free}}}\right)^2 C_{6\mathrm{AA}}^{\mathrm{free}}, \tag{2.33}$$

where V_A^{free} is the volume of the free atomic species and V_A^{eff} represents the effective volume of the species in the compound[185]. The so-called **van der Waals radius** is defined as

$$R_{\mathrm{eff}} = \left(\frac{V_A^{\mathrm{eff}}}{V_A^{\mathrm{free}}}\right)^{1/3} R_{\mathrm{free}}. \tag{2.34}$$

Since corrections using the C_6 coefficients are valid only for long range distances, where the series does not diverge and higher order terms are negligible, a *damping function* must be used for shorter distances. Following Tkatchenko-Scheffler (xc) a Fermi type damping function has been employed in this work,

$$f_{\mathrm{damp}}(r_{\mathrm{AB}}) = \frac{1}{1 + e^{-d(r_{\mathrm{AB}}/(s_R R^{\mathrm{AB}}_{\mathrm{free}})-1)}}, \tag{2.35}$$

where $R^{\mathrm{AB}}_{\mathrm{free}} = R^{\mathrm{A}}_{\mathrm{free}} + R^{\mathrm{B}}_{\mathrm{free}}$ and d, s_R are parameters set equal to 20 and to 0.94 respectively for PBE calculations[184].
The total ground state energy as a post-processing correction then reads

$$E = E_{\mathrm{PBE}} + \sum_{ij} f_{\mathrm{damp}}(r_{\mathrm{ij}}) \frac{C_{6ij}}{r^6_{ij}}, \tag{2.36}$$

where the indices represent summations over the atoms of the system considered, and r_{ij} the distance between two given atoms.

2.6 Basis Set: Which one?

Hilbert space has an infinite dimension, and to represent a given state we need in principle an infinite number of orthonormal states. Such states can be determined analytically only in few cases, where the symmetry of the system allows a representation in special functions (in particular plane waves, spherical harmonics, spherical Hankel and Bessel functions, Slater and Gaussian functions, confluent hypergeometric functions[3,9,30,103]). However, only a relative small number of basis functions is often required to describe to a sufficient accuracy our observables of interest, like the ground state energy, equilibrium geometries, band gaps and electron density[67,80]. MP2 and RPA/RPA+ methods need a certain amount of excited -also know as *empty* or *virtual* states- to be considered, so that the amount of basis sets necessary to converge ground state properties, is slower than in other methods, e.g. Hartree-Fock and DFT[50,67,80].
Since it is often not possible to find an orthonormal basis set for each system of interest, it is fundamental to find the smallest and most accurate basis set expansion. For periodic systems the obvious choice are plane-waves[3,9,13,43,59,80] . In atoms and molecules the most common approach is a linear combination of atomic orbitals (LCAO), where we define the atom-centered basis functions in spherical coordinates[13,80] or even wavelets[24]. We can then expand the wave functions of our isolated system of interest as

$$\phi_i(\mathbf{x}) = \sum_{im} c_{im} \psi_m(\mathbf{x}), \tag{2.37}$$

where ϕ_i is an eigenstate of the system, and

$$\psi_m(\mathbf{x}) = \sum_{k=K_{min},l=L_{min}}^{K_{max},L_{max}} \frac{u_{mk}(r)}{r} Y_{kl}(\theta, \phi), \tag{2.38}$$

where c_{im} are expansion coefficients, optimized with certain procedures[80], r, θ, ϕ spherical coordinates, and ψ_m the basis set of choice centered on atoms and of angular part Y_{kl}. u_{mk} are the radial parts with quantum numbers m and k. K and L refers to the range of the angular expansion. Such a range is naturally chosen as the analytical solutions of the hydrogenoid Schrödinger equation, and is therefore chosen as $0 < K < m$ and $L < |k|$, but in many cases higher angular quantum numbers are included in order to achieve a better convergence of the correlation energy (as for Gaussian basis sets)[80]. This is particularly important for numerical simulations, where a limited amount of resources is available and a high efficiency in needed.
In the history of quantum computations in condensed matter, the first basis sets employed for molecular systems or crystals where plane waves and the so-called Slater type orbitals (STO)[173]. Such functions have the same shape as for the hydrogenoid solution of an atom, i.e. an exponential decay, so they were thought to efficiently describe molecular orbitals (MO). This has been indeed the case, but numerical codes were made faster by expanding such functions in Gaussian basis sets[21,66], also known as Gaussian type orbitals (GTO), and later on only by using Gaussian functions as basis set[65]. Gaussian basis sets have the advantage of being analytically tractable, so that integrals can be easily calculated. The disadvantage of such basis functions is that they do not have a correct asymptotic behaviour, i.e. they decay is too steep and they do not diverge in the atomic center[73,80,87,95,172,196].
For these reasons, a viable alternative has been represented by numerical atomic orbitals (NAO)(ref.[19] and references therein), and is the basis set we are going to employ in our study. Such a basis set has an angular part represented by spherical harmonics and a radial part which can be, in principle, of the shape we wish, i.e. ionic, Slater, Gaussian-like or a mixture of all of them, and it is numerically tabulated, thus allowing a high flexibility[19].

2.7 Scaling

Taken a method of choice and assigned a basis set, the major issue, if we want to calculate our system within a given accuracy, is that we have to face the problem of how much a method scales computationally. This means we need to evaluate the number of required calculations as a function of the basis set size. Moreover, it should be determined if such a method is size consistent, i.e. it scales linearly with the system size. It can be shown that local and semi-local functionals in density functional theory, since they depend on the electron density, scale like N^3, where N is the number of basis set functions. Functionals involving non-local terms and wave functions calculations, like for the exchange term, yield a N^4 order scaling. Hartree-Fock approximation involves the calculation of the exchange term, where the so-called **electron repulsion integrals** (ERIs) -or four center integrals- have to be calculated. Therefore the scaling is of the order of N^4. When we move towards correlated methods like MP2 and RPA the situation is more problematic, since the scaling is proportional to N^5, while RPA scaling can be lowered to N^4, [51,168].

However there exist numerical methods which reduce the scaling to linear, and thus they reduce dramatically the computational effort for large systems[15,67,80,83,92,144,167,193].
For what concerns the memory, local and semi-local functionals and PBE+vdW have a lower amount of memory to be stored since they involve density integrals, while other quantities can be calculated on-the-fly. Wavefunction methods, like MP2 and RPA, involve the storage of the product of wave functions spanning the excited states and of the Coulomb matrix, i.e. the projection of the Coulomb potential on the basis set. To cope with such a problem, the not required quantities can be stored on disk and the needed quantities are calculated on-the-fly [67,80]. The present version of our code[19,161] calculates efficiently the ERIs terms through the resolution of the identities technique. The scaling for HF and RPA/RPA+ is still of the order of N^4, for MP2 is N^5, and N^3 for DFT local and semi-local functionals and PBE+vdW, but with low prefactors. Further features like disk-storage to decrease the demanding amount of computer memory have not yet been implemented and are planned for future development.

2.8 Resolution of Identities Technique

In the previous sections, we noticed the problem of calculating ERIs of the kind

$$(ia|jb) \equiv \int_{\mathcal{V},\mathcal{V}'} \phi_i(\mathbf{x})\phi_j(\mathbf{x}')\phi_a(\mathbf{x})\phi_b(\mathbf{x}')V(\mathbf{x}-\mathbf{x}') = \int_{\mathcal{V},\mathcal{V}'} \frac{\phi_i(\mathbf{x})\phi_j(\mathbf{x}')\phi_a(\mathbf{x})\phi_b(\mathbf{x}')}{|\mathbf{x}-\mathbf{x}'|}, \quad (2.39)$$

where i, j are occupied states and a, b are excited states. To cope with this issue, a technique known as the **resolution of the identities**, or in certain cases as **density fitting**, has been developed throughout the years[48,49,80,108,111,116,188]. It is a completeness insertion in the ERIs, which allows to split the matrices into products of smaller matrices. The advantage of such a technique is that calculations are relatively faster (fewer indices in matrices are more easily accessed by a computer), reportedly ten times faster[80,89], and at little cost of accuracy. Of the so-called **SVS**, **S** and **V** schemes, it has been reported that the V scheme as the most satisfactory, which is confirmed by tests done with our code[161]. With such a scheme I implemented the Møller-Plesset perturbation theory, while X. Ren (FHI) implemented the RPA method[161].
The product between two local basis functions of a chosen basis set, e.g. NAO, are *fitted* with an *auxiliary* basis set, P_μ -which have to be optimized- and a projection of a state of the system can always be expanded in terms of such a basis set, so that

$$\phi_i(\mathbf{x})\phi_j(\mathbf{x}) \approx \sum_{ij\mu} O_{ij\mu}P_\mu(\mathbf{x}), \quad (2.40)$$

where $O_{ij\mu}$ varies according to the chosen scheme.
In the V scheme Eq. (2.39) reads

$$(ia|jb) \equiv \int_{\mathcal{V},\mathcal{V}'} \phi_i(\mathbf{x})\phi_j(\mathbf{x}')\phi_a(\mathbf{x})\phi_b(\mathbf{x}')V(\mathbf{x}-\mathbf{x}') = O_{ia\mu}V^{-1}_{\mu\nu}O_{jb\nu}, \quad (2.41)$$

where

$$O_{ij\mu} = V_{\mu t}^{-1} \int_{\mathcal{V},\mathcal{V}'} \phi_i(\mathbf{x})\phi_j(\mathbf{x})V(\mathbf{x}-\mathbf{x}')P_t(\mathbf{x}'), \tag{2.42}$$

and where $V_{\mu\nu}^{-1}$ is the inverse of the Coulomb potential projected on the auxiliary basis set, $V_{\mu\nu} = \int_{\mathcal{V},\mathcal{V}'} P_\mu(\mathbf{x})V(\mathbf{x}-\mathbf{x}')P_\nu(\mathbf{x}')$. The present in-house code FHI-AIMS[19,161] has been developed with such a functionality for wavefunction methods, i.e. Hartree-Fock, MP2, RPA, and such a technique, differently from what was used in literature[48,49,80,108,111,116,188], is applied to all integrals involving four wave functions. The reason is that for numerical atomic orbitals, all integrals have to be calculated on a real-space grid, while Gaussian type orbital integrals over occupied states are efficiently calculated analytically, thus it is does not make any sense to apply the resolution of identities technique in Hartree-Fock implementations. Integrals are evaluated in FHI-AIMS using the V scheme and using a multi-step procedure when available[159]. Moreover we apply the singular valued decomposition (SVD)[159] technique for the inversion of the Coulomb potential[19,161].

3 Monolayer and Bilayer Graphene

3.1 Background and Main Assumptions

Graphitic systems represent an important benchmark for the study of extended aromatic systems and are the basis for more complex nanostructured ones. In our study we focus on graphene and bilayer graphene, and we are interested in determining the equilibrium geometry, cohesive and binding energy of such systems. Previous studies with local and semi-local DFT functionals, i.e. LDA and GGA, showed how the interaction between two graphene sheets is poorly described, while the accurate equilibrium geometries obtained in LDA are attributed to error cancellations[78,133]. At the same time cohesive energies are not described accurately in LDA, while in PBE they are relatively close to the experimental results[78,145]. Since the interactions between two graphene sheets and more in general, in graphite bulk, are weak, the cohesive energy is not much affected. On the other side experimental results, due to the scale of the interactions, have always shown a considerable error bar. This is caused by the fact that measurements are indirectly extrapolated from thermal desorption of aromatic molecules on surfaces or are extrapolated from models based on exfoliation of nanotubes, so that surface contributions are intrinsically taken into account[17,197].
For such a reason a benchmark of new, improved functionals as well as post-Hartree-Fock methods is important as advances in computational resources and algorithms become available. In the previous chapter we have highlighted the importance of correlation, in particular beyond the Hartree-Fock approximation (HF) and semi-local DFT. Such contribution is very important in determining the correct equilibrium geometries and binding energies. We described several suitable and computationally less demanding theories and methodologies, e.g. PBE+vdW, MP2, RPA/RPA+, formulated in order to cope with weakly interacting systems, where the repulsive exchange contribution is relatively small compared to the other contributions. Correlation is, for isolated systems in the non-relativistic Casimir-Lifshitz region[136], an attractive contribution, without which two graphene sheets cannot bind as we will see. On the other side, if we consider multiple graphene sheets, depending on the stacking, they contain quadrupole contributions which could tend to cancel the attractive behaviour of the correlation[27]. On the computational side, the so-called wavefunction methods such as MP2 and RPA, have been mainly used for cluster calculations. Periodic implementations exist, and have been successfully implemented[63,157], but when it comes to systems close to metallicity, or zero-gap semiconductors, like graphite, there are technical difficulties [39]. The second order perturbation theory, MP2, is known to diverge for metals in three dimensions[47](as well as second order perturbation DFT theory, i.e. the Görlitz-Levy approach), due to the bare Coulomb potential[47]. However for two dimensional systems, it can be shown,

starting from a jellium model, this is not the case[160]. Hence the use of MP2 for two dimensional metallic or semi-metallic systems is justified.
In this study we will first evaluate properties like the equilibrium distance and cohesive energy of graphene with the in-house numerical atomic orbital (NAO) code, using DFT functionals already applied to graphene in literature. Such reported computations usually employ plane waves, hence pseudopotentials [59,121], or linear augmented plane waves techniques[59]. We will use a tigh-binding approach starting from cluster calculations, which will be subsequently validated with the corresponding bulk calculations and then we will proceed to the evaluation of the corresponding quantities via the wavefunction methods (MP2, RPA, RPA+). We will then apply the same methodologies to evaluate equilibrium distance, cohesive and binding energy of AB-stacked bilayer graphene.
Such an approach can also represent an alternative way to estimate physical properties for presently too demanding methodologies like coupled cluster at the third order in perturbative excitations (CCSD(T)), which has been shown to provide accurate results for aromatic systems[84].

3.2 Preliminary Consideration on Geometry

Graphene has been discovered only recently[142], and it has been mostly studied on substrates, ranging from silicon oxide and carbide[120,169,189] to transition metals[178], graphite (accurate measurements can be done nowadays on highly-oriented pyrolitic graphite (HOPG)) and then only in 2007 as a suspended graphene sheet[129]. It has been debated in the past over the possible symmetry breaking, from six-fold to three-fold, or even two-fold and it has been argued by Pauling[148] that *quinoid* structures were possible. X-rays techniques did not provide strong evidence for this though[72] Experiments using scanning tunneling microscopy (STM) became available much later[18] and revealed often only half of the surface atoms, since in graphitic structures only three atoms of the honeycomb lattice have an atom underneath. Moreover it was not possible to accurately evaluate bonds in graphite, and often disturbances like Moireé and Kekulé patterns form on such surfaces[138]. Even movements of graphene layers have been reported during STM experiments, due to the weak interlayer bonding. In particular electron density modulation has been observed at low voltages[85], and it has been sometimes associated with STM tip effects[68,199]. Studies on graphene and nanotubes, which can be imagined as rolled graphene sheets, reported similar effects, but it has been shown that they come from a wavefunction modulation, as can be seen from *ab-initio* calculations as well[85,105]. Furthermore, atomic force microscopy (AFM) experiments provided the visualization of the full honeycomb structure[68], and no quinoid structures have been found within the accuracy limits. Thus the structure of graphite has been widely accepted as hexagonal, with different arrangements of the stacked graphene sheets (ABA, ABC structures[110]), and with equally spaced carbon atoms[72]. A six-fold symmetry break due to the variation of the in-plane carbon bonds can be found instead as a result of the finite temperature and phonon modes[131], which are beyond the scope of our study due to computationally demanding techniques we are going to apply. Recent experiments on suspended graphene

showed the absence of perfect two dimensional structures, but ripples, even though bond distances of carbon atoms were not modulated. Such ripples can be present also on certain surfaces[117,189]. Because of the large length scale of such warping and since we are interested mostly in the cohesive energy and equilibrium distances between graphene layers we can assume graphene as approximately flat. By all these considerations, in the zero temperature limit, it is not expected that this approximation creates drastic differences with respect to accurate experimental measurements of the cohesive and binding energies of the graphitic structures i.e. we will assume no modulation is present in the in-plane distances, and we assume a perfect two dimensional structure. Hence we can calculate the properties of mono and bilayer graphene, as we will see in the following sections, only using two degrees of freedom, i.e. we vary the in-plane lattice constant and the interlayer distance.

3.3 Periodic Graphene

The aim of the first part of our study is the investigation of the properties of a graphene sheet using different quantum chemical methods, i.e. LDA, GGA-PBE, PBEsol, PBE+ vdW DFT functionals and MP2, RPA and RPA+. Our properties of interest are equilibrium geometries, cohesive and binding energies. As a first step we study the convergence of density-functional theory periodic calculations to provide accurate references that afterwards will be compared to the bulk limits obtained from cluster calculations. Once established that bulk extrapolations from clusters are reliable for various DFT methods, we extrapolate the bulk limit from MP2 and RPA/RPA+ calculations and compare our periodic and extrapolated values with the theoretical and experimental references presently available.

3.3.1 The LDA and GGA-PBE Functionals

We consider a graphene layer and study the convergence of the cohesive energy per atom first with respect to the basis set size, then with respect to the number of k-points and in the end we consider the effects of vacuum size and the order of the multipole expansion (see Appendix A.2.1). Calculations are performed with PW-LDA[152] and GGA-PBE[150] DFT functionals.
The cohesive energy per atom is defined as

$$E_{\mathrm{coh}} = \frac{E_{\mathrm{tot}}}{N_{\mathrm{C}}} - E_{\mathrm{C}}, \tag{3.1}$$

where N_{C} is the number of carbon atoms in the supercell of energy E_{tot} and E_{C} the energy of the isolated carbon atom. The way the free atom reference is computed is important, in particular when atoms have partly occupied levels, like in the carbon case. The present implementation of the code FHI-AIMS[19] does not take the Hund's rules into account, and the electron population is eventually equally distributed among the degenerate valence levels. To avoid this, we break the spacial symmetry using an external perturbation and smear the Fermi level slightly in order to make such a symmetry-break

easier. As perturbation we choose a small external electric field, which we apply for the first few self-consistency cycles. In this way the self consistency is directed into the *right* attractor basin of the ground state of the employed DFT functional, i.e. the $^3P_0$ ground state. A similar effect can be obtained when a spin-collinear Hartree-Fock calculation is preliminarily done and Hartree-Fock wave functions are used as a starting point for DFT calculations. We also note that in Eq. (3.1) E_{tot} does not contain the vibrational zero-point energy (ZPE) contribution, estimated to be about $0,166$ eV/atom for ABA stacked graphene layers[7].
The basis sets in this study are NAOs, and in particular the LDA optimized sets provided within FHI-AIMS[19]. In Appendix A.2.1 we report the convergence evaluations and we conclude the following settings are enough for an accuracy at the meV/atom level: "sb", an (18x18x1) k-mesh, $l_{\text{hartree}} = 4$ and an interplane distance of 20 Å.
In Fig. (3.1) we show the resulting cohesive energy curve as a function of the in-plane constant a.

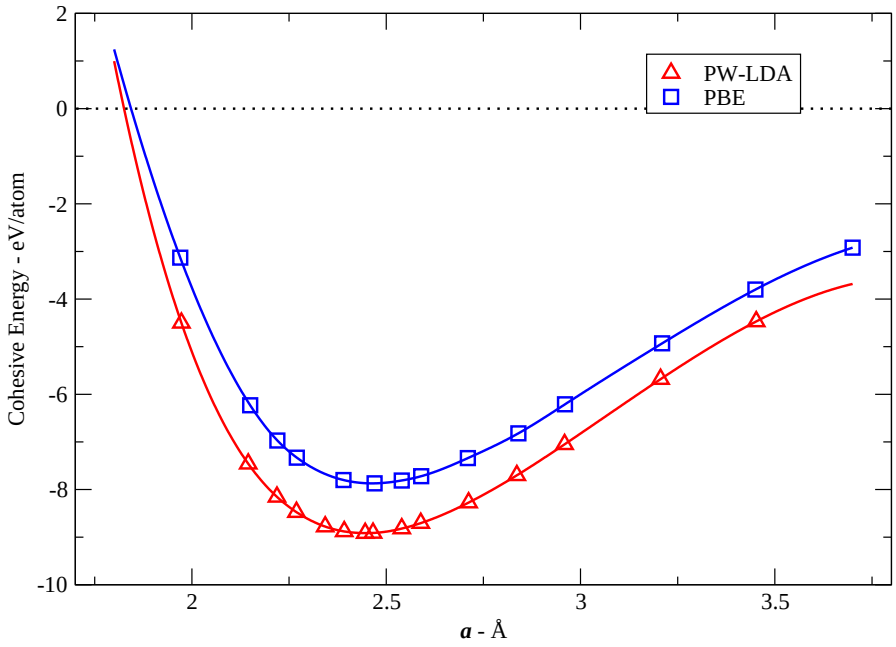

Figure 3.1: Dependence of the graphene cohesive energy on the in-plane lattice constant computed at optimized computational settings ("sb" basis set, (18x18x1) k-mesh, $l_{\text{hartree}} = 4$, and intersheet distance of 20 Å).

We interpolate the DFT curves shown in Figure (3.1) with cubic splines, to obtain the cohesive energies and equilibrium distances shown in Table (3.1). Our results agree well with literature, in particular with ref.[64], and differences are at most of the order of 4%.

Both PW-LDA and GGA-PBE functionals yield lattice constants in close agreement to experimental values. As shown in refs.[129,133] using a suspended graphene sheet, the in-plane lattice constants of graphene and graphite are very similar, so that the comparison to experimental data from graphite is permissible.

Table 3.1: Comparison of the computed graphene in-plane lattice constant a and cohesive energy E_{coh} with existing DFT literature and experiment. The values for E_{coh} reported for refs.[62,64,78,145] are estimated from the published graphite binding and interaction energy. The experimental values are zero-point energy corrected using the value for graphite of ref. [7] and are considered at lower precision because the interaction energy between two graphite layers is known only with a certain error bar. More LDA values can be found in reference[64]. For simplicity in all the tables of this work the sign of cohesive energies is reversed in principle being negative.

a (Å)	E_{coh} (eV/atom)	DFT method
2,446	8,92	PW-LDA (this work)
2,441	8,89	PW-LDA (PP)[64]
2,447	8,98	PW-LDA (FP-LAPW)[78]
2,452	8,57	HL-LDA (LCGTO-FF)[186]
2,441	8,53	PZ-LDA (PP)[145]
2,463	7,87	GGA-PBE (this work)
2,461	7,87	GGA-PBE (PP)[64]
2,462	7,75	GGA-PBE (PP)[145]
2,46		Exp.[129]
2,461		Exp. (293 K)[40,187]
2,459	$\sim$ 7,5	Exp. (303 K)[62], ZPE from ref.[7]

3.3.2 The PBEsol Functional

As the PBEsol functional has been optimized for jellium bulk and surface properties, we are interested in how this functional behaves for a two dimensional graphene sheet.
As for the previous section we determine the accuracy of the PBEsol DFT functional[151] with respect to the cohesive energy of a graphene sheet and convergence tests are reported in Appendix A.2.2. We conclude that the same settings as those applied to PW-LDA and GGA-PBE are valid. The atomic references are calculated as we already mentioned in the last section. Fig. (3.2) shows the variation of the cohesive energy as a function of the lattice constant a. In Table (3.2) we summarise the results and we compare them with the previous calculations for PW-LDA and GGA-PBE DFT functionals and experiment. The lattice constant, already very close to the experimental one for the GGA-PBE functional, now matches it exactly. However, as expected for solids and as reported in literature[151], the cohesive energy is worse than for the GGA-PBE functional.

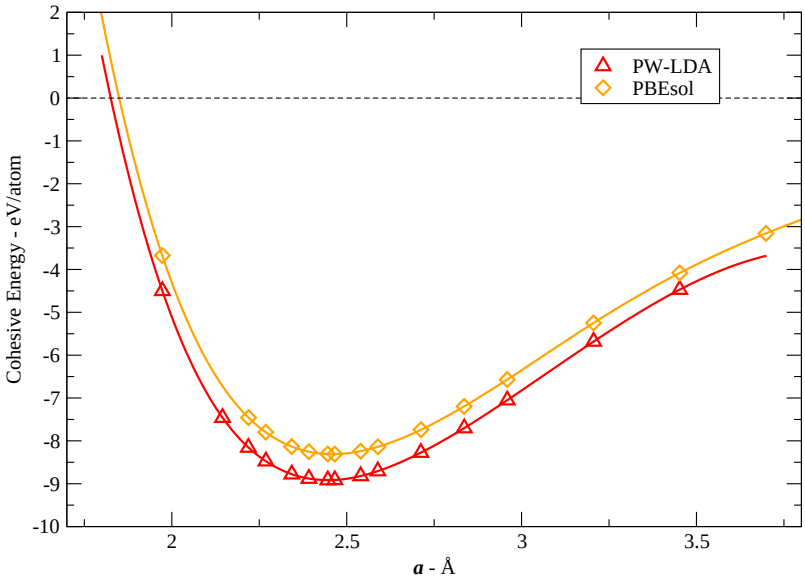

Figure 3.2: Dependence of the graphene cohesive energy on the in-plane lattice constant computed at the optimized computational settings ("sb" basis set, (18x18x1) k-mesh, $l_{\mathrm{hartree}} = 4$, and intersheet distance of 20 Å.

In conclusion the PBEsol functional provides a very accurate geometry, as it has been built for [151], but energies lie between PW-LDA and GGA-PBE.

Table 3.2: Comparison of the PBEsol functional computed graphene in-plane lattice constant a and cohesive energy E_{coh} with the PW-LDA and GGA-PBE DFT functionals and experiment. The values for E_{coh} reported for refs.[62,64,78,145] are estimated from the published graphite binding and interaction energy. The experimental values are zero-point energy corrected using the value for graphite of ref.[7] and are considered at lower precision because the interaction energy between two graphite layers is known only with a certain error bar.

a (Å)	E_{coh} (eV/atom)	DFT method
2,446	8,92	PW-LDA (this work)
2,463	7,87	GGA-PBE (this work)
2,459	8,31	PBEsol (this work)
2,46		Exp.[129]
2,461		Exp. (293 K)[40,187]
2,459	$\sim$ 7,5	Exp. (303 K)[62], ZPE from ref.[7]

3.3.3 The PBE+vdW Functional

In the previous sections we have shown how a semi-local functional like GGA-PBE recovers relatively well the cohesive energy with respect to the experimental data. We consider now to a first extent the effect of the dispersion interaction on the cohesive energy using the PBE+vdW method elaborated by A. Tkatchenko and M. Scheffler[184]. Convergence tests are shown in Appendix A.2.3 and we employ the following settings: "sb", an (18x18x1) k-mesh, $l_{\text{hartree}} = 4$ and an interplane distance of 20 Å and *vdw_cells* as (10 10 0) grid. In Fig.(3.3) we show the cohesive energy curve calculated using the PBE+vdW functional compared to the underlying GGA-PBE functional. The van der Waals interaction correction, as expected, does not provide substantial changes in the cohesive energy equilibrium minimum, but only a small shift in the cohesive energy since the free atom reference is the same as for the GGA-PBE functional.

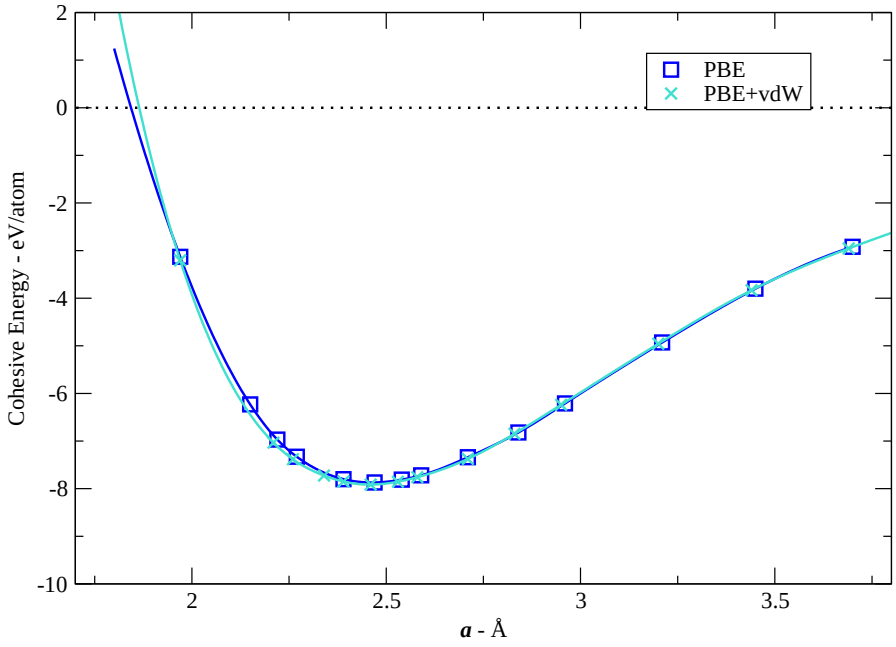

Figure 3.3: Dependence of the graphene cohesive energy on the in-plane lattice constant computed at the optimized computational settings ("sb" basis set, (18x18x1) k-mesh, $l_{\text{hartree}} = 4$, and intersheet distance of 20 Å).

In Table (3.3) we compile the comparison between the PBE+vdW method and all other tested functionals. As said previously the cohesive energy given by the addition of pair-wise summations over van der Waals interactions is small and appears to be worse than the PBE functional when comparing it to experiments. However a correct consideration of the multiconfigurational atomic reference should be included as well.

Table 3.3: Comparison of the PBE+vdW computed graphene in-plane lattice constant a and cohesive energy E_{coh} with other DFT functionals and experiment. The values for E_{coh} reported for refs.[62,64,78,145] are estimated from the published graphite binding and interaction energy (see text). The experimental values are zero-point energy corrected using the value for graphite of ref.[7] and are considered at lower precision because the interaction energy between two graphite layers is known only with a certain error bar.

a (Å)	E_{coh} (eV/atom)	DFT method
2,446	8,92	PW-LDA (this work)
2,463	7,87	GGA-PBE (this work)
2,459	8,31	PBEsol (this work)
2,460	7,91	PBE+vdW (this work)
2,46		Exp.[129]
2,461		Exp. (293 K)[40,187]
2,459	$\sim$ 7,5	Exp. (303 K)[62], ZPE from ref.[7]

3.4 Graphene Sheet, Cluster Extrapolations

In many quantum chemical methods, the study of periodic systems is not straightforward and at the present time in some cases it is restricted to non-conducting systems[157]. In order to compute the bulk properties of our interest, i.e. the cohesive energy and the equilibrium geometry, we have therefore investigated as an alternative to periodic calculations the use of cluster extrapolations to the bulk limit. For this, we consider a set of clusters with the geometric parameters of the periodic systems previously calculated. As shown in Fig. (3.4) these clusters are saturated with peripheral hydrogens, at the experimental C-H distance in benzene. This way we avoid problems due to the open-shell nature of carbon and mimick better the properties of sp^2-hybridized carbon in the infinite sheets. However, the fact that clusters have borders and are saturated with hydrogens, makes the straightforward convergence of the cohesive energy towards the bulk limit rather slow. A suitable procedure is then needed to eliminate such edge effects, and make an extrapolation efficient. To achieve this goal without parametrization, we consider a formula of the type

$$E_{\mathrm{tot}} = N_{\mathrm{C}} E_{\mathrm{C}} + N_{\mathrm{H}} E_{\mathrm{H}} + E_{\mathrm{coh}} \sum_c f(c) N_c + E_{\mathrm{CH}} N_{\mathrm{H}}, \tag{3.2}$$

where E_{tot} is the total energy of the cluster, E_{C} the spin-polarized atomic references for C and H, N_{C} and N_{H} the number of carbon and hydrogen atoms in the cluster respectively, c the coordination number of carbon atoms, $f(c)$ a function of the coordination number, N_c the number of carbon atoms with c-fold coordination, E_{CH} the carbon-hydrogen interaction and E_{coh} the extrapolated infinite bulk cohesive energy per atom. As long as the unspecified function f assumes the right limit of $f(3) = 1$, this equation yields the correct infinite sheet cohesive energy. Motivated by tight-binding[174] we have chosen $f(c) = \sqrt{c/3}$ to obtain the values for singly and doubly coordinated carbon. Next, let us reorder the previous equation in the following form,

$$g(N_{\mathrm{H}}/b) \equiv \frac{E_{\mathrm{tot}} - N_{\mathrm{C}} E_{\mathrm{C}} - N_{\mathrm{H}} E_{\mathrm{H}}}{b} = E_{\mathrm{coh}} + E_{\mathrm{CH}} \frac{N_{\mathrm{H}}}{b}, \tag{3.3}$$

where $b \equiv \sum_c f(c) N_c$. From this form we can see that the intercept of a least-square interpolated linear function $g(N_{\mathrm{H}}/b)$ with the ordinates provides the bulk limit extrapolation in absence of hydrogens while the slope of such a curve gives the C-H binding, i.e. border, contribution.

3.4.1 The LDA and GGA-PBE Functionals

We apply this approach first to determine the graphene cohesive energies for PW-LDA and GGA-PBE and compare to the previously established periodic reference values. As said previously, we built hydrogen saturated graphene flakes of the same geometry as in periodic graphene. The in-plane constant of PW-LDA is taken as a reference C-C distance for all methods and clusters and we consider a set of progressively growing

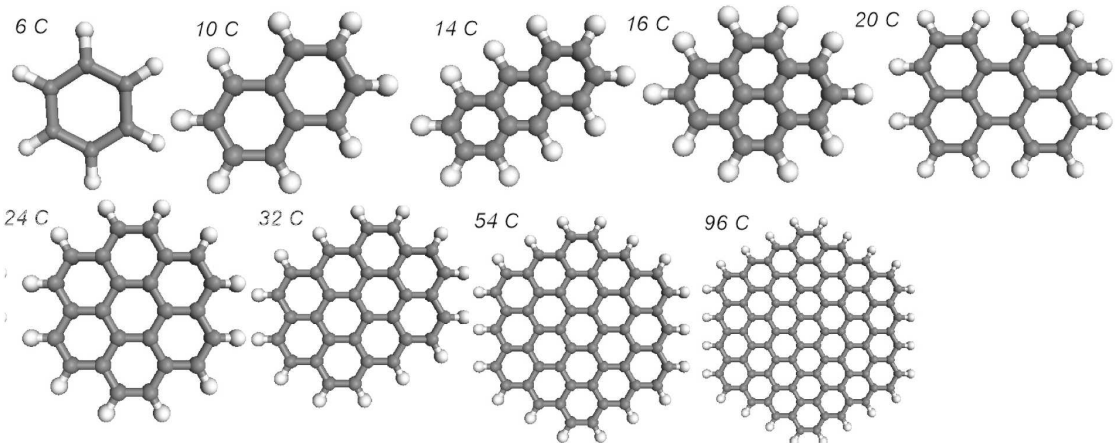

Figure 3.4: Clusters used in the present graphene calculations.

clusters starting from benzene to a flake of 120 atoms (C and H) as shown in Figure (3.4).
Fig. (3.5) shows the computed data as obtained from Eq. (3.3), and using a C[min+2s2p3d4f] H[min+2s2p] basis set, called "t1+f". The values obtained for larger basis sets lie on parallel lines to the ones shown in Fig. (3.5) and on the scale of Fig. (3.5) they are essentially superimposed on the lines shown. The fact that calculated values lie on the fitted linear curve shows how rapidly the E_{CH} contribution per atom in Eq. (3.3) converges to a constant value for a given method.
In table (A.1) in Appendix A.3.1 we compile the extrapolated cohesive energies using different basis sets and different linear regressions, i.e. we considered different sets of cluster sizes that are used in the least-square fit. We also compare the difference between the cohesive energies computed with PW-LDA and GGA-PBE and obtain an absolute error that is smaller with respect to the periodic calculations than for PW-LDA and GGA-PBE separately. If we neglect the results for the smallest clusters (primarily "6 C") the accuracy of the bulk limit with respect to the known periodic case further improves for both PW-LDA and GGA, and in the (PW-LDA - GGA-PBE) difference the extrapolated value lies now within ±10 meV/atom of the periodic reference value.

3.4.2 The PBEsol Functional

As a further test we calculate the cohesive energy extrapolation from clusters shown in Fig. (3.3) using the PBEsol DFT functional. The geometries considered are the same as employed in the previous section, and we considered again the same progressively growing clusters up to 120 atoms. Fig. (3.6) shows the computed extrapolated data at the "t1+f" basis set level. For the PBEsol DFT functional the values obtained for different basis sets lie on parallel lines, superimposed at the scale shown in such a figure. In Table (A.2) in Appendix A.3.2 we show the results obtained using different linear extrapolation ranges

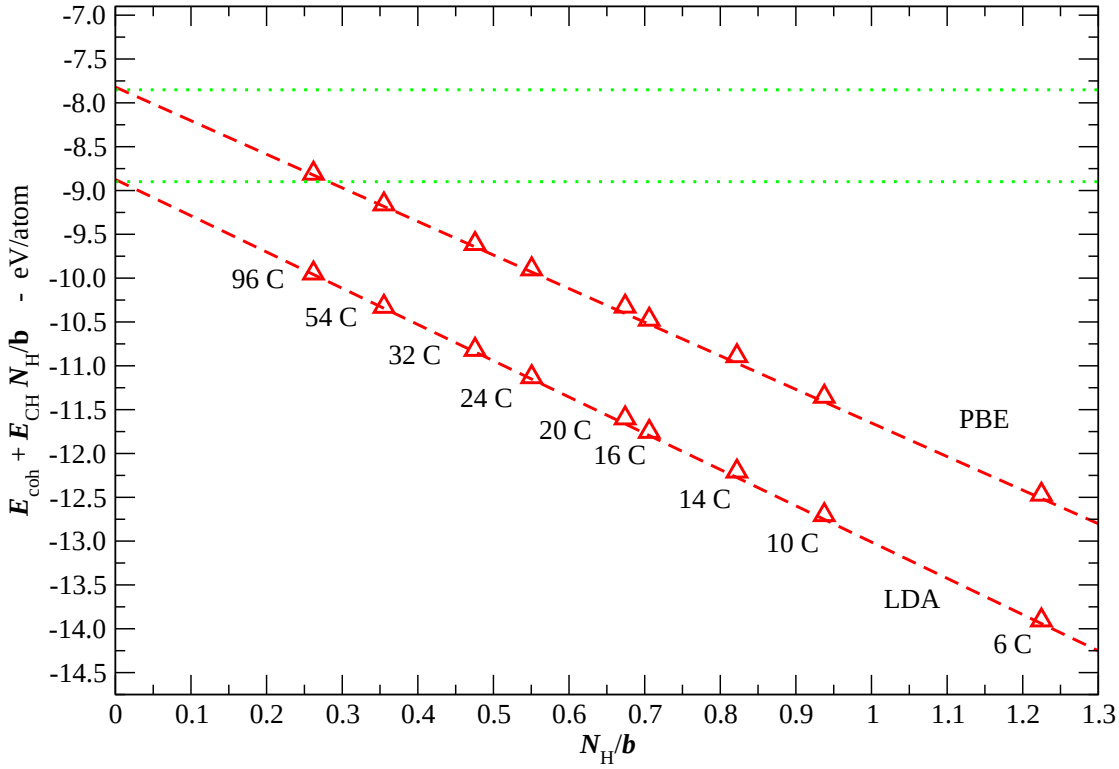

Figure 3.5: Convergence of PW-LDA and GGA-PBE extrapolated cohesive energies for graphene taken at an in-plane lattice constant $a = 2,446$ Å. The intercepts with the ordinates represent the bulk limit extrapolation. Dashed lines represent the linear regressions and dotted lines the periodic reference values described before. The labels at every point correspond to the number of carbon atoms in the corresponding cluster, starting at benzene (labelled "6 C", cf. Fig. (3.4)).

and using progressively growing basis sets. Again, the behaviour of the cohesive energy with respect to the basis set size and clusters range appears very similar to the behaviour already discussed in the previous section for PW-LDA and GGA-PBE functionals, and the same conclusions are therefore valid. In particular the energy differences among two different methods are more accurate (within 10 meV/atom) with respect to the periodic calculations.

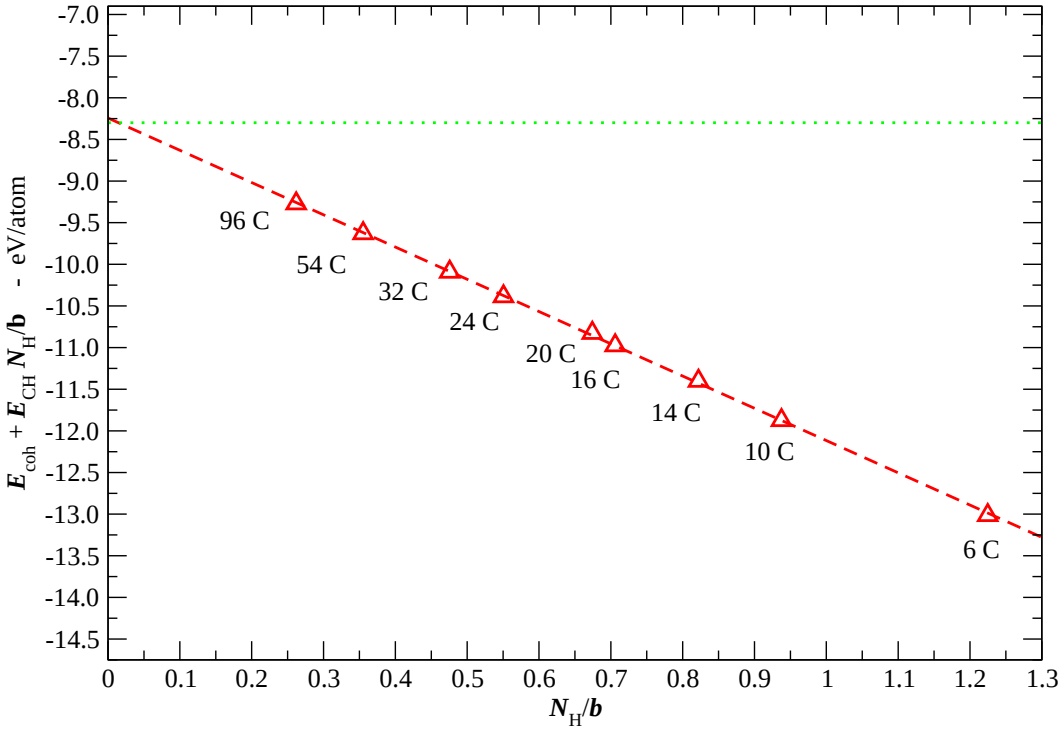

Figure 3.6: Convergence of PBEsol extrapolated cohesive energy for graphene taken at an in-plane lattice constant $a = 2,446$ Å. The intercepts with the ordinates represent the bulk limit extrapolation. Dashed lines represent the linear regressions and dotted lines the periodic reference values described before. The labels at every point correspond to the number of carbon atoms in the corresponding cluster, starting at benzene (labelled "6 C", cf. Fig. (3.4)).

3.4.3 The PBE+vdW Functional

We validate the cluster extrapolation approach also with the PBE+vdW van der Waals correction scheme[184]. We compute all clusters with the same settings as in the previous sections. In Fig. (3.7) we show the extrapolated data at at "t1+f" basis set level, since different basis sets data lie on parallel lines superimposed at such a scale. The behaviour of the PBE+vdW functional with respect to clusters size and basis set convergence is fairly similar to the other functionals previously employed. Again, in Table (A.3) we report the results obtained for the most accurate basis sets and as for PW-LDA and GGA-PBE DFT functionals, results are converged at meV/atom level. The difference in cohesive energy between DFT local and semi-local functionals and PBE+vdW functionals are more precise then the results obtained using one functional, and values lie within 10 meV/atom from values obtained from periodic calculations.

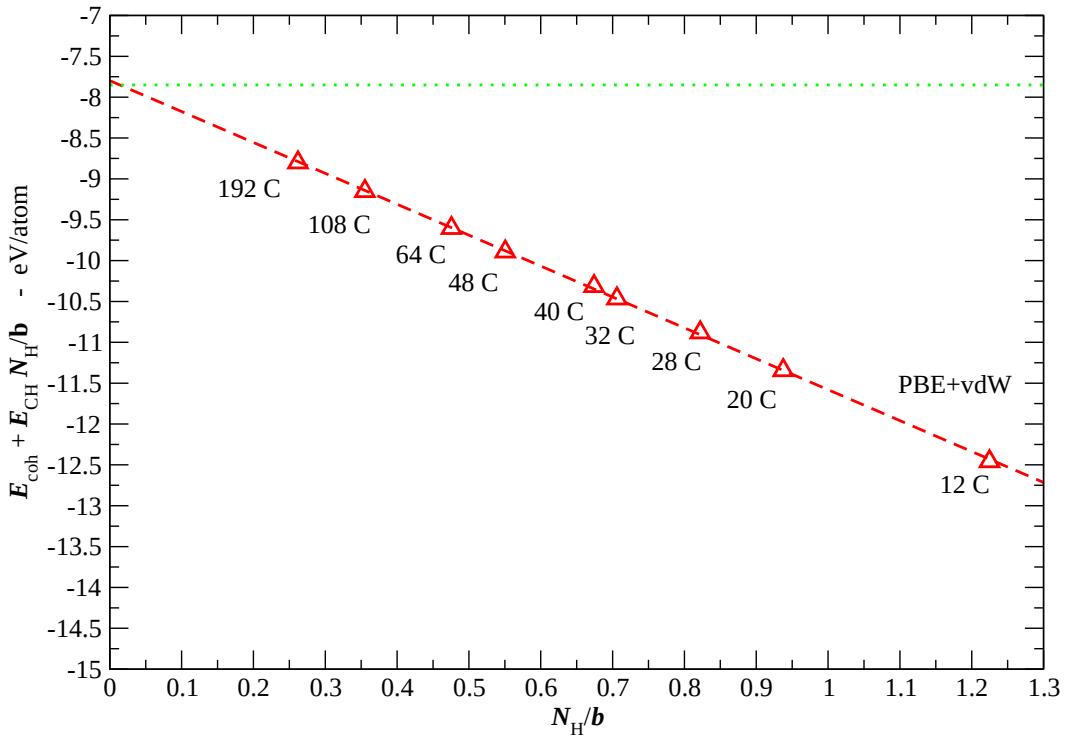

Figure 3.7: Convergence of PBE+vdW extrapolated cohesive energy for graphene taken at an in-plane lattice constant $a = 2,446$ Å. The intercepts with the ordinates represent the bulk limit extrapolation. Dashed lines represent the linear regressions and dotted lines the periodic reference values described before. The labels at every point correspond to the number of carbon atoms in the corresponding cluster, starting at benzene (labelled "6 C", cf. Fig. (3.4)).

3.4.4 The MP2 Method

Having demonstrated the feasibility of our approach for DFT we consider the MP2 method. Now the atomic reference values have also been corrected with the counterpoise correction method (BSSE-CP)[22], which is not necessary for DFT functionals, according to the settings and basis sets applied. In Figure (3.8) we plot the extrapolated cohesive energies using different basis sets. The cohesive energies lie on the fitted linear curve with good approximation. Moreover different basis sets provide parallel lines like in the DFT case. In Table (A.4) in Appendix A.3.4 we show the extrapolated cohesive energies corresponding to the "t1+f", "sb", "t2", "t3", "t4C" and "t4Cp" basis sets, setting product basis threshold to 4 (3 for hydrogens) and basis set product cut-off threshold of 10^{-4} (10^{-3} for largest clusters and basis sets). The variation among different sets of clusters are again very small and particularly in the difference to one of the DFT functionals we obtain extrapolated values that scatter only within ±20 meV/atom. For the DFT functionals the "t3", "t4C" and "t4Cp" basis sets are converged at the sub-meV/atom level. However, as expected, the convergence of the MP2 value with basis set size is

much slower than in the case of the DFT functionals, and it is monotonically reached at the "t4C" basis set level. Tentatively, we therefore assign a conservative error bar of ~ 0.06 eV/atom to the "t4Cp" values (accounting for extrapolation) and quote the latter as the final result.

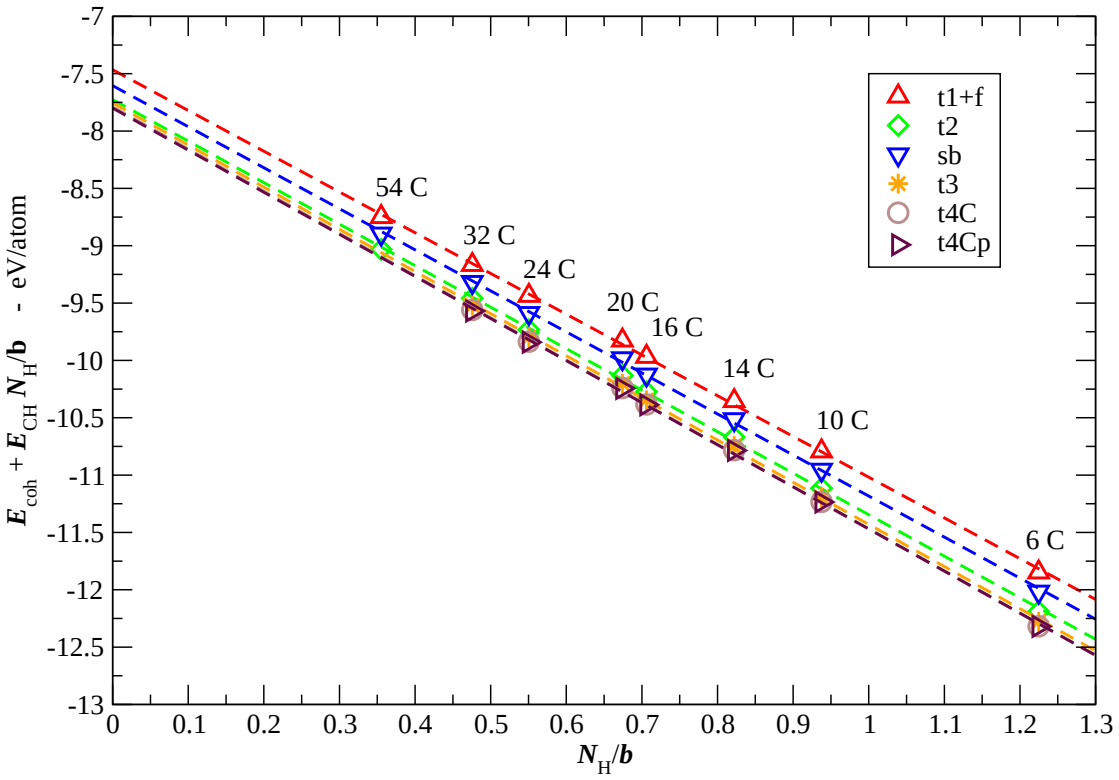

Figure 3.8: Convergence of MP2 extrapolated cohesive energy for graphene taken at $a = 2,446$ Å and starting from benzene (labelled "6 C"). The intercepts with the ordinates represent the bulk limit extrapolation. The dashed lines represent the linear regressions.

3.4.5 The RPA method

We consider next the RPA method[42,101]. The atomic references have been corrected, as before, with the counterpoise correction method (BSSE-CP)[22]. Fig. (3.9) shows the linear regressions for "t1+f", "sb", "t2", "t3", "t4C" and "t4Cp" basis sets and with the following parameters: number of basis set products are set to 4 (3 for hydrogens), basis set product cut-off threshold set to 10^{-4} and *frequency_points* set to 80. RPA calculations are based on PW-LDA, and for such a reason atomic references have to be computed in the same way as for DFT, i.e. introducing an electric field or doing a preliminary Hartree-Fock calculation. In Fig. (3.9) we show the extrapolated cohesive energy for different basis sets. Also in this case the curves are linear and parallel. In Table (A.5) in Appendix A.3.5 we compile the results for different extrapolations and basis sets. The differences in each clusters' set are reduced when energy differences with the other methods are taken into account. The convergence with respect to the basis set size is again slow and it is essentially reached at the t4C level. We assign a similar error bar as for MP2 of $0,06$ eV/atom, which takes account of the extrapolations.

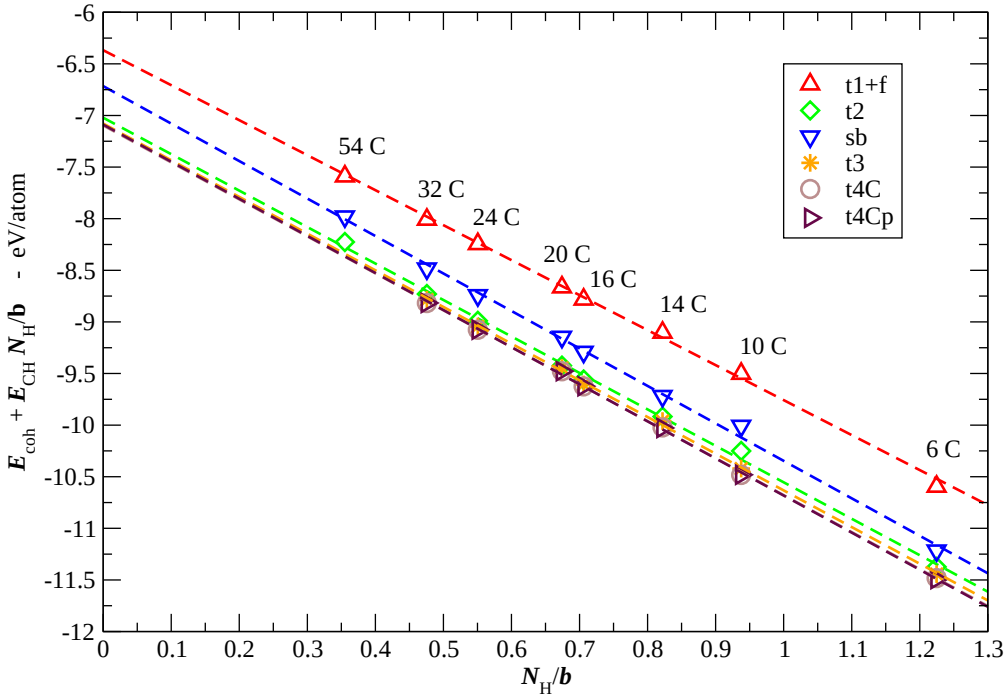

Figure 3.9: Convergence of RPA extrapolated cohesive energy for graphene taken at $a = 2,446$ Å and starting from benzene (labelled "6 C"). The intercepts with the ordinates represent the bulk limit extrapolation. The dashed lines represent the linear regressions.

3.4.6 The RPA+ method

Finally we consider the RPA+ method[94]. This method is based on exactly the same computational framework of RPA, so that we do not need further parameters or conditions in principle: number of basis set products are set to 4 (3 for hydrogens) and *frequency_points* are set to 80, basis set product cut-off threshold is set to 10^{-4}. In Fig. (3.10) we demonstrate that the extrapolated cohesive energy curves for different basis sets are linear and parallel. In Table (A.6) in Appendix A.3.6 we show the results for various extrapolation ranges and basis sets. Again the differences for each cluster set with other DFT functionals improves the overall accuracy of the cohesive energy extrapolations. The convergence with respect to the basis set size is slow and is reached at the t4C level. We assign again an error bar of $0,06$ eV/atom which takes into account the extrapolation error bars.

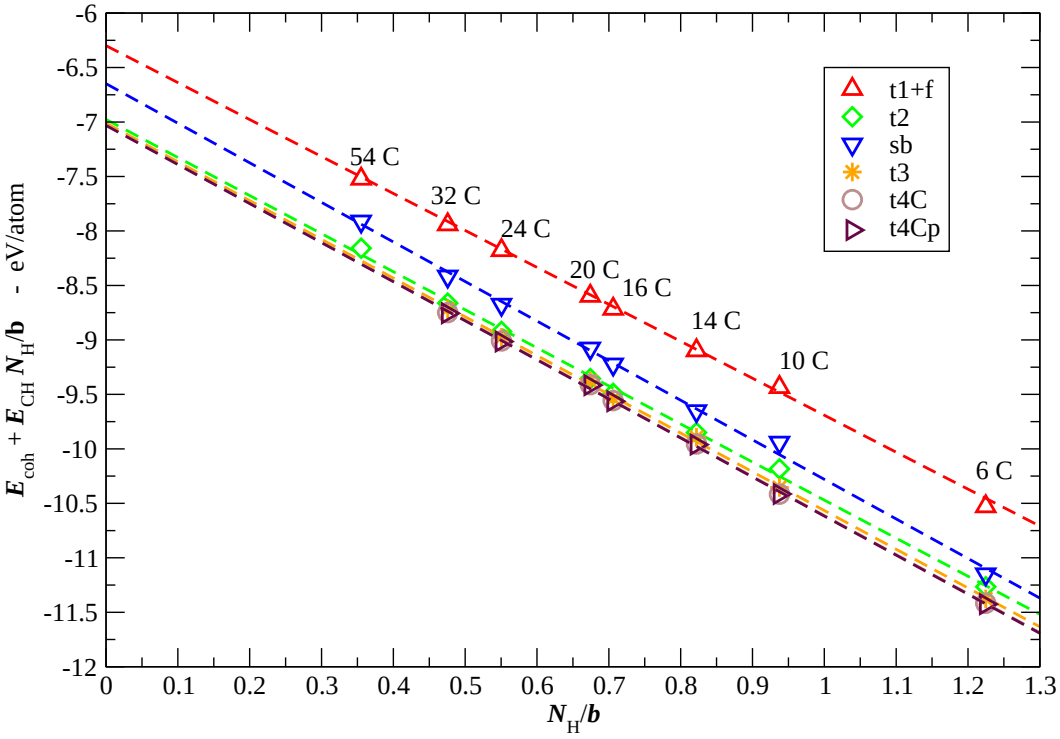

Figure 3.10: Convergence of RPA+ extrapolated cohesive energy for graphene taken at $a = 2,446$ Å and starting from benzene (labelled "6 C"). The intercepts with the ordinates represent the bulk limit extrapolation. The dashed lines represent the linear regressions.

3.4.7 Summary of the Results for Graphene

We summarise all extrapolation results for this isolated graphene sheet in Table (3.4) and Figure (3.11). For the comparison to the periodic reference values and to assess the wavefunction methods' results one has to keep in mind that the cluster extrapolation was only done for all methods at the fixed in-plane lattice constant of the PW-LDA periodic calculations, $a = 2,446$ Å. While it would, of course, be possible to do the cluster extrapolation at different lattice constants to obtain the equation of state, the similarity of the optimized periodic PW-LDA, GGA-PBE, PBEsol and PBE+vdW in-plane lattice constants, c.f. Table (3.1), should already now permit the intended proof-of-concept. Moreover, as to the MP2 and RPA/RPA+ extrapolations, we repeated an extrapolation using the cluster size range "6 C - 54 C" and the "sb" basis set at the experimental in-plane constant $a = 2,461$ Å [129,187] and obtained a shift at the meV level in the cohesive energy compared to the extrapolation results obtained with the same settings at the PW-LDA in-plane lattice constant $a = 2,446$ Å. As long as the real MP2 and RPA/RPA+ optimized lattice constants are not too far from these values, the energetic hierarchy seen in Table (3.4) will thus prevail.

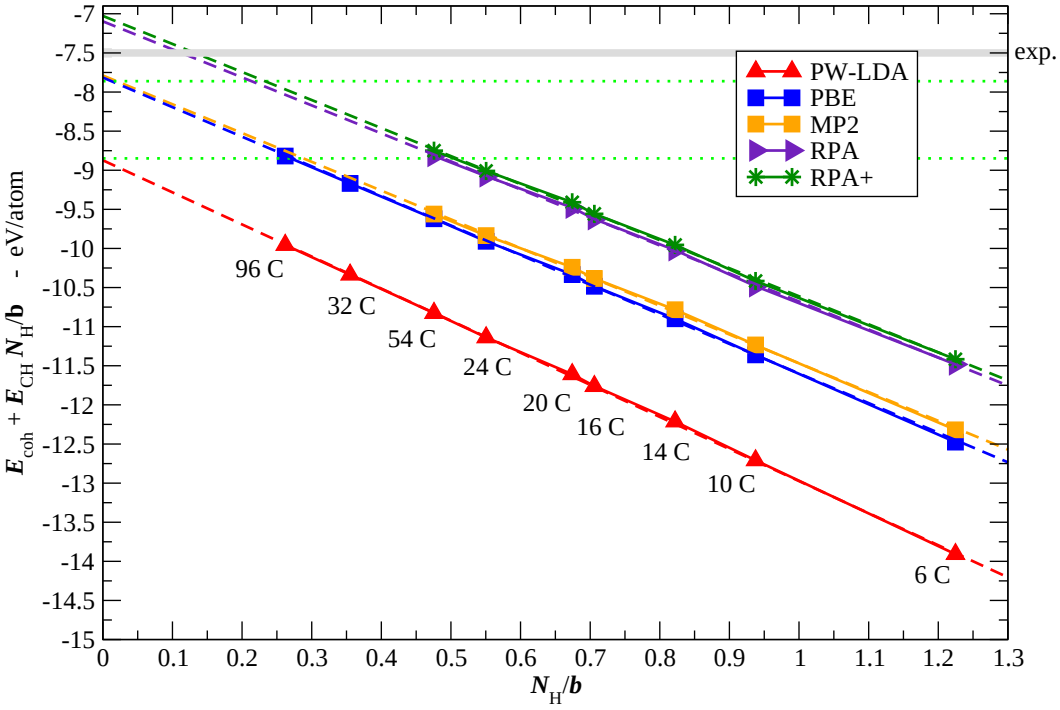

Figure 3.11: Comparison of regression curves for different chemical methods for graphene at in-plane distance $a = 2,446$ Å starting from benzene (bottom left points). Dotted lines represent the periodic calculation reference values and dashed lines the linear regressions. The intercepts with the ordinates represent the bulk limit extrapolations. Calculations shown here are computed with the "t3" basis set for DFT functionals and the "t4C" basis set for the MP2, RPA, RPA+ methods.

Table 3.4: Cohesive energy extrapolations compared with periodic calculations when available. For GGA-PBE, PBEsol, PBE+vdW and wavefunction methods also the difference of the extrapolations with respect to the other methods are considered. The basis set used corresponds to the converged "t3" basis set for the DFT functionals applied and the "t4Cp" for the wavefunction methods. The error is estimated from the basis set convergence behaviour and extrapolation scatter observable from the corresponding tables in the Appendix.

E_{coh} (eV/atom)	method
8,90 $\pm 0,03$	PW-LDA extrapolated
8,92	PW-LDA periodic
7,84 $\pm 0,03$	GGA-PBE extrapolated
7,86 $\pm 0,01$	GGA-PBE periodic + $\delta_{\text{PW-LDA}}$ extrapolated
7,86	GGA-PBE periodic
8,28 $\pm 0,03$	PBEsol extrapolated
8,29 $\pm 0,01$	PBEsol periodic + $\delta_{\text{PW-LDA}}$ extrapolated
8,28 $\pm 0,01$	PBEsol periodic + $\delta_{\text{GGA-PBE}}$ extrapolated
7,88 $\pm 0,03$	PBE+vdW extrapolated
7,89 $\pm 0,01$	PBE+vdW periodic + $\delta_{\text{PW-LDA}}$ extrapolated
7,89 $\pm 0,01$	PBE+vdW periodic + $\delta_{\text{GGA-PBE}}$ extrapolated
7,84 $\pm 0,06$	MP2 extrapolated
7,85 $\pm 0,02$	PW-LDA periodic + δ_{MP2} extrapolated
7,85 $\pm 0,02$	GGA-PBE periodic + δ_{MP2} extrapolated
7,84 $\pm 0,02$	PBE+vdW periodic + δ_{MP2} extrapolated
7,11 $\pm 0,06$	RPA extrapolated
7,12 $\pm 0,02$	PW-LDA periodic + δ_{RPA} extrapolated
7,12 $\pm 0,02$	GGA-PBE periodic + δ_{RPA} extrapolated
7,11 $\pm 0,02$	PBE+vdW periodic + δ_{RPA} extrapolated
7.04 $\pm 0,06$	RPA+ extrapolated
7.05 $\pm 0,02$	PW-LDA periodic + $\delta_{\text{RPA+}}$ extrapolated
7.05 $\pm 0,02$	GGA-PBE periodic + $\delta_{\text{RPA+}}$ extrapolated
7.04 $\pm 0,02$	PBE+vdW periodic + $\delta_{\text{RPA+}}$ extrapolated
$\sim$ 7,5	Exp. (303K)[62], ZPE from ref.[7]

3.5 Periodic Bilayer Graphene

Graphene can be stacked to form graphite bulk in three different ways, namely AAA, ABA (hexagonal graphite) and ABC (rhombohedral graphite). Graphite found in nature exhibits mainly ABA stacking[110]. However, for two stacked graphene sheets we have the choice of only AA and AB-stacking, and we undertake the study of the latter. We proceed again as we did for graphene, i.e. we first converge the properties of interest in the periodic systems using the DFT functionals and then we compare the results to the DFT cluster extrapolation. We consider first the cohesive energy and then the binding energy per atom.
Two definitions are given about the interactions between graphene sheets: the **exfoliation energy**, i.e. the energy required to remove a layer from graphite surface, and the **binding energy**, which is the energy required to bring each layer infinitely far away. Of the two notions we will focus on the binding energy and we will apply the definition used for molecules, and mainly in literature, as the difference in total energies of the entire systems minus the total energy of each layer. We note that sometimes in literature this quantity is simply written as the difference between the cohesive energies per atom of the graphitic systems and graphene, i.e. exactly half of what we will call in our work *binding energy*. In summary, the cohesive energy is defined as in the graphene case, i.e.

$$E_{\text{coh - AB}} = \frac{E_{\text{tot}}}{N_{\text{C}}} - E_{\text{C}}, \tag{3.4}$$

where N_{C} is the number of carbon atoms in the supercell of energy E_{tot} and E_{C} the energy of the isolated spin-polarized carbon atom in the $^3\text{P}_0$ ground state. The binding energy per atom, or interaction energy, is defined in this study as the difference of the cohesive energy of two stacked graphene sheets (AB) and two single sheets of graphene (monomer):

$$E_{\text{bind - AB}} = 2(E_{\text{coh - AB}} - E_{\text{coh - monomer}}). \tag{3.5}$$

where the two-factor takes into account the fact that cohesive energies are calculated per atom.

3.5.1 The LDA and GGA-PBE Functionals

In Appendix A.4.1 we describe the convergence tests and conclude that the following settings are sufficient to describe cohesive and binding energies at a high accuracy, i.e. the sub-meV/atom level: "sb", a (18x18x1) grid of 326 k-points in the full Brillouin zone, 25 Å vacuum and $l_{\text{hartree}} = 4$.
Figure (3.12) shows the binding curves of two stacked graphene sheets as a function of the interlayer distance obtained with this computational setup. Sample points on the curve were also calculated with much higher converged parameters ($l_{\text{hartree}} = 6$, (24x24x1) mesh with 576 k-points in the full Brillouin zone) and the results agree at the order of the 1 meV/atom for cohesive and at the sub-meV/atom level for binding

energy. In Table (3.5) we summarise the results obtained and compare with literature and experiment.
As in the graphene case, the GGA-PBE cohesive energy is closer to the experimental value. However, its binding energy is very small and the interlayer distance is too large. PW-LDA, because of error cancellation[133], gives also for the graphite case geometric constants close to experiments, but cohesive energies that are rather far from the experimental values. This behaviour of local and semi-local functionals with respect to the graphite binding energy is consistent with what is already described in literature (see Table (3.5)), i.e. LDA tends to underbind, but GGA-PBE tends to overcorrect LDA.

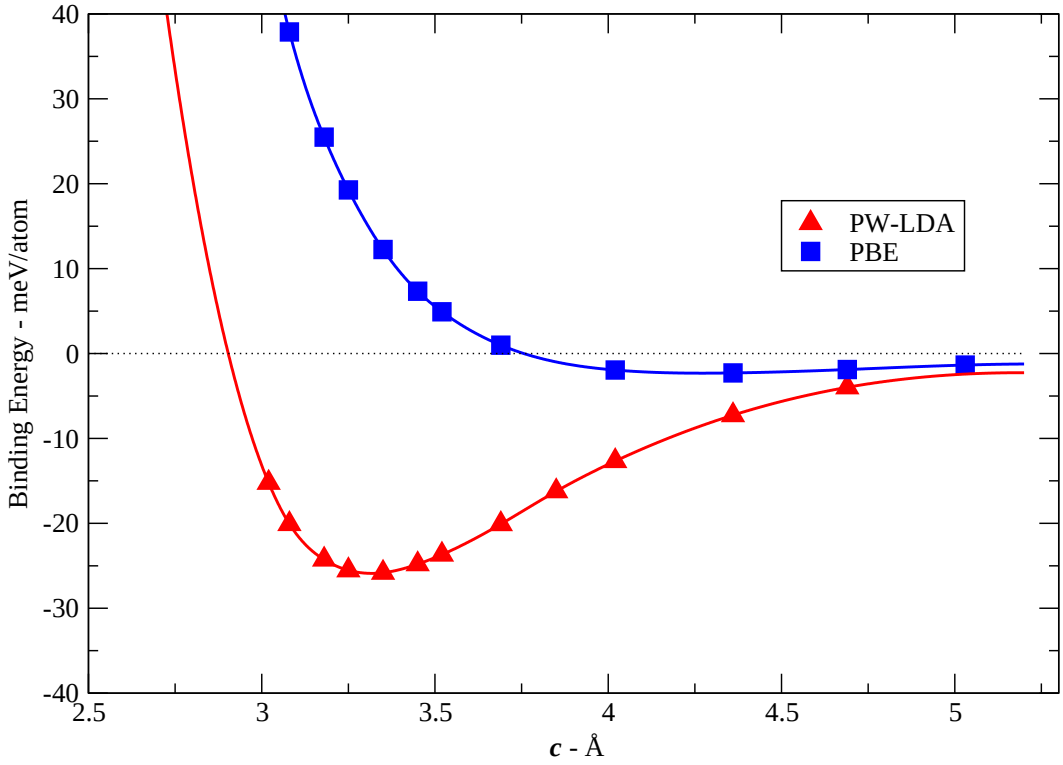

Figure 3.12: Binding energy between the stacked sheets as a function of the interlayer constant *c*. Shown are data for PW-LDA and GGA-PBE at optimized graphene in-plane equilibrium distances (see Table (3.1)) and using the "sb" basis set and (18x18x1) k-points.

Table 3.5: Comparison of the computed graphite AB bilayer interlayer distances (c), cohesive energies (E_{coh}) and binding energies (E_{bind}) per atom with existing DFT literature and experiment. The ZPE correction is estimated for the cohesive energy as in Table (3.1).

c (Å)	E_{coh} (eV/atom)	E_{bind} (eV/atom)	DFT method
3,32	8,93	0,026	PW-LDA (this work)
3,32	8,90	0,028	PW-LDA (PP)[64]
3,436	8,60	0,060	HL-LDA (LCGTO-FF)[186]
3,33	8,78	0,024	PZ-LDA (PP)[145]
4,27	7,87	$\sim 0,002$	GGA-PBE (this work)
$\sim$ 4,5	7,87	$\sim 0,002$	GGA-PBE (PP)[64]
$\sim$ 4,45	7,72	$\sim 0,002$	GGA-PBE (PP)[145]
3,35	6,88		Increments (SCF/MRCI)[149,177]
3,35	7,54-7,56	0,054	Exp. (303K)[186], ZPE from ref.[7]
3,35			Exp. (293 K)[40,187]

3.5.2 The PBEsol Functional

Using the optimized parameters (see Appendix A.4.2) we show in Fig. (3.13) the binding curve of two stacked graphene sheets for the PBEsol functional compared to PW-LDA and in Table (3.6) we report the results compared to literature and experimental values. Both curves have been interpolated with cubic splines. The PBEsol functional shows better agreement with experimental values regarding the equilibrium distances, but worse cohesive energies. The binding energy at equilibrium distance is still strongly underestimated compared to experiment.

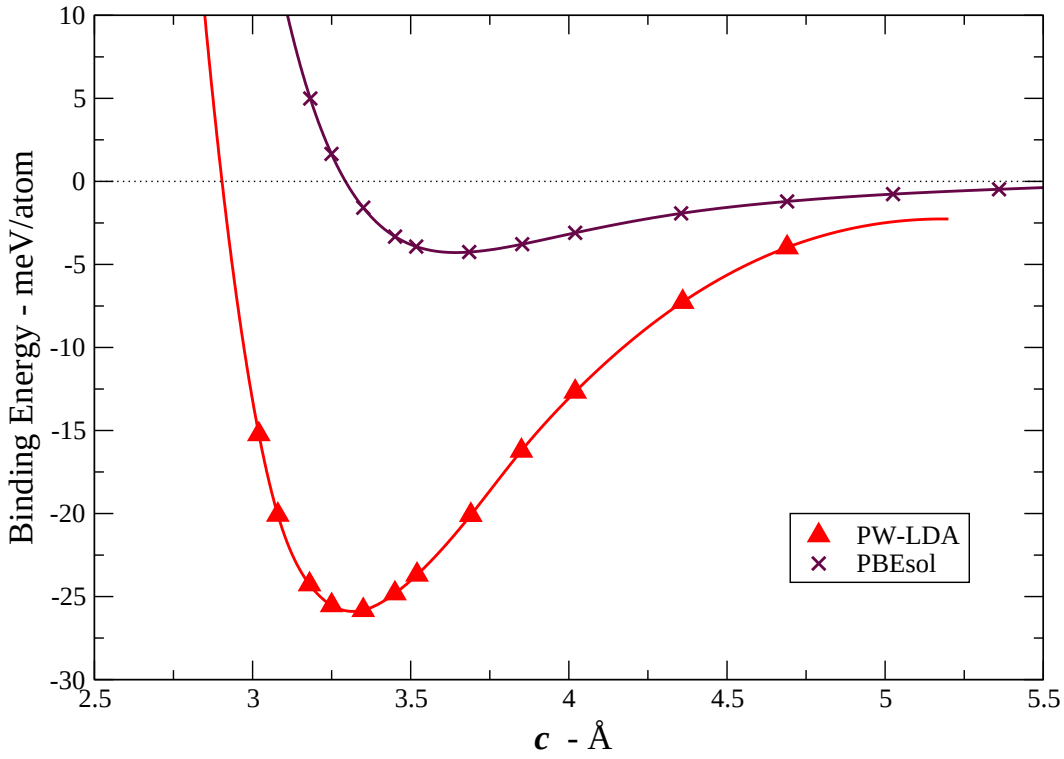

Figure 3.13: Binding energy between the stacked sheets as a function of the interlayer constant c. Shown are data for PW-LDA and PBEsol at optimized graphene in-plane equilibrium distances (see Table (3.1)) and using the "sb" basis set and (18x18x1) k-points.

Table 3.6: Comparison of the computed graphite AB-stacked graphene interlayer distances (c), cohesive energies (E_{coh}) and binding energies (E_{bind}) per atom with experimental values. The ZPE correction is estimated for the cohesive energy as in Table (3.1).

c (Å)	E_{coh} (eV/atom)	E_{bind} (eV/atom)	DFT method
3,32	8,93	0,026	PW-LDA (this work)
4,27	7,87	$\sim$ 0,002	GGA-PBE (this work)
3,65	8,30	$\sim 0,002$	PBEsol (this work)
3,35	6,88		Increments (SCF/MRCI)[149,177]
3,35	7,54-7,56	0,054	Exp. (303K)[186], ZPE from ref.[7]
3,35			Exp. (293 K)[40,187]

3.5.3 The PBE+vdW Functional

Fig. (3.14) shows the binding energy curves interpolated using cubic splines (see Appendix A.4.3 for convergence tests) between two AB-stacked graphene sheets for the PBE+vdW method compared to the underlying GGA-PBE functional. In Table (3.7) results are compared to other *ab-initio* calculations and experiment. Equilibrium geometries are in very good agreement with experiment and cohesive energies are slightly worse then the underlying GGA-PBE functional. On the other hand van der Waals forces are partly overestimated.

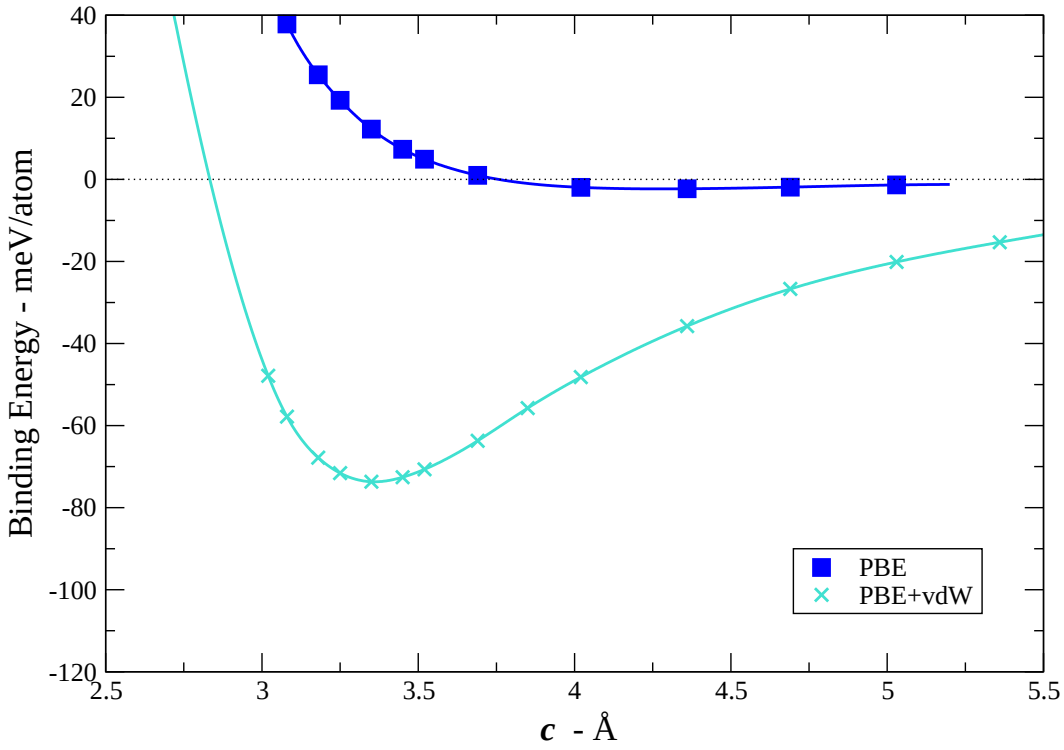

Figure 3.14: Binding energy between the stacked sheets as a function of the interlayer constant c. Shown are data for GGA-PBE and PBE+vdW at optimized graphene in-plane equilibrium distances (see Table (3.1)) and using the "sb" basis set and (18x18x1) k-points.

Table 3.7: Comparison of the computed graphite AB-stacked graphene interlayer distances (c), cohesive energies (E_{coh}) and binding energies (E_{bind}) per atom with experimental values. The ZPE correction is estimated for the cohesive energy as in Table (3.1).

c (Å)	E_{coh} (eV/atom)	E_{bind} (eV/atom)	DFT method
3,32	8,93	0,026	PW-LDA (this work)
4,27	7,87	$\sim$ 0,002	GGA-PBE (this work)
3,65	8,30	$\sim 0,002$	PBEsol (this work)
3,36	7,95	0,074	PBE+vdW (this work)
3,35	6,88		Increments (SCF/MRCI) [149,177]
3,35	7,54-7,56	0,054	Exp. (303K) [186], ZPE from ref. [7]
3,35			Exp. (293 K) [40,187]

3.6 Bilayer Graphene, Cluster Extrapolations

Two graphene sheets, and more in general non covalently stacked systems, interact weakly[84]. We can then make the hypothesis that at "stacking" distances close or larger than the equilibrium distance, border effects of finite flakes can be treated in the same way as for the monomers. This means that we consider border effects in the same way as for one graphene sheet, and apply the equation (3.3) to calculate the extrapolated cohesive energies per atom.
In Fig. (3.15) we show the clusters used to model the AB-stacking of hexagonal graphite at the equilibrium PW-LDA in-plane constant $a = 2,446$ Å and at the experimental interlayer distance of $c = 3,35$ Å. The flakes are chosen to avoid open shell -or unsaturated- systems, i.e. we have constructed the clusters' geometries such as to have an even number of carbon and hydrogen atoms in both monomers.

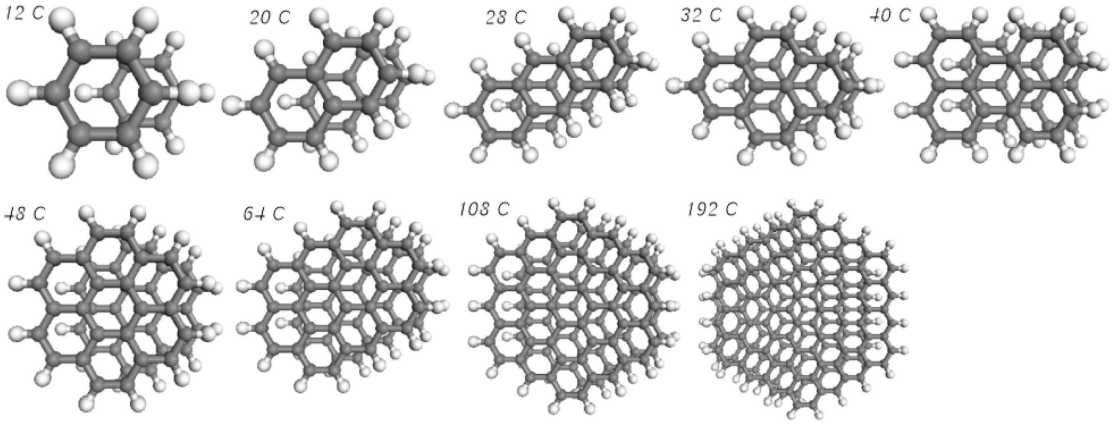

Figure 3.15: Clusters used in the present graphitic calculations.

3.6.1 The LDA and GGA-PBE Functionals

Fig. (3.16) shows the computed data as obtained from Eq. (3.3), and using a C[min+2s2p 3d4f] H[min+2s2p] basis set, called "t1+f". The values obtained for larger basis sets lie on parallel lines to the ones shown in Fig. (3.16) and on the scale of Fig. (3.16) they are superimposed on the lines shown. As in the graphene case the fact that calculated values lie on the fitted linear curve shows how rapidly the E_{CH} contribution per atom in Eq. (3.3) converges to a constant value for the chosen method.
In Table (A.7) in Appendix A.5.1 we compile the extrapolated cohesive energies using progressively growing basis sets and different linear regressions, i.e. we considered different sets of cluster sizes that are used in the least-square fit. As for the graphene case, we compare the difference between the cohesive energies computed with PW-LDA and GGA-PBE. If we neglect the results for the smallest clusters the accuracy of the bulk limit with respect to the known periodic case further improves for both PW-LDA and GGA,

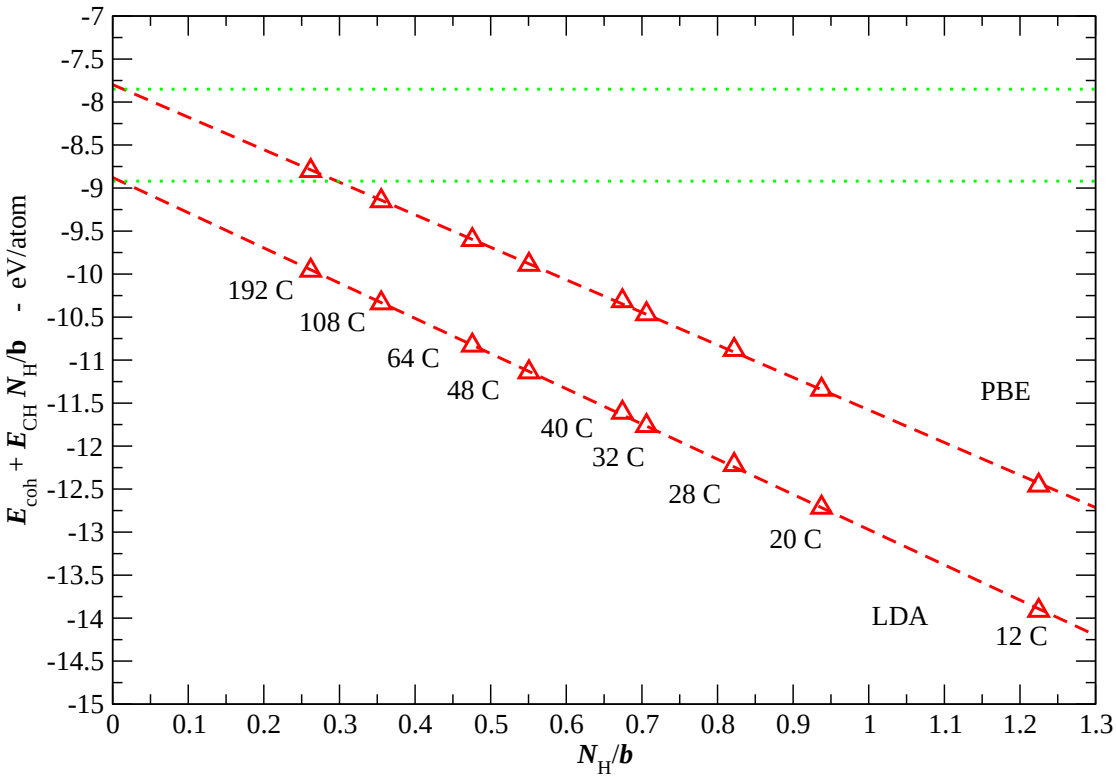

Figure 3.16: Convergence of PW-LDA and GGA-PBE extrapolated cohesive energies for two stacked graphene sheets taken at in-plane lattice constant $a = 2,446$ Å and interlayer constant $c = 3,35$ Å. The intercepts with the ordinates represent the bulk limit extrapolation. Dashed lines represent the linear regressions and dotted lines the periodic reference values described before. The labels at every point correspond to the number of carbon atoms in the corresponding cluster, starting at the benzene dimer (labelled "12 C", cf. Fig. (3.15)).

and particularly in the difference the extrapolated values are within ±10 meV/atom of the periodic reference when smallest clusters are excluded. We also observe a convergence behaviour with basis set size similar to the graphene case, and conclude that the "sb" values are essentially converged.

We now additionally apply the same extrapolation procedure to the binding energy. Figure (3.17) shows the corresponding data as obtained from Eq. (3.5), and using the "t1+f" basis set. The values obtained for larger basis sets are on this scale essentially superimposed on the curves shown.

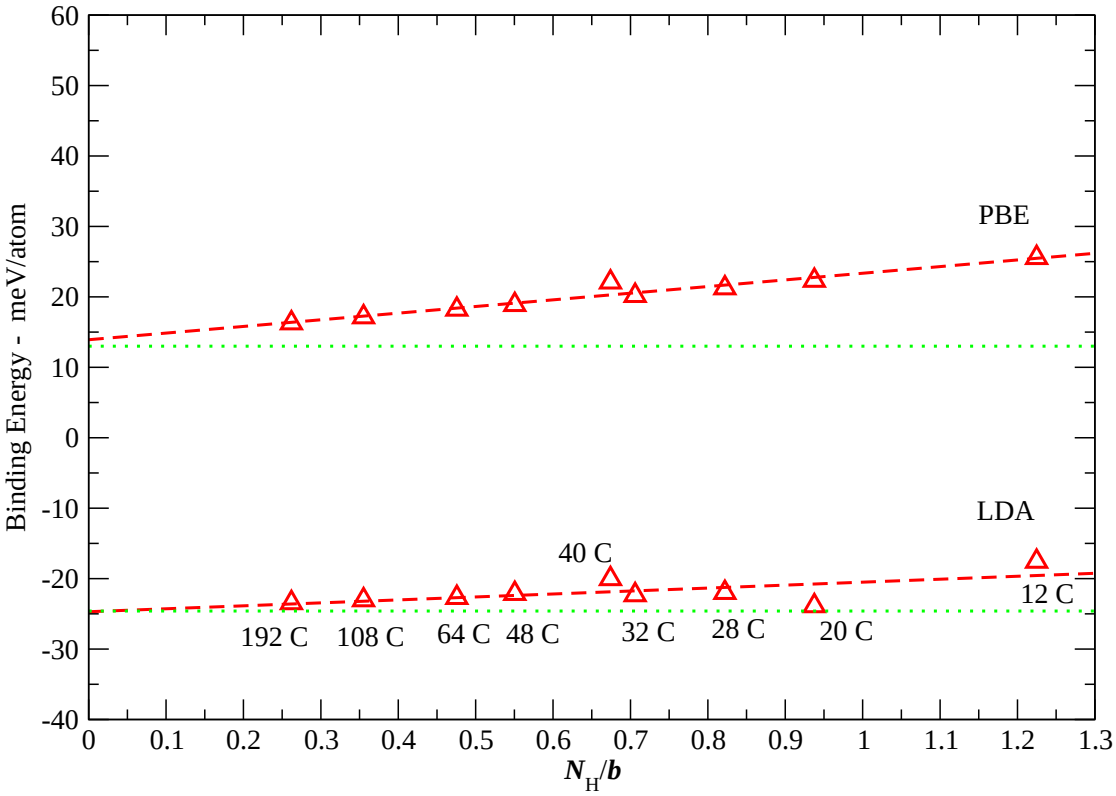

Figure 3.17: Convergence of PW-LDA and GGA-PBE extrapolated binding energies for two stacked graphene sheets taken at an in-plane lattice constant $a = 2,446$ Å and interlayer constant $c = 3,35$ Å. The intercepts with the ordinates represent the bulk limit extrapolation. Dashed lines represent the linear regressions and dotted lines the periodic reference values described before. The labels at every point correspond to the number of carbon atoms in the corresponding cluster, starting at the benzene dimer (labelled "12 C").

In Table (A.8) in Appendix A.5.1 we show the extrapolated binding energies using different basis sets and different linear regressions. We also compare the difference between the binding energies computed with PW-LDA and GGA-PBE functionals. Already for interpolations including only the smallest clusters the accuracy of the bulk limit with respect to the known periodic cases is about 2 meV for both PW-LDA and GGA, except for the smallest ranges of cluster sizes. Since the binding energy is very small, in the

comparisons shown in Table (A.8) we use very fine parameters, a (24x24x1) grid with 576 points in the full Brillouin zone and $l_{hartree} = 6$ and a large vacuum of 25 Å for the periodic reference values. Unlike in the cohesive energy case, the energy differences among the two DFT functionals applied in this study do not provide any further improvements. Intriguingly, the extrapolation procedure is applicable even for the GGA which does not bind at the considered intersheet distance.

3.6.2 The PBEsol Functional

Similarly to what we have done in the previous section, we employ now the PBEsol functional to determine the cluster extrapolations. Fig. (3.18) shows the cohesive energies computed using Eq. (3.3) for "t1+f" basis set. Since values for more precise basis sets provide superimposed parallel lines at such a scale, they have been omitted. Again values lie with a good approximation on the fitted linear curves. In Table (A.9) in Appendix A.5.2 we compile the different extrapolations using different ranges of clusters. Again the difference with respect to the periodic calculations of E_{CH} lie within ± 10 meV/atom when smallest clusters are excluded in extrapolations.

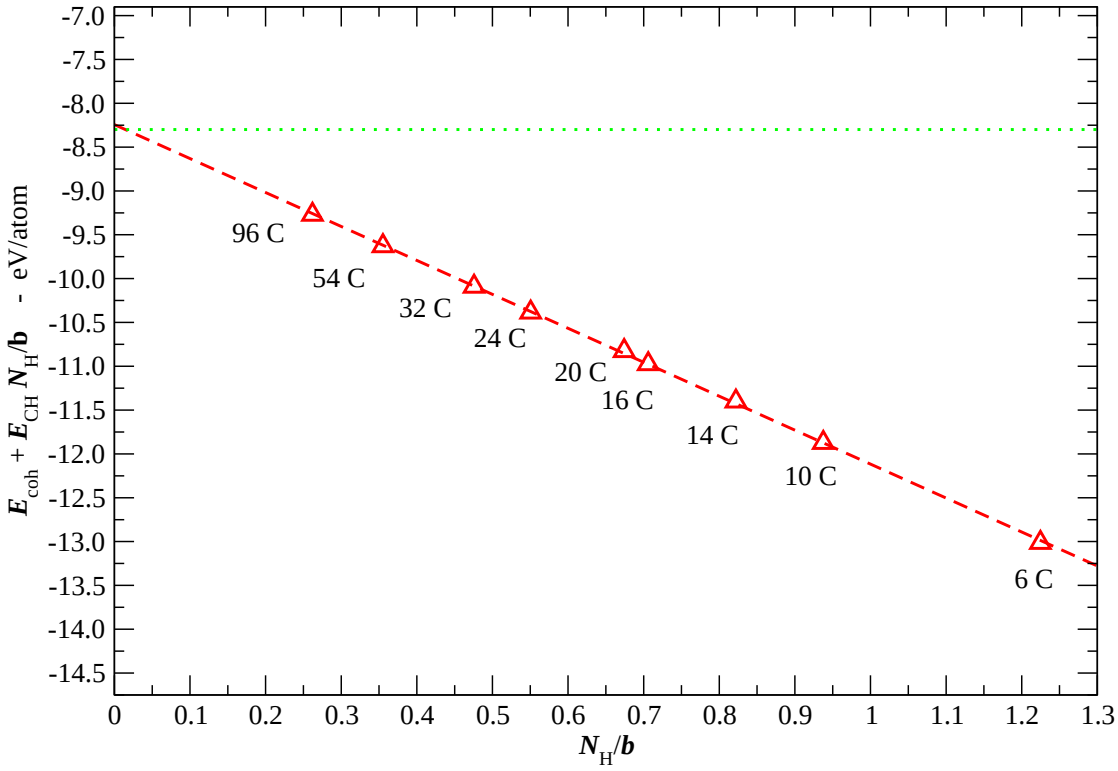

Figure 3.18: Convergence of PBEsol extrapolated cohesive energies for two stacked graphene sheets taken at in-plane lattice constant $a = 2,446$ Å and interlayer constant $c = 3,35$ Å. The intercepts with the ordinates represent the bulk limit extrapolation. Dashed lines represent the linear regressions and dotted lines the periodic reference values described before. The labels at every point correspond to the number of carbon atoms in the corresponding cluster, starting at the benzene dimer (labelled "12 C", cf. Fig. (3.15)).

Furthermore we compute the binding energy with Eq. (3.5) and results are shown in Fig. (3.19). In Table (A.10) in Appendix A.5.2 data are compiled with all extrapolations. Again values lie on linear curves as we can see from the figure and data scatter in the table.

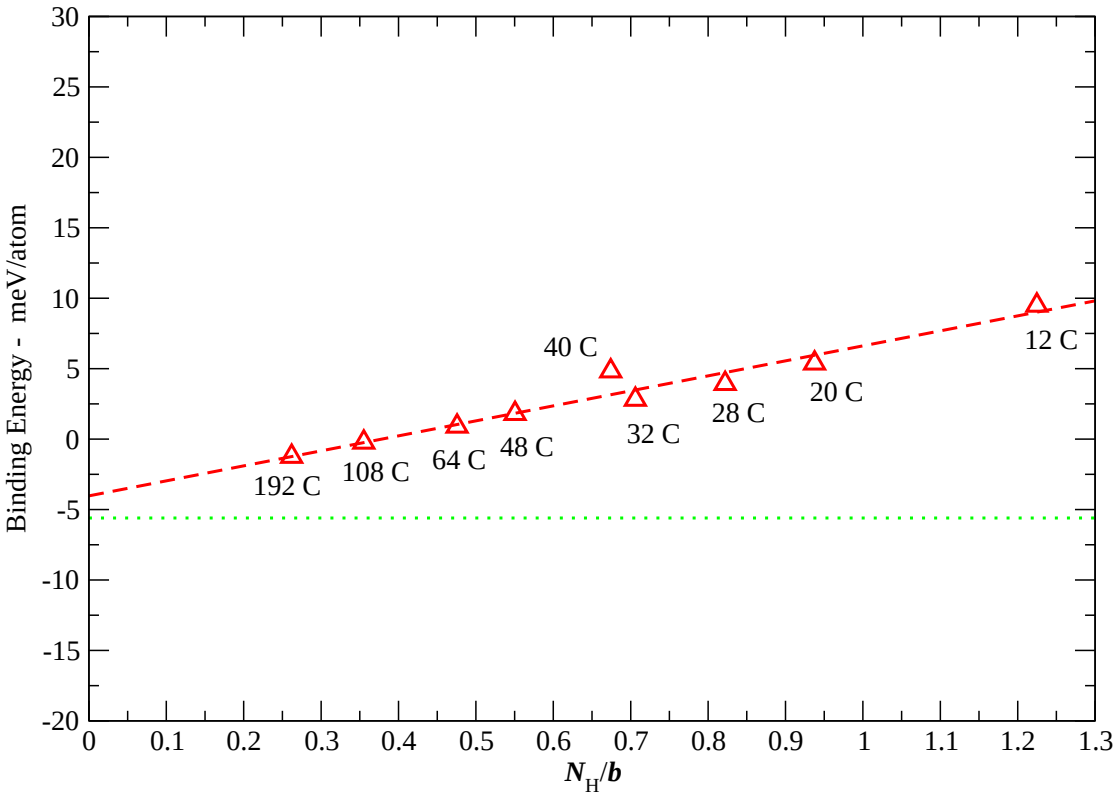

Figure 3.19: Convergence of PBEsol extrapolated binding energy for two stacked graphene sheets taken at an in-plane lattice constant $a = 2,446$ Å and interlayer constant $c = 3,35$ Å. The intercepts with the ordinates represent the bulk limit extrapolation. Dashed lines represent the linear regressions and dotted lines the periodic reference values described before. The labels at every point correspond to the number of carbon atoms in the corresponding cluster, starting at the benzene dimer (labelled ”12 C”).

3.6.3 The PBE+vdW Functional

So far we demonstrated our approach for graphene's cohesive energy using various *ab-initio* techniques, we then have evaluated graphite cohesive and binding energy for different DFT functionals. We proceed now to evaluate the dispersion forces contribution to the binding energy in bilayer graphene. Settings are alike to what was used in previous sections. In Fig. (3.20) are shown the extrapolation data and linear fitting for the cohesive energy using a "t1+f" basis set and the PBE+vdW functional. All basis sets are superimposed at this scale and for such a reason they are not shown in figure. In Table (A.11) in Appendix A.5.3 we report the extrapolations for different ranges of clusters, and the same conclusions are valid as for the other DFT functionals.

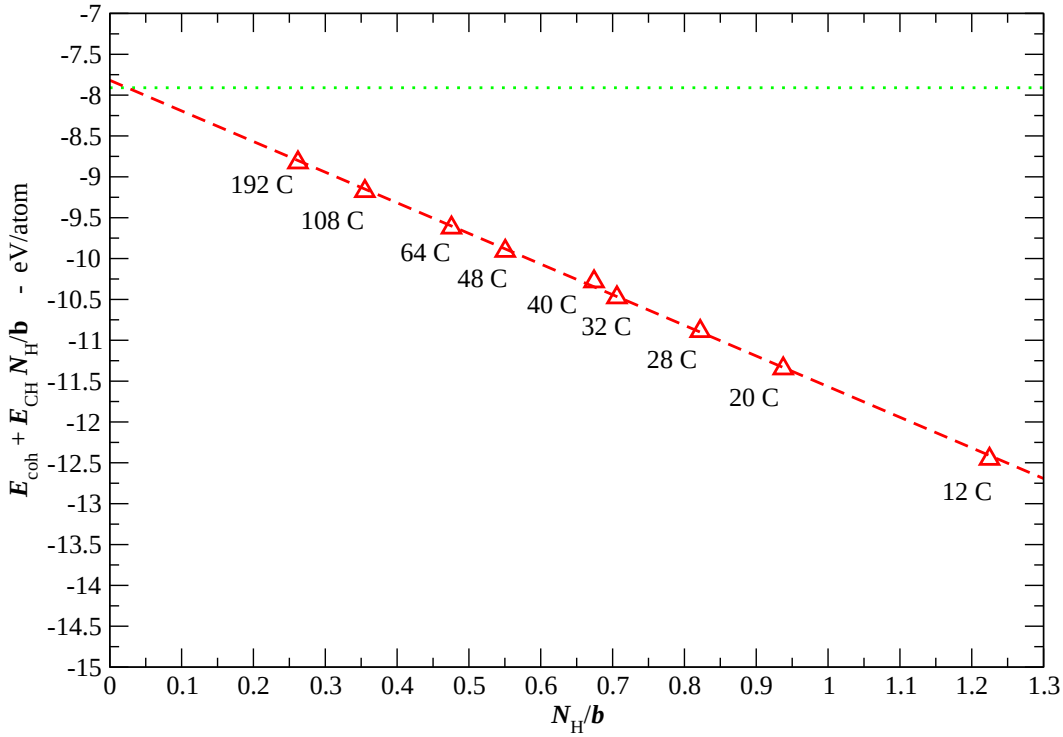

Figure 3.20: Convergence of PBE+vdW extrapolated cohesive energies for two stacked graphene sheets taken at in-plane lattice constant $a = 2,446$ Å and interlayer constant $c = 3,35$ Å. The intercepts with the ordinates represent the bulk limit extrapolation. Dashed lines represent the linear regressions and dotted lines the periodic reference values described before. The labels at every point correspond to the number of carbon atoms in the corresponding cluster, starting at the benzene dimer (labelled "12 C", cf. Fig. (3.15)).

Applying the same procedure to the binding energy we obtain values lying, with good approximation, on linear curves, as shown in Fig. (3.21). We notice that adding the dispersion correction to the PBE functional provides an increase of the slope of the linear regression in Fig. (3.21). This slope is small for local and semi-local DFT functionals because they do not have any long-range dispersion contribution except the contributions coming from exchange-correlation. In Table (A.12) in Appendix A.5.3 we report the extrapolations using different basis and clusters sets, confirming that the data scatter is relatively small.

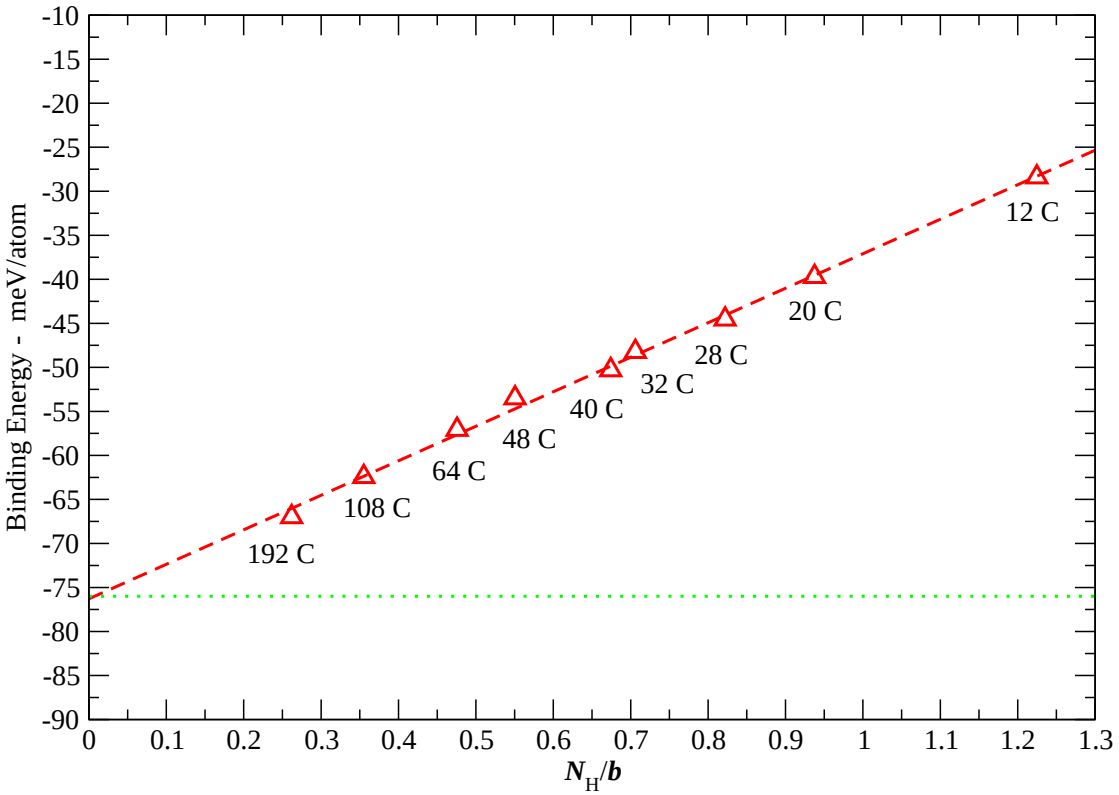

Figure 3.21: Convergence of PBE+vdW extrapolated binding energy for two stacked graphene sheets taken at an in-plane lattice constant $a = 2,446$ Å and interlayer constant $c = 3,35$ Å. The intercepts with the ordinates represent the bulk limit extrapolation. Dashed lines represent the linear regressions and dotted lines the periodic reference values described before. The labels at every point correspond to the number of carbon atoms in the corresponding cluster, starting at the benzene dimer (labelled ”12 C”).

3.6.4 The MP2 Method

Having demonstrated the feasibility of our approach for DFT functionals, we now consider the MP2 method. In Fig. (3.22) we plot the extrapolated cohesive energies using different basis sets. Since for MP2 the basis set superposition is relatively large, we have corrected the total energies of the flakes with the interlayer counterpoise BSSE[22], and we have then applied the same BSSE-corrected free atom references previously used for the graphene flakes. The cohesive energies lie again on fitted linear curves with good approximation. Moreover different basis sets provide parallel lines like in the DFT case. In Table (A.13) in Appendix A.5.4 we show the extrapolated cohesive energy as obtained with the "t1+f", "sb", "t2", "t3" and "t4C" basis sets, setting product basis threshold to 4 (3 for hydrogens) and basis set product cut-off threshold of 10^{-4} (10^{-3} for largest clusters and basis sets). For the largest basis sets available ("t3", "t4C" and "t4Cp") we have not been able to compute the largest clusters. Unfortunately, calculations at the "t4Cp" basis set level could also not be performed up to sufficiently large cluster sizes to dare make a safe extrapolation. However the behaviour of the cohesive energy as a function of the basis set is similar to the graphene case. At the smaller basis sets where larger clusters could be computed, we again obtain extrapolated values for the cohesive energy that depend little on the range of cluster sizes included in the fit. A reliable extrapolation is even obtained when using only the restricted cluster range up to "40 C", i.e. forty C atoms in the cluster, that is available at the "t4C" level, in particular in the difference to DFT functionals. From the extrapolations compiled in Table (A.13) in Appendix A.5.4 we therefore estimate that the extrapolated value at the "t4C" level still has an uncertainty of 0.06 eV/atom due to the extrapolation procedure. In Fig. (3.23) we summarise the comparison among DFT methods and MP2 (using "t4C" basis set). We can see how the curves are relatively parallel one to each other, showing that the short range physics is captured in the same way by all DFT functionals and the MP2 method.

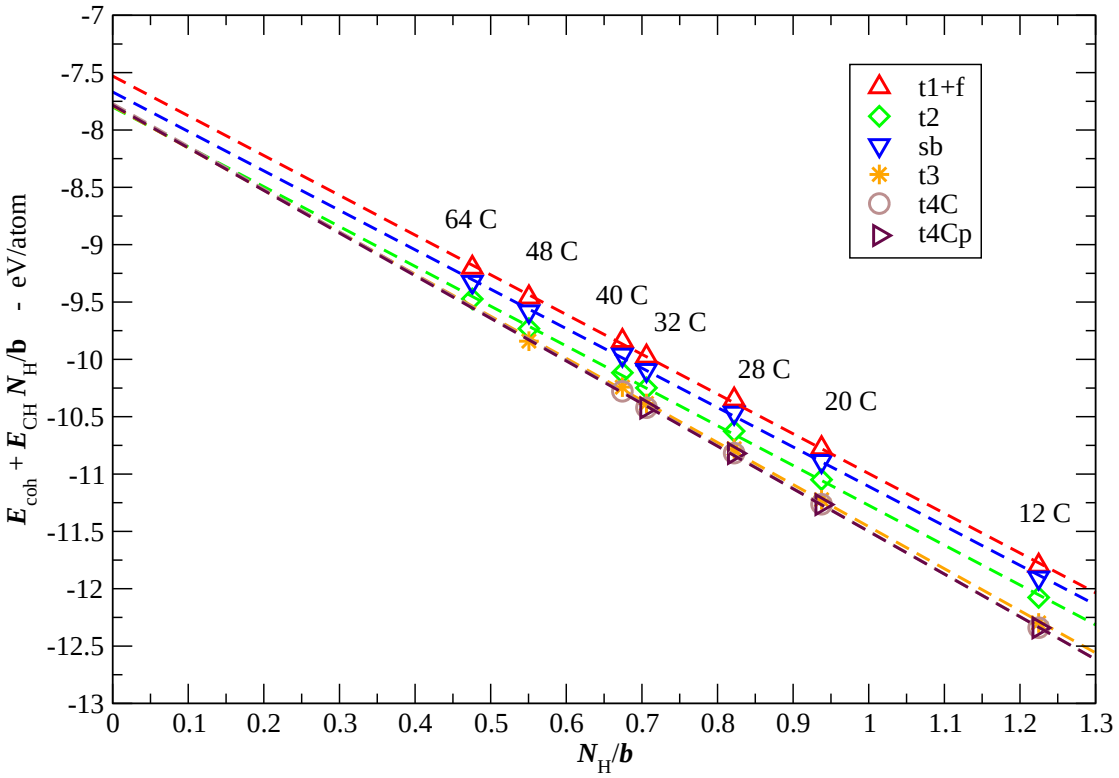

Figure 3.22: Convergence of MP2 extrapolated cohesive energy for two stacked graphene sheets taken at the in-plane constant $a = 2,446$ Å and interlayer constant $c = 3,35$ Å starting from benzene dimer (labelled "12 C"). The intercepts with the ordinates represent the bulk limit extrapolation. The dashed lines represent the linear regressions.

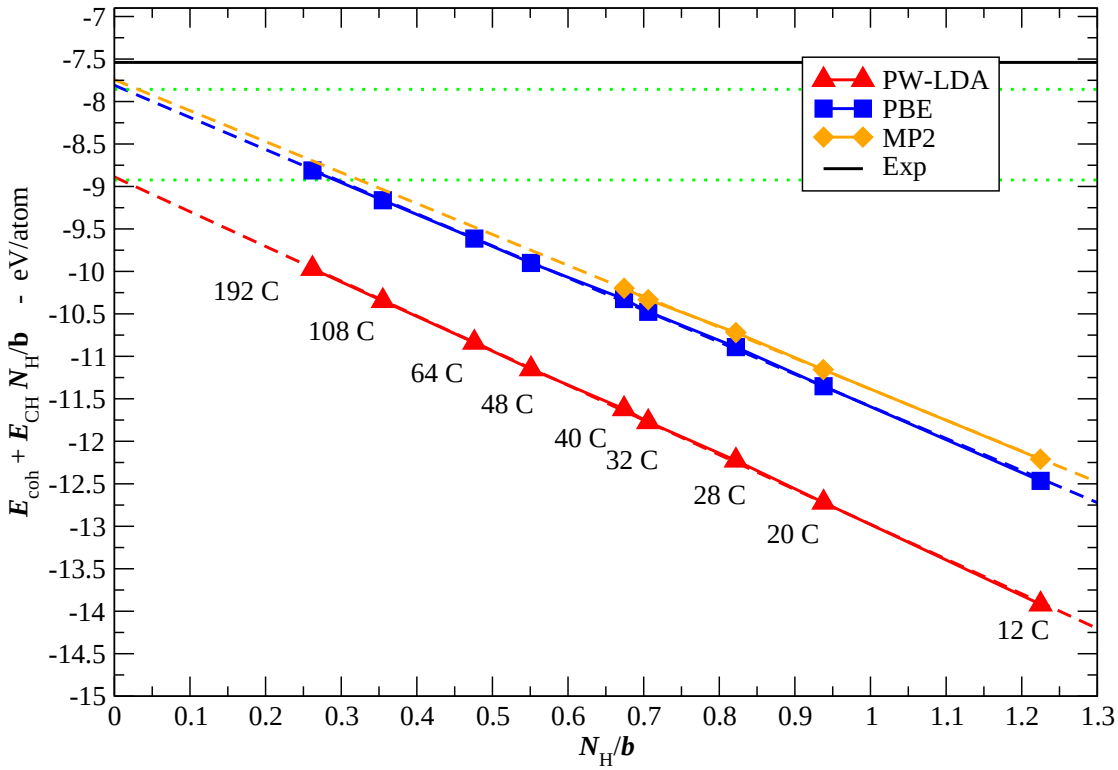

Figure 3.23: Summary of regression curves for the cohesive energy of two stacked graphene sheets at $a = 2,446$ Å, $c = 3,35$ Å, starting from the benzene dimer (bottom right points). Dotted line represents the periodic calculations, and dashed lines the linear regressions. The basis set considered are the converged "t2" for DFT functionals and "t4C" for the MP2 method. The ZPE corrected experimental value of about $-7,54$ eV/atom is shown for comparison. PBE+vdW method is not shown because the relative curve is superimposed on the GGA-PBE and MP2 curves at such a scale.

As the next step, we proceed to the extrapolation of the MP2 binding energy. All monomers have been corrected with the counterpoise correction method[22] as usual. In Table (A.14) in Appendix A.5.4 we show the results obtained using different basis sets, namely "t1+f", "sb", "t2", "t3" and "t4C". The scatter of the extrapolated binding energies when using different cluster size ranges is few meV/atom for both the MP2 method and its differences with respect to the DFT functionals. Considering the restricted size range available this is rather remarkable. In Fig. (3.24) we show the computed data as obtained from Eq. (3.5), and using different basis sets, namely "t1+f", "sb", "t2", "t3", "t4C" and "t4Cp". As expected, the convergence with basis set size is slower than for the DFT methods. For the "t3" basis set data for the smallest six clusters are available, which thus allows a safe extrapolation for the range of clusters up to "12 C - 48 C". For the "t4C" and "t4Cp" basis sets only the five and four smallest clusters, respectively, can be computed. However, for such clusters, the binding energy obtained for the "t3" basis set is converged at the sub-meV/atom level with respect to the "t4C" basis set and the largest basis set available "t4Cp". Nevertheless, taking this value and all the data in Table (A.14) we see that the largest limitation is the extrapolation. From the data scatter in the table we conclude on an estimated error of about 4 meV/atom. In Fig. (3.25), we summarise the comparison among the DFT methods and MP2 again, and conclude again that the extrapolation approach is well applicable.

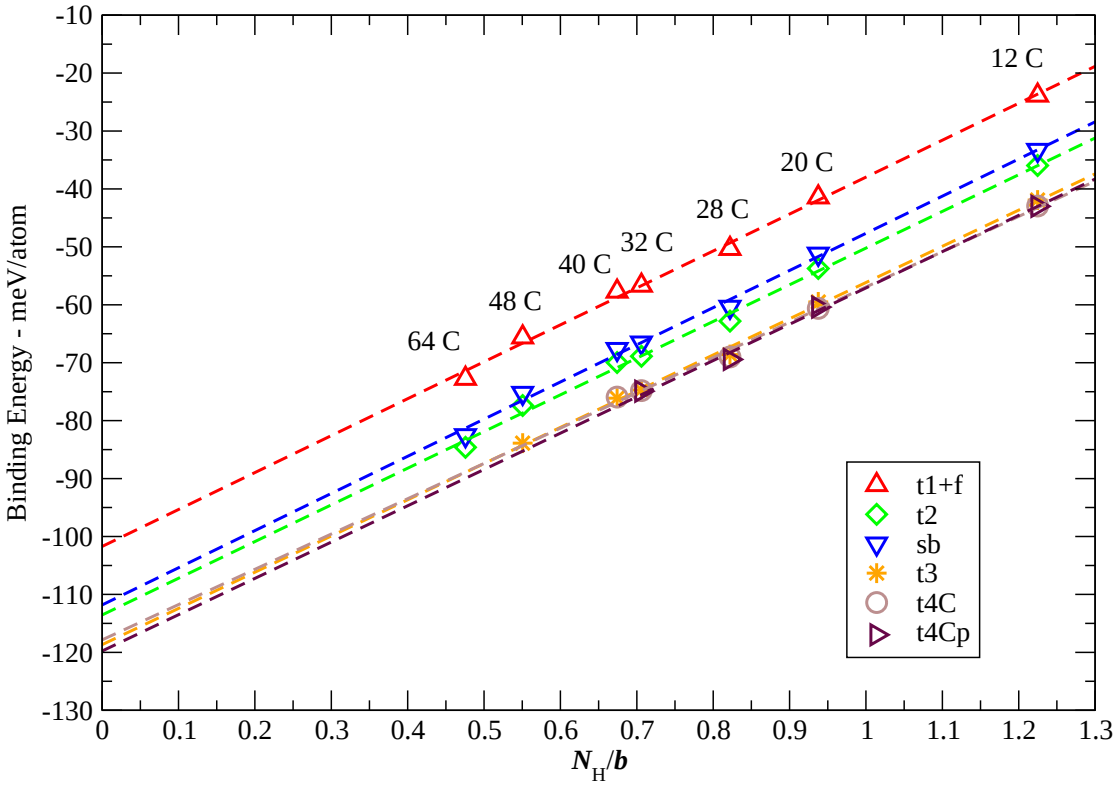

Figure 3.24: Convergence of MP2 extrapolated binding energy for two stacked graphene sheets taken at the in-plane constant $a = 2,446$ Å and interlayer constant $c = 3,35$ Å starting from the benzene dimer (labelled "12 C"). The intercepts with the ordinates represent the bulk limit extrapolation. The dashed lines represent the linear regression.

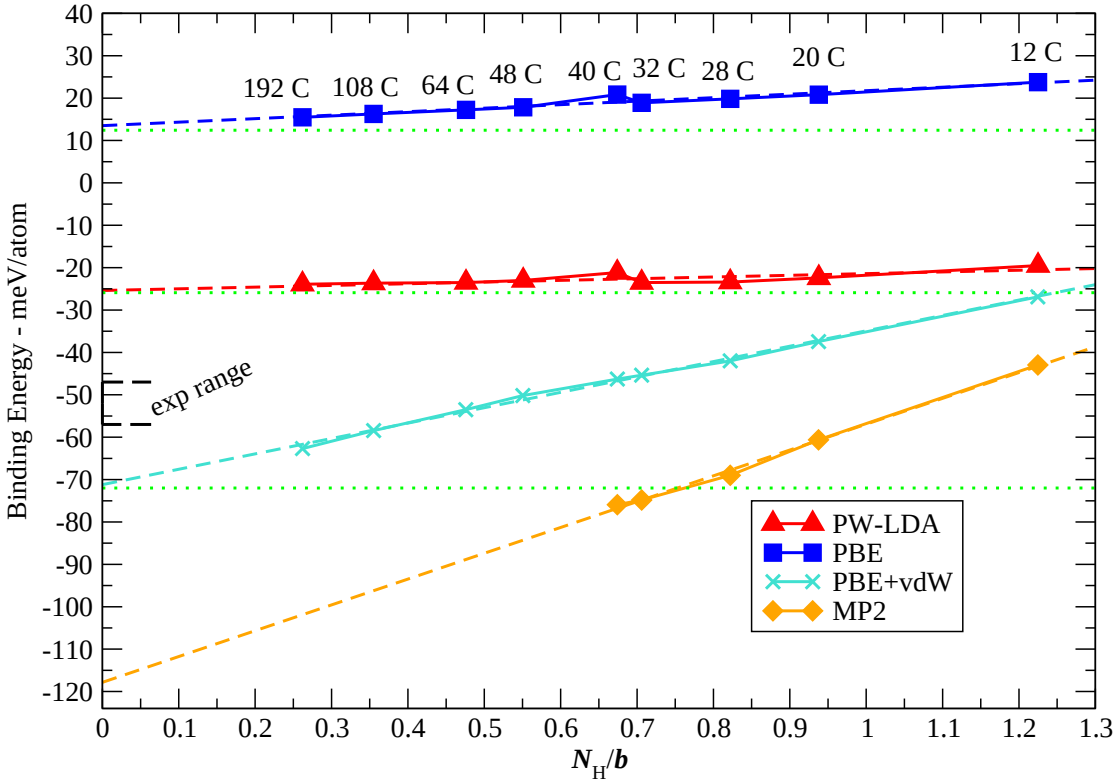

Figure 3.25: Summary of the regression curves for the binding energy between two stacked graphene sheets and for different methods, using the converged "t2" basis set for DFT functionals and the "t4C" basis set for wavefunction methods. Geometries are taken at in-plane constant $a = 2,446$ Å and interlayer constant $c = 3,35$ Å, starting from the benzene dimer (bottom right points). Dotted line represents the periodic calculations, and dashed lines the linear regressions. The experimental range taken from reference[197] is shown for comparison.

3.6.5 The RPA method

In addition we apply the RPA method. In Fig. (3.26) we show the extrapolated cohesive energy for different basis sets, i.e. "t1+f", "sb", "t2", "t3", "t4C" and "t4Cp", number of basis set products are set to 4 (3 for hydrogens), *frequency_points* are set to 80 and basis set product cut-off threshold is set to 10^{-4}. As in all previous cases the flakes interlayer total energies have been corrected with the counterpoise correction method (CP-BSSE)[22], and we have applied the same atomic reference as for the graphene flakes. For the RPA method all regression curves lie parallel to each other, and we notice how the computational requirements are rather similar to the MP2 method. Hence the sizes of the permissible clusters which can be computed are similar, even though, at the present level of implementation, MP2 and RPA methods scale like the fifth and fourth power with respect to the number of basis functions, respectively. However, the code is efficient and basis sets are still relatively small so that clusters are not large enough to clearly exploit such a behaviour. This is due to the memory requirements of the underlying calculations of the exact exchange, prior to MP2 and RPA calculations.
Table (A.15) in Appendix A.5.5 shows the extrapolated cohesive energy as obtained with the "t1+f", "sb", "t2", "t3" and "t4C" basis sets. For the largest basis sets available ("t3", "t4C" and "t4Cp") we have not been able to compute the largest clusters. Unfortunately, calculations at the "t4Cp" basis set level could also not be performed up to sufficiently large cluster sizes to dare make a safe extrapolation. However the behaviour of the cohesive energy as a function of the basis set size is similar to what was already observed in the graphene case.

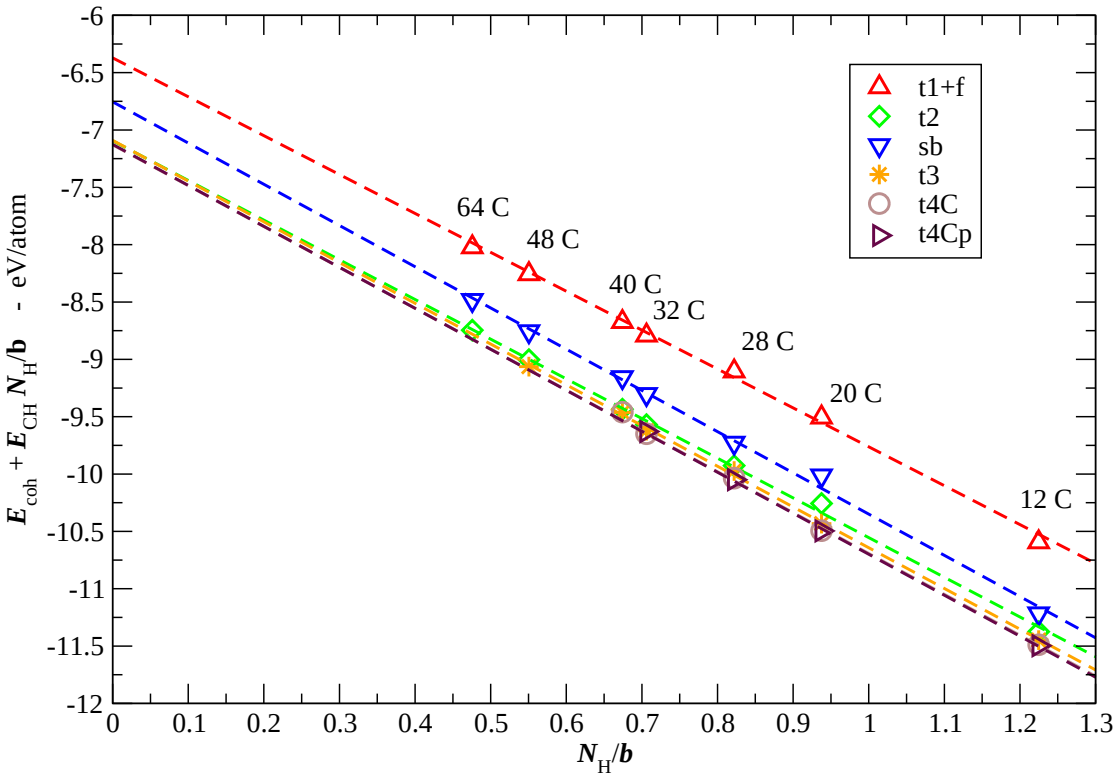

Figure 3.26: Convergence of RPA extrapolated cohesive energy for two stacked graphene sheets taken at the in-plane constant $a = 2,446$ Å and interlayer constant $c = 3,35$ Å starting from the benzene dimer (labelled "12 C"). The intercepts with the ordinates represent the bulk limit extrapolation. The dashed lines represent the linear regressions.

In Fig. (3.27) we summarise the results for the cohesive energies with the RPA method. Again the curves are relatively parallel one to each other, as in all previous cases, and this behaviour is due to the dominance of the short range interactions for what concerns the cohesive energy, as we can see in the figure. Moreover, while GGA-PBE and PBE+vdW functionals and the MP2 method tend to overestimate the cohesive energy, the RPA method is prone to underestimate it.

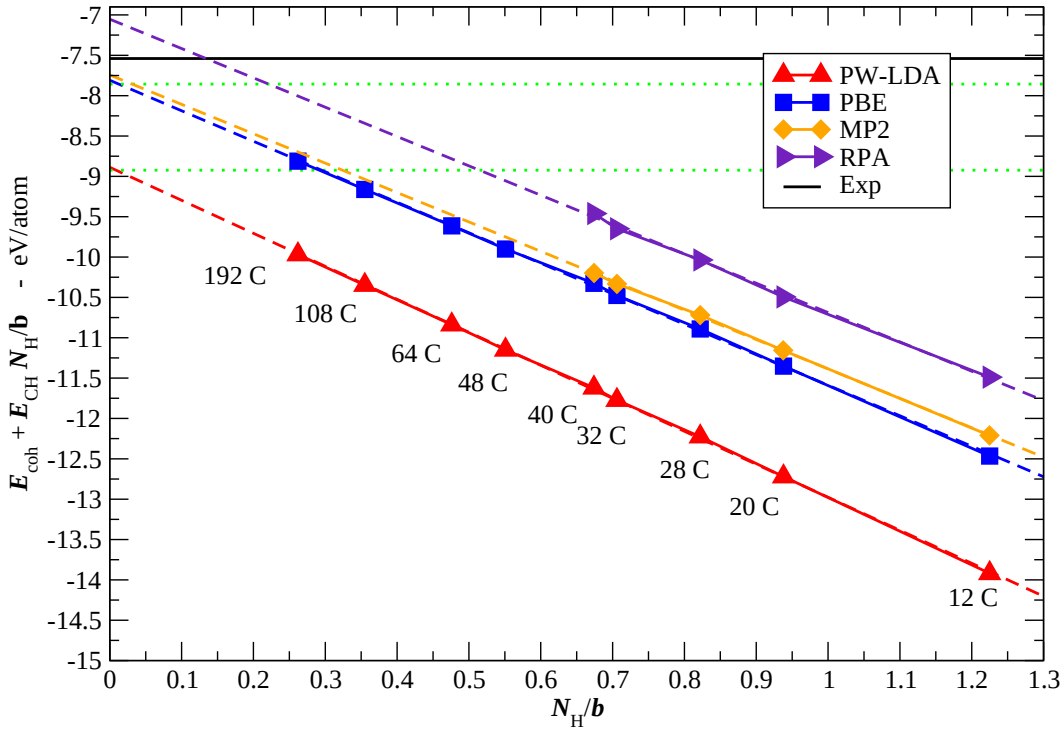

Figure 3.27: Summary of regression curves for the cohesive energy of two stacked graphene sheets at $a = 2,446$ Å, $c = 3,35$ Å, starting from the benzene dimer (bottom right points). Dotted line represents the periodic calculations, and dashed lines the linear regressions. The basis sets considered are the converged "t2" for DFT functionals and "t4C" for wavefunction methods. The ZPE corrected experimental value of about $-7,54$ eV/atom is shown for comparison. The PBE+vdW method is not shown because the curve is superimposed on the GGA-PBE and MP2 curves at this scale.

Once proven the reliability of our approach for RPA cohesive energies, we employ it additionally to evaluate the interlayer interaction. Fig. (3.28) shows the regression curves of the calculated binding energy for all basis sets. The calculations are performed using the interlayer CP-BSSE counterpoise correction [22]. As expected all curves lie parallel to each other also for the RPA method. Table (A.16) in Appendix A.5.5 shows the results for different regressions with respect to different basis sets, i.e. "t1+f", "sb", "t2", "t3", "t4C" and "t4Cp", where the number of basis set products are set to 4 (3 for hydrogens), *frequency_points* are set to 80 and basis set product cut-off threshold is set to 10^{-4}. The convergence of the binding energy with respect to the basis set in this case is slightly worse than for the MP2 method, and the "t3" basis set is converged at the meV/atom level. With the RPA method only few clusters can be calculated with the larger basis sets, i.e. "t4C" and "t4Cp". From the data scatter in Table (A.16), we conclude on an error of about 4 meV/atom.

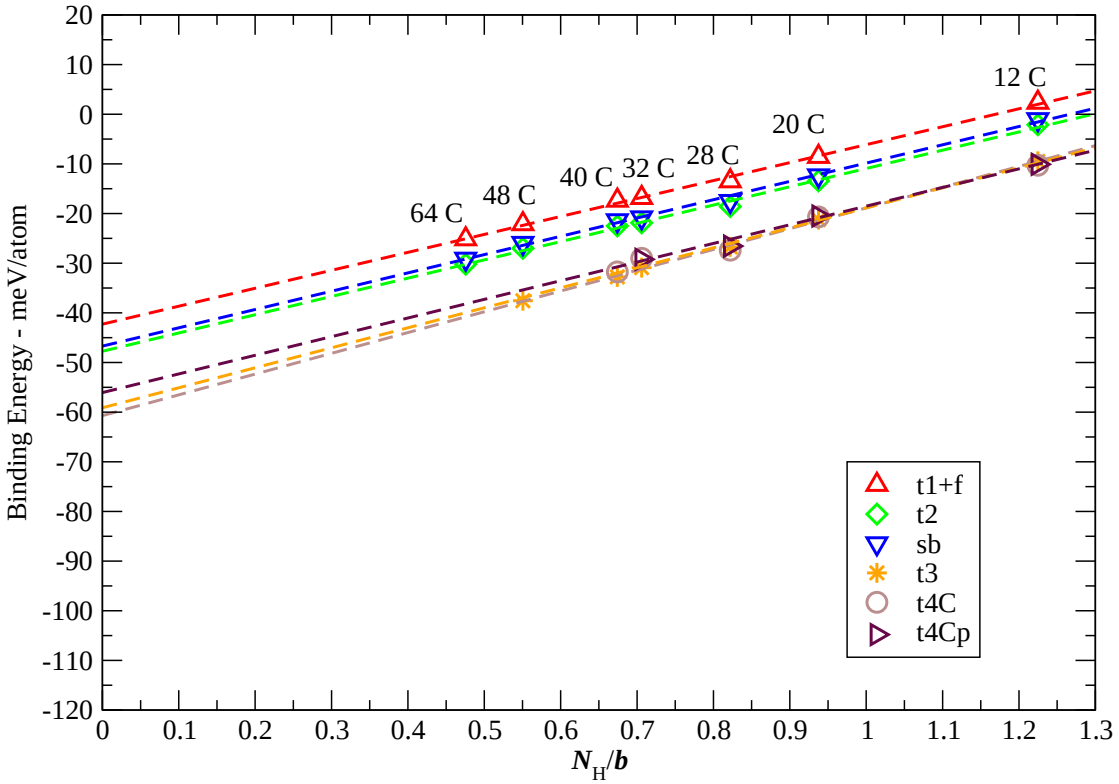

Figure 3.28: Convergence of RPA extrapolated binding energy for two stacked graphene sheets taken at the in-plane constant $a = 2,446$ Å and interlayer constant $c = 3,35$ Å starting from the benzene dimer (labelled "12 C"). The dashed lines represent the linear regression.

In Fig. (3.29) we summarise the results for the RPA binding energy compared to the other *ab-initio* methods. The slope of the RPA curve is relatively similar to the PBE+vdW method, indicating a similar dispersion interaction contribution. The RPA method recovers the correct correlation energy in the limit of infinite distances, hence it may be used as an additional proof of the reliability of the PBE+vdW method.

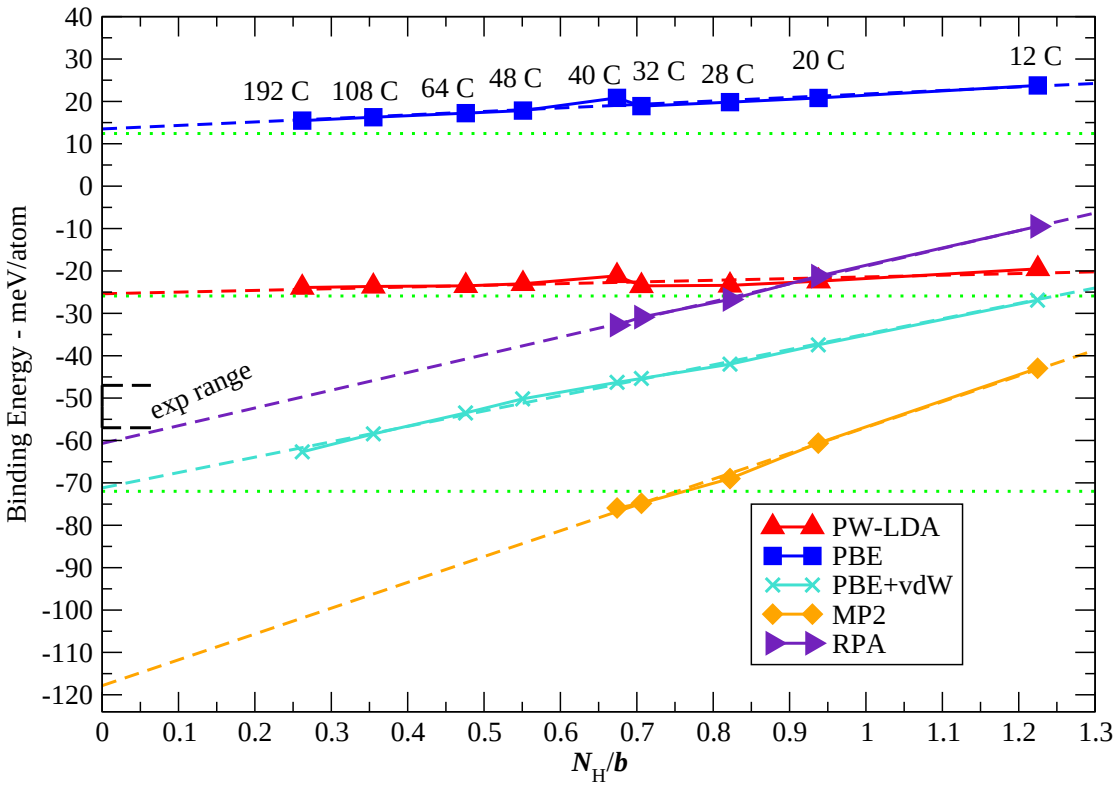

Figure 3.29: Summary of the regression curves for the binding energy between two stacked graphene sheets and for different methods, using the "t2" basis set for DFT functionals and the "t4C" basis set for wavefunction methods. Geometries are taken at in-plane constant $a = 2,446$ Å and interlayer constant $c = 3,35$ Å, starting from the benzene dimer (bottom right points). Dotted line represents the periodic calculations, and dashed lines the linear regressions. The experimental range taken from reference[197] is shown for comparison.

3.6.6 The RPA+ Method

Finally we calculate the RPA+ approximation to evaluate the effect on cohesive and binding energy of AB-stacked graphene with the introduction of PW-LDA DFT short range correlation.
The computational settings are exactly as for RPA method. Also the behaviour of the energies with respect to the cluster sizes and basis sets is absolutely comparable. We show in Fig. (3.30) the extrapolated cohesive energy and we compile the data in Table (A.17) in Appendix A.5.6.

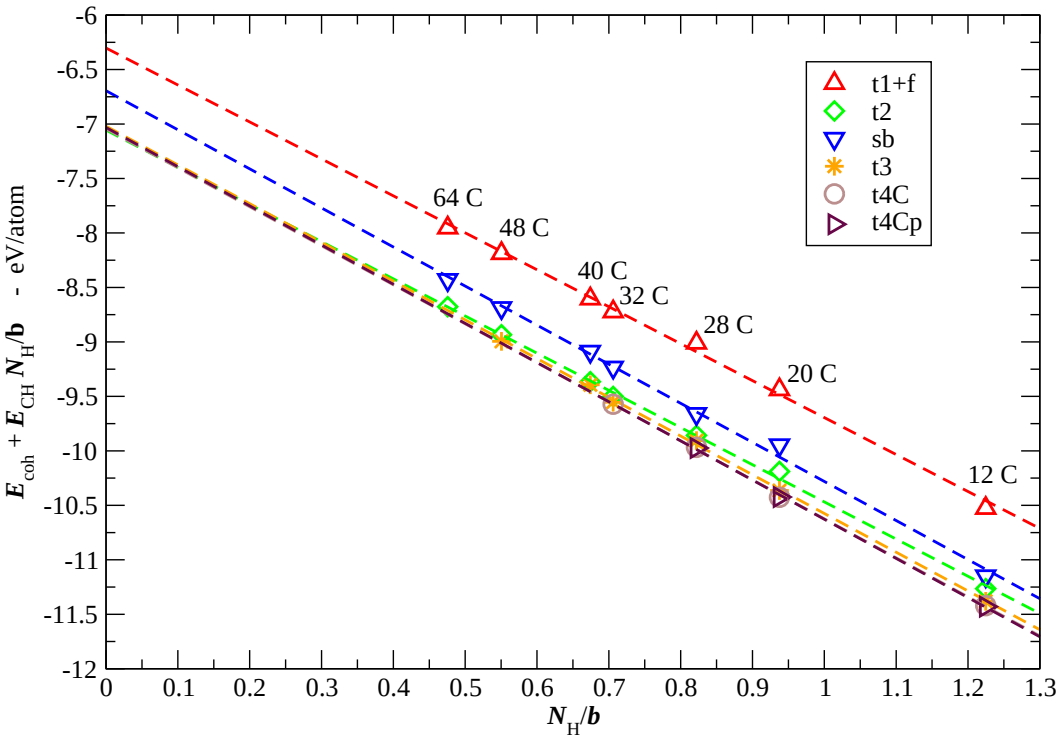

Figure 3.30: Convergence of RPA+ extrapolated cohesive energy for two stacked graphene sheets taken at the in-plane constant $a = 2,446$ Å and interlayer constant $c = 3,35$ Å starting from benzene dimer (labelled "12 C"). The intercepts with the ordinates represent the bulk limit extrapolation. The dashed lines represent the linear regressions.

In Fig. (3.31) we compare our new findings on the cohesive energy with the previous results using other *ab-initio* methods, such as DFT, MP2 and RPA. The RPA+ method shows a slighlty more repulsive behaviour with respect to the RPA method. Moreover it does not provide any substantial improvement with respect to the RPA method. The effect of the short range correlation coming from underlying DFT calculations is thus relatively small.

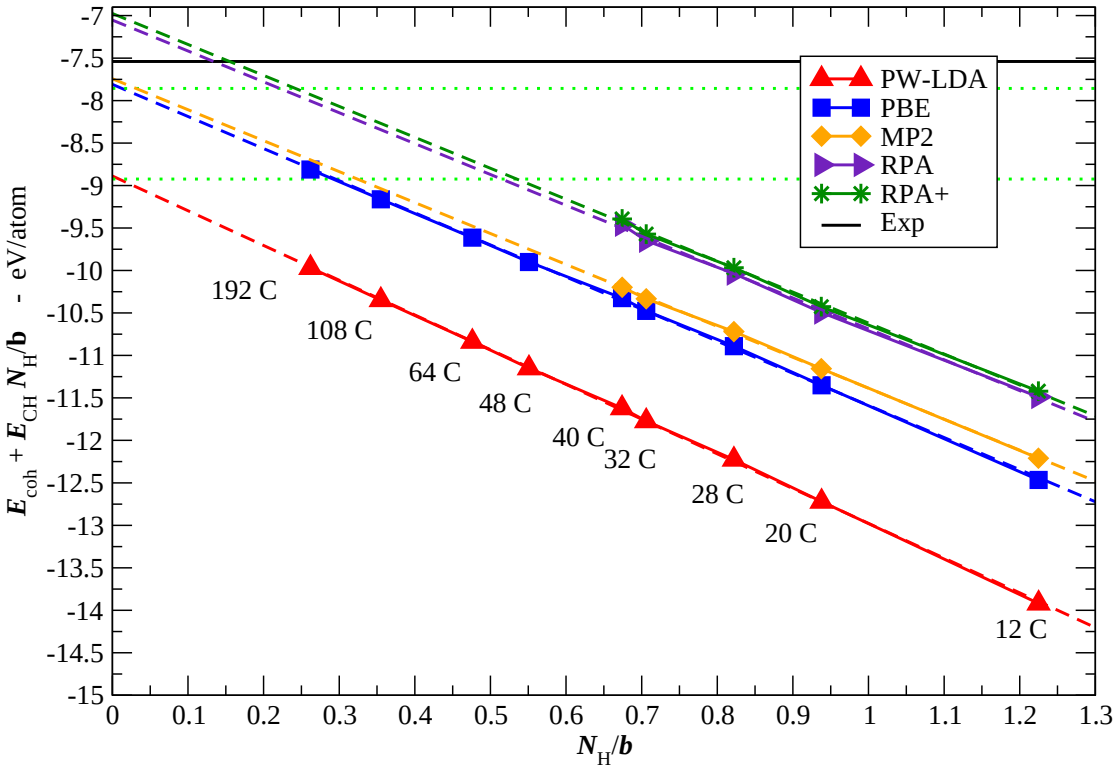

Figure 3.31: Summary of regression curves for the cohesive energy of two stacked graphene sheets at $a = 2,446$ Å, $c = 3,35$ Å, starting from the benzene dimer (bottom right points). Dotted line represents the periodic calculations, and dashed lines the linear regressions. The basis set considered are the converged "t2" for DFT functionals and "t4C" for wavefunction methods. The ZPE corrected experimental value of about $-7,54$ eV/atom is shown for comparison. The PBE+vdW method is not shown because the curve is superimposed on the GGA-PBE and MP2 curves at this scale.

Furthermore we calculate the binding energy using the RPA+ approximation. Extrapolations are shown in Fig. (3.32) and data are compiled in Table (A.18) in Appendix A.5.6. From Table (A.18) we again conclude on an error of about 4 meV/atom.

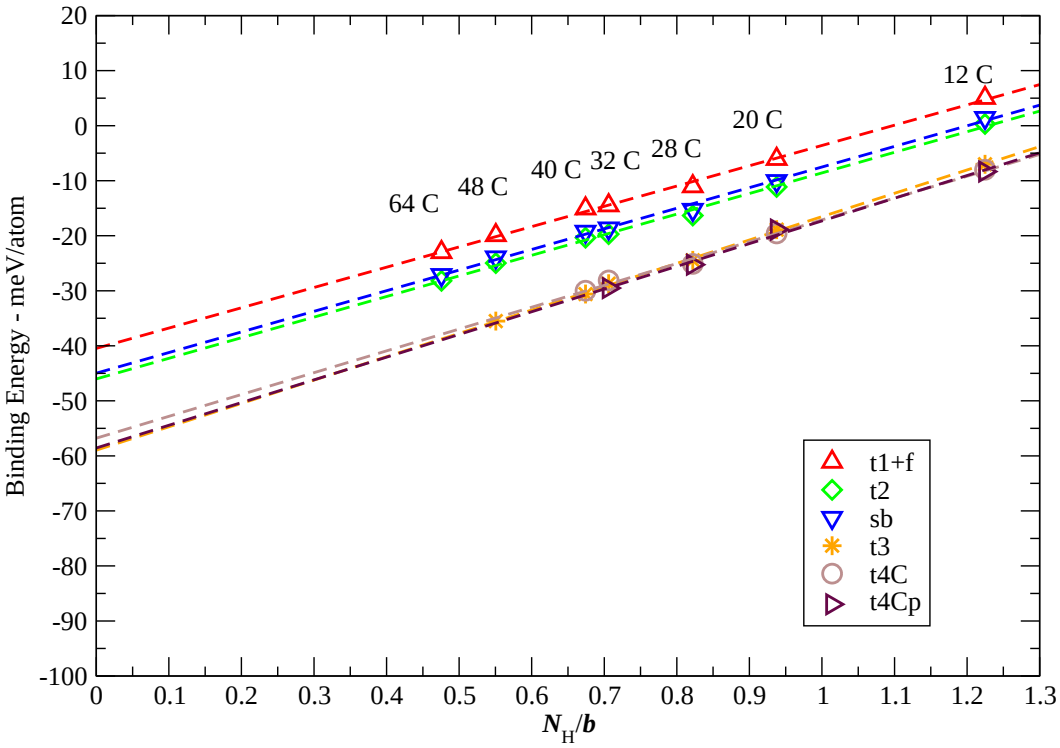

Figure 3.32: Convergence of RPA+ extrapolated binding energy for two stacked graphene sheets taken at the in-plane constant $a = 2,446$ Å and interlayer constant $c = 3,35$ Å starting from the benzene dimer (labelled "12 C"). The intercepts with the ordinates represent the bulk limit extrapolation. The dashed lines represent the linear regression.

In Fig. (3.33) we summarise the results for the RPA+ binding energy compared to the other methods. There are no major improvements to the RPA approximation, indicating that in AB-stacked graphene the short range correlation correction provided by the underlying calculation to the RPA+ method, has little influence on the binding energy.

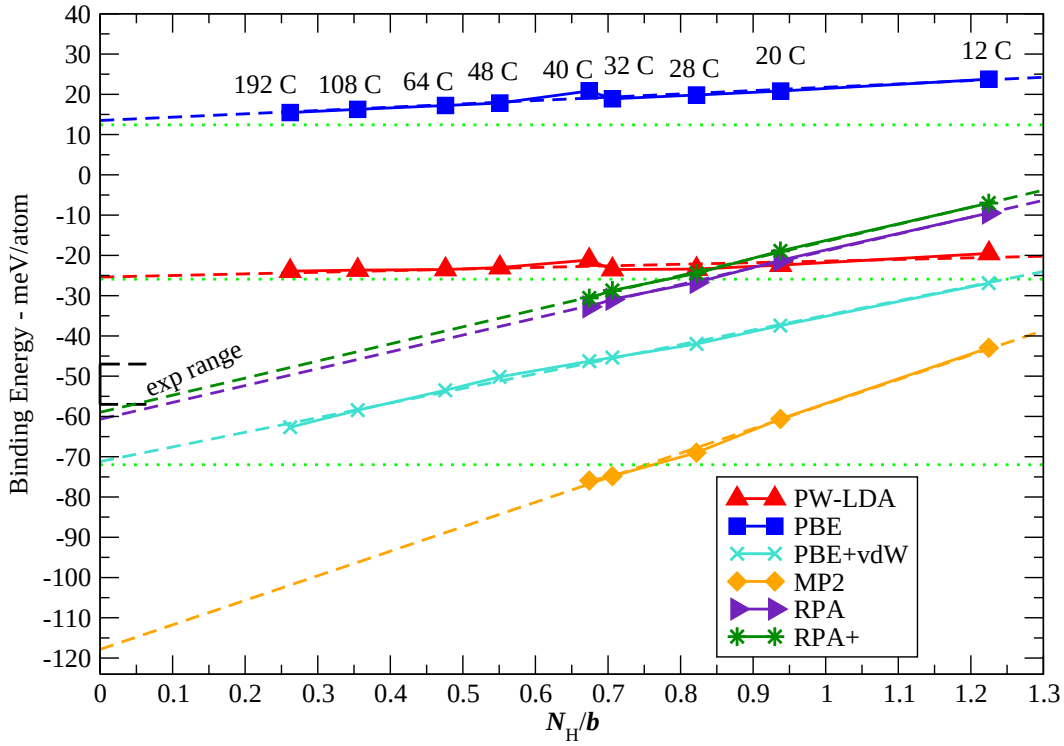

Figure 3.33: Summary of the regression curves for the binding energy between two stacked graphene sheets and for different methods, using the converged "t2" basis set for DFT functionals and the "t4C" basis set for wavefunction methods. Geometries are taken at in-plane constant $a = 2,446$ Å and interlayer constant $c = 3,35$ Å, starting from the benzene dimer (bottom right points). Dotted line represents the periodic calculations, and dashed lines the linear regressions. The experimental range taken from reference[197] is shown for comparison.

3.6.7 Summary of the Results on Interaction Energies

Having established and validated the extrapolation approach for one specific intersheet distance, we finally proceed to the calculation of the entire binding energy curve as a function of the intersheet distance for all wave functions methods, i.e. MP2, RPA and RPA+, keeping a fixed in-plane lattice constant of $a = 2,461$ Å in all cases (see discussion at the end of Section 3.4.7). For this we assume a similar validity of the extrapolation procedure at the other distances and use the computed energetics for the set of clusters "12 C - 40 C" at the "t3" basis set level (converged within 1 meV/atom for binding energies), to obtain the extrapolated values. Figure (3.34) summarises the obtained results, where we additionally include the binding energy curve as obtained from the computed Hartree-Fock data (we remember the reader MP2 calculations are based on HF) and using the same extrapolation approach.
Using cubic splines to interpolate, the minimum of the MP2 binding energy curve is at a distance of $3,02$ Å and the binding energy is about 135 meV/atom. In the same figure we include the results of the RPA, RPA+ calculations and the equilibrium distances are found to be at about $3,2$ and $3,3$ Å respectively, while the binding energies are found at about 61 and 58 meV/atom respectively.

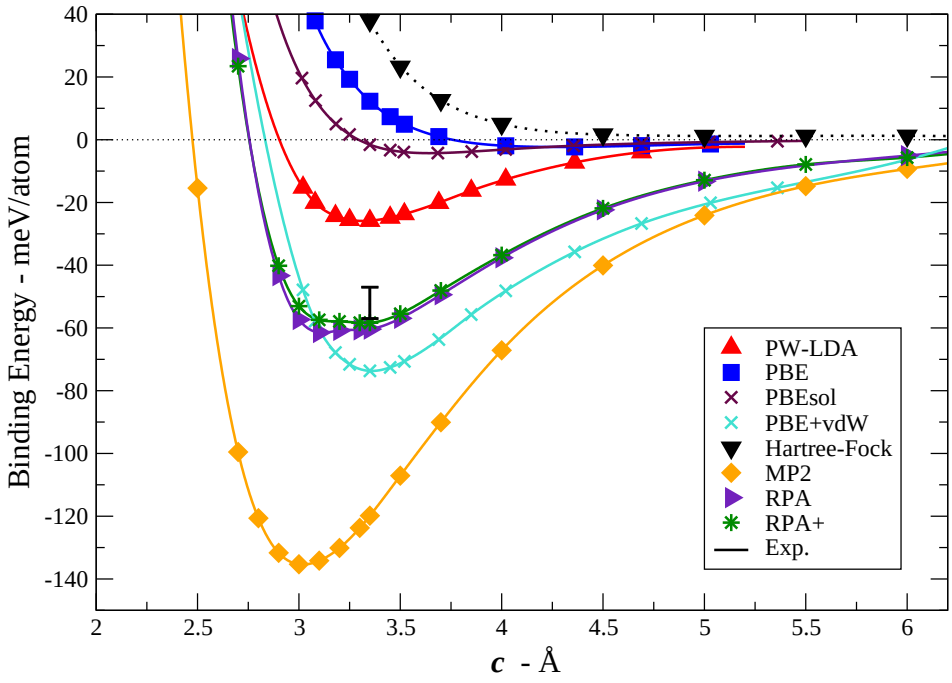

Figure 3.34: Binding energy curves for two stacked graphene sheets at the experimental in-plane lattice constant $a = 2,461$ Å for the wavefunction methods and the relative equilibrium in-plane lattice constants for the DFT functionals (see table 3.4 in Section 3.4.7). Experiment refers to data from ref. [186].

We summarise our results for MP2, RPA and RPA+ wavefunction methods compared to literature and our DFT calculations in Table (3.8). Here the binding energy has been corrected with the interlayer vibrational ZPE obtained using the "frozen phonon" method applied to each curve of Fig. (3.34), i.e. the fundamental frequency has been calculated using the harmonic approximation considering only the second derivative of the binding curves at their minimum interlayer distances. The obtained ZPE corrections are ~ 1, 4 and 6 meV/atom for GGA-PBE, PW-LDA/PBE+vdW/RPA/RPA+ and MP2, respectively. Using calculations based on the dispersion-corrected B97-D functional, ref.[57] showed that adding further layers to a graphite stack affects the binding energy by a small percentage. This suggests that it is permissible to compare our data for the two AB-stacked graphene sheets with the experimental binding energy of graphite.
In particular, from the results obtained with PBE+vdW, MP2 and RPA/RPA+ methods we conclude that dispersion plays a major role in determining the correct equilibrium distance and the binding energy itself. RPA/RPA+ and PBE+vdW share similar dispersion contributions, thus enabling us to say that such a dispersion allows us to recover the binding energy in the experimental range with a relatively good accuracy.
Worth of notice is the recent work of L. Spanu, S. Sorella and G. Galli[175] where they calculate the binding energy of graphite bulk, using the lattice regularized diffusion Monte Carlo (LRDMC) method. Quantum Monte Carlo methods are well known to eventually yield accurate *ab-initio* results. Even though the results of L. Spanu *et al.* are not fully converged, with an extrapolation procedure they estimate a binding energy close to the experiment of Zacharia *et al.* [197] (see Table (3.8)).
Moreover, we have undertaken a study of long range distances and asymptotics, where energies are of the order of -or below- 1 meV/atom. However, for large distances, e.g. over 10 Å, the linearity of the extrapolations is compromised for small clusters, so that large clusters are required to recover the correct periodic limit. Unfortunately this is not possible to-date for a computationally demanding methods as MP2 and RPA (RPA+ is only a short range correlation correction and it does not affect the long range of distances and the asymptotic properties as dispersion), and the asymptotes cannot yet be determined and compared with previous analytical studies[39].

Table 3.8: AB-stacked graphene extrapolation results for interlayer distances (c), cohesive energy (E_{coh}) and binding energy (E_{bind}) per atom compared with periodic calculations when available. The experimental cohesive energies are ZPE-corrected using the value from ref.[7]. As the ZPE contribution to the experimental binding energy is unknown, such a correction is not possible there. Instead, the theoretical values have been corrected by adding the ZPE as estimated from Fig. (3.34) (see text). The error is estimated from the basis set convergence behaviour and extrapolation scatter observable from the corresponding tables in the Appendix.

c (Å)	E_{coh} (eV/atom)	E_{bind}(eV/atom)	method
3,32	8,93	0,020	PW-LDA periodic (this work)
4,27	7,87	0,002	GGA-PBE periodic (this work)
3,36	7,95	0,073 ± 0,004	PBE+vdW periodic (this work)
3,02	7,91 ± 0,06	0,128 ± 0,004	MP2 (this work)
3,2	7,13 ± 0,06	0,061 ± 0,004	RPA (this work)
3,3	7,06 ± 0,06	0,058 ± 0,004	RPA+ (this work)
3,35		0,062	B97-D[57]
3,35		0,066	rev-PBE + vdW[171]
3,337		0,062	GS + vdW3+4 [55]
3,426		0,060 $\pm 0,005$	LRDMC (300K) [175]
3,35	7,54-7,56		Exp. (303K)[115], see also ref. [186], ZPE from ref.[7]
	7,54		Exp (300K)[133], ZPE from ref.[7]
		0,052 ± 0,005	Exp.[197]
		$0,035^{+0,015}_{-0,010}$	Exp.[17]

As an additional proof of the reliability of the extrapolated van der Waals interaction calculated at a fixed carbon-hydrogen distance, we have briefly analysed the role of the border effects on van der Waals radii and C_6 coefficients calculated using the PBE+vdW method. We evince from such an analysis that:

i) the convergence of the binding energy with respect to the cluster size is essentially not affected by small variations of the C-H distance.

ii) the effect of the borders with respect to the dispersion contribution is rather localized.

4 Conclusions

In many quantum chemical methods, the study of periodic systems is not straightforward and at the present time in some cases they are restricted to non-conducting systems[157]. Among these methods are the Møller-Plesset perturbation theory, the Random Phase Approximation (RPA) and its variant RPA+. We have implemented Møller-Plesset perturbation theory at the second order (MP2) into our in-house code (FHI-AIMS) along with the BSSE-CP correction method[161]. With the thus available computational tools we have undertaken a study of graphene and bilayer graphene.
In order to compute bulk properties of interest, like the cohesive and binding energy and the equilibrium geometry, as an alternative to periodic calculations we have investigated the use of cluster extrapolations to the bulk limit. We have shown how an equation of the type of Eq. (3.3) can be applied with good approximation to sp^2-systems like graphene and stacked graphene, thereby reducing significantly the overall computational cost compared to studies aiming at a brute-force convergence[57]. For what concerns cohesive energies, they are computed at a similar level of accuracy for MP2, RPA/RPA+ and PBE/PBE+vdW methods.
Moreover we note that already a benzene molecule and benzene dimer, i.e. the smallest representative clusters, lie, with a good approximation, on the fitted linear curves regarding graphene and bilayer graphene respectively. Calculations made for $\pi - \pi$ stacked non-covalent weak bonds in molecules[79,84] show that Møller-Plesset theory at the second order is not sufficient to properly account for dispersion forces. On the other side RPA and RPA+ methods tend to underestimate such a contribution in small systems[161]. However, for large and infinite systems the dispersion contributions are larger, and eventually the binding energy is correctly evaluated for RPA/RPA+ or it is even more overestimated in the MP2 case. Additional analyses on the computed atomic C_6 coefficients, show that border effects are rather localized on the evaluation of the atomic contribution to the dispersion in bilayer graphene, and the carbon-hydrogen distance is not essentially relevant, while PBE+vdW and RPA tackle the dispersion at a similar level. The dispersion is thus fundamental to recover the correct binding energy in bilayer graphene.
Of all the methodologies we applied, PBE+vdW, is the computationally cheapest methodology and it provides dispersion corrections to functionals lacking by construction of such a contribution, e.g. GGA-PBE. Besides it provides results relatively close to experiments on one side and the random phase approximation, on the other.
Tables (4.1) and (4.2) summarise the present findings for the cohesive energy of graphene and AB-stacked graphene and the interaction energy between two layers. Since our approach can be applied in principle to more accurate and predictive quantum chemical methods (for which the computational cost of direct calculations would be prohibitive),

this study paves the way to safe reference values also for extended systems.

Table 4.1: Cohesive energy extrapolations for a graphene layer compared with periodic calculations when available. For GGA-PBE, PBEsol, PBE+vdW and wavefunction methods also the difference of the extrapolations with respect to the other methods are considered. The error is estimated from the basis set convergence behaviour and extrapolation scatter observable from the corresponding tables in the Appendix.

E_{coh} (eV/atom)	method
8,90 $\pm 0,03$	PW-LDA extrapolated
8,92	PW-LDA periodic
7,84 $\pm 0,03$	GGA-PBE extrapolated
7,86 $\pm 0,01$	GGA-PBE periodic + $\delta_{\text{PW-LDA}}$ extrapolated
7,86	GGA-PBE periodic
8,28 $\pm 0,03$	PBEsol extrapolated
8,29 $\pm 0,01$	PBEsol periodic + $\delta_{\text{PW-LDA}}$ extrapolated
8,28 $\pm 0,01$	PBEsol periodic + $\delta_{\text{GGA-PBE}}$ extrapolated
7,88 $\pm 0,03$	PBE+vdW extrapolated
7,89 $\pm 0,01$	PBE+vdW periodic + $\delta_{\text{PW-LDA}}$ extrapolated
7,89 $\pm 0,01$	PBE+vdW periodic + $\delta_{\text{GGA-PBE}}$ extrapolated
7,84 $\pm 0,06$	MP2 extrapolated
7,85 $\pm 0,02$	PW-LDA periodic + δ_{MP2} extrapolated
7,85 $\pm 0,02$	GGA-PBE periodic + δ_{MP2} extrapolated
7,84 $\pm 0,02$	PBE+vdW periodic + δ_{MP2} extrapolated
7,11 $\pm 0,06$	RPA extrapolated
7,12 $\pm 0,02$	PW-LDA periodic + δ_{RPA} extrapolated
7,12 $\pm 0,02$	GGA-PBE periodic + δ_{RPA} extrapolated
7,11 $\pm 0,02$	PBE+vdW periodic + δ_{RPA} extrapolated
7.04 $\pm 0,06$	RPA+ extrapolated
7.05 $\pm 0,02$	PW-LDA periodic + $\delta_{\text{RPA+}}$ extrapolated
7.05 $\pm 0,02$	GGA-PBE periodic + $\delta_{\text{RPA+}}$ extrapolated
7.04 $\pm 0,02$	PBE+vdW periodic + $\delta_{\text{RPA+}}$ extrapolated
$\sim$ 7,5	Exp. (303K)[62], ZPE from ref.[7]

Table 4.2: AB-stacked graphene extrapolation results for interlayer distances (c), cohesive energy (E_{coh}) and binding energy (E_{bind}) per atom compared with periodic calculations when available. The experimental cohesive energies are zero point energy (ZPE) corrected using the value from ref.[7]. As the ZPE contribution to the experimental binding energy is unknown, such a correction is not possible there. Instead, the theoretical values have been corrected by adding the ZPE as estimated from Fig. (3.34) (see text). The error is estimated from the basis set convergence behaviour and extrapolation scatter observable from the corresponding tables in the Appendix.

c (Å)	E_{coh} (eV/atom)	E_{bind}(eV/atom)	method
3,32	8,93	0,020	PW-LDA periodic (this work)
4,27	7,87	0,002	GGA-PBE periodic (this work)
3,36	7,95	0,073 ± 0,004	PBE+vdW periodic (this work)
3,02	7,91 ± 0,06	0,128 ± 0,004	MP2 (this work)
3,2	7,13 ± 0,06	0,061 ± 0,004	RPA (this work)
3,3	7,06 ± 0,06	0,058 ± 0,004	RPA+ (this work)
3,35		0,062	B97-D[57]
3,35		0,066	rev-PBE + vdW[171]
3,337		0,062	GS + vdW3+4 [55]
3,426		0,060 $\pm 0,005$	LRDMC (300K)[175]
3,35	7,54-7,56		Exp. (303K)[115], see also ref. [186], ZPE from ref.[7]
	7,54		Exp (300K)[133], ZPE from ref.[7]
		0,052 ± 0,005	Exp.[197]
		$0,035^{+0,015}_{-0,010}$	Exp.[17]

4.1 Physical Effects Beyond Current Assumptions

When dealing with aromatic systems, it is important to consider effects which are beyond the classical two-body additive summation, since none of the approximations we are going to employ, in particular PBE+vdW, MP2 and RPA/RPA+ take into account dispersion non additive effects, and all fail to describe the Axilrod-Teller-Muto triple dipoles[14,137], the so-called *three body* effects[86]. Such effects can be described in more sophisticated theories like coupled cluster (CC) approximation[12,16] starting from third order perturbative excitations (CCSD(T)), but they are still too demanding for extended systems. Based on calculations published in literature on representative $\pi - \pi$ systems as well as non-covalent crystals as bilayer graphene, such an effect is repulsive and is expected to provide a substantial correction to the cohesive and binding energies[191], even though it is expected to be in part counterbalanced by higher order dispersion terms[143]. Since we consider clusters to derive the properties of bulk bilayer graphene, bulk effects, like plasmon-plasmon interactions cannot be calculated (they add another contribution to the asymptotic behaviour of the dispersion interactions between two layers[39,55]). From tight-binding considerations on the band structure on layered structures an independent electron dielectric function model, J.F. Dobson, A. White and A. Rubio estimated such an effect[39], which provides a decay as the third order with respect to the interlayer distance instead of the faster decaying fourth order (given by C_6 summations over surfaces) as provided by pairwise summations. However by definition, such an effect is asymptotic, hence in regions not far from the equilibrium distance, additive summations for the dispersion interaction can still hold. In their study electrostatic quadrupolar effects (repulsive for AB-stacked structures) are not considered, since they are assumed to be negligible for infinite layers. In fact quadrupole interactions[76,190] (see Appendix A.1) do not decay monotonically with the distance, but they have an oscillating behaviour, so that the overall repulsive contribution is almost negligible.
All techniques employed have all the same underlying assumption of the adiabatic Born-Oppenheimer (ABO) approximation, which is valid for pure infinite graphene layers with respect to band structure, geometry and ground state calculations. Moreover it has been shown that graphene violates the ABO approximation in certain cases[156], like in the study of Raman spectra.

4.2 Possible Future Developments

The techniques elaborated in this study allow a comprehension of the mechanism at the basis of $\pi - \pi$ systems, and show how relatively well RPA and PBE+vdW methods can determine the binding energy between two extended π systems like in graphite. Such a benchmark provides a cheap tool which can be applied to study corresponding systems. Once established that such technique can be evaluated through cluster expansions, it would be valuable to calculate the potential energy surfaces (PES) for different configurations and stackings with complex and accurate techniques like CCSD(T) and higher orders, where for example, three body interactions are naturally taken into account. This

would be possibly the basis for studies on bulk elastic properties, and on the friction between graphene layers with accurate and fully *ab-initio* calculations. Moreover our methodology can be applied in principle to other systems, like multilayer or epitaxial graphene, graphite with intercalated materials and physisorption and nanomesh studies on layers or surfaces.

A Appendices

A.1 Quadrupole-Quadrupole Interactions

It is often assumed that the quadrupole contribution to the interaction energy can be calculated by taking a summation over point quadrupoles. We estimate the interaction between two *point* quadrupoles of axial symmetry along the $\hat{e}_z$ direction, normal to the graphene plane, and quadrupole moment Q_0. Such a traceless tensor can be written as

$$\mathbf{Q} = \begin{pmatrix} -\frac{Q_0}{2} & 0 & 0 \\ 0 & -\frac{Q_0}{2} & 0 \\ 0 & 0 & Q_0, \end{pmatrix} \tag{A.1}$$

The quadrupole term in the expansion of the Coulomb potential around the origin, can be written as

$$\phi(\mathbf{r}) = -\frac{1}{2r^5} \sum_{i,j=1}^{3} x_i x_j Q_{ij} = \frac{-\frac{Q_0 x^2}{2} - \frac{Q_0 y^2}{2} + Q_0 z^2}{2\left(x^2+y^2+z^2\right)^{5/2}} \tag{A.2}$$

where by definition $r = (x^2 + y^2 + z^2)^{1/2}$ while the energy of a quadrupole interacting with an external field, in this case another quadrupolar field, is given by

$$W_q = \frac{1}{6} \sum_{i,j=1}^{3} Q_{ij} \frac{\partial}{\partial x_i \partial x_j} \phi(0), \tag{A.3}$$

where the Hessian is given by the espression (A.4)

$$\mathbf{H} = [\partial_{\mathbf{ij}}\phi] =$$

$$\begin{pmatrix} \frac{3Q_0\left(4x^4-y^4+3y^2z^2+4z^4+3x^2\left(y^2-9z^2\right)\right)}{4\left(x^2+y^2+z^2\right)^{9/2}} & \frac{15Q_0xy\left(x^2+y^2-6z^2\right)}{4\left(x^2+y^2+z^2\right)^{9/2}} & \frac{15Q_0xz\left(3x^2+3y^2-4z^2\right)}{4\left(x^2+y^2+z^2\right)^{9/2}} \\ \frac{15Q_0xy\left(x^2+y^2-6z^2\right)}{4\left(x^2+y^2+z^2\right)^{9/2}} & \frac{3Q_0\left(-x^4+4y^4-27y^2z^2+4z^4+3x^2\left(y^2+z^2\right)\right)}{4\left(x^2+y^2+z^2\right)^{9/2}} & \frac{15Q_0yz\left(3x^2+3y^2-4z^2\right)}{4\left(x^2+y^2+z^2\right)^{9/2}} \\ \frac{15Q_0xz\left(3x^2+3y^2-4z^2\right)}{4\left(x^2+y^2+z^2\right)^{9/2}} & \frac{15Q_0yz\left(3x^2+3y^2-4z^2\right)}{4\left(x^2+y^2+z^2\right)^{9/2}} & -\frac{3Q_0\left(3x^4+3y^4-24y^2z^2+8z^4+6x^2\left(y^2-4z^2\right)\right)}{4\left(x^2+y^2+z^2\right)^{9/2}}, \end{pmatrix} \tag{A.4}$$

Thus, the energy of the interaction of two quadrupoles between two graphene layers is given by

$$W_q = \frac{3Q_0^2\left(3x^4+3y^4-24y^2z^2+8z^4+6x^2\left(y^2-4z^2\right)\right)}{16\left(x^2+y^2+z^2\right)^{9/2}}, \tag{A.5}$$

In ref [190] an expression for two axial quadrupoles displaced along the $\hat{e}_x$ direction (following the results of ref.[158]) has been published,

$$W_q = \frac{3Q_0^2\left(35d^4-30d^2\left(x^2+y^2+z^2\right)+3\left(x^2+y^2+z^2\right)^2\right)}{4\left(x^2+y^2+z^2\right)^{9/2}}, \tag{A.6}$$

where d is the component of the distance of the two quadrupoles along the $\hat{e}_z$ axis. Comparing the two equations at a given distance, expression (A.5) contains a pre-factor 4 with respect to the expression we derived (our findings have been evaluated using the Mathematica code[2]). Regardless of the prefactor, we nevertheless see that the interaction does not decay monotonically with the distance between two point quadrupoles.

We calculated using Eq. (A.5), the interaction of AB-stacked graphene layers via point quadrupoles, i.e. the estimated quadrupoles of the carbon atoms, using the experimental value considered in refs.[190,194], i.e. $1,31B$. In Fig (A.1) we show the resulting energy of the quadrupole-quadrupole interaction as a function of the distance of two graphene sheets, which is negligible at all relevant distances compared to the binding energy computed in this thesis.

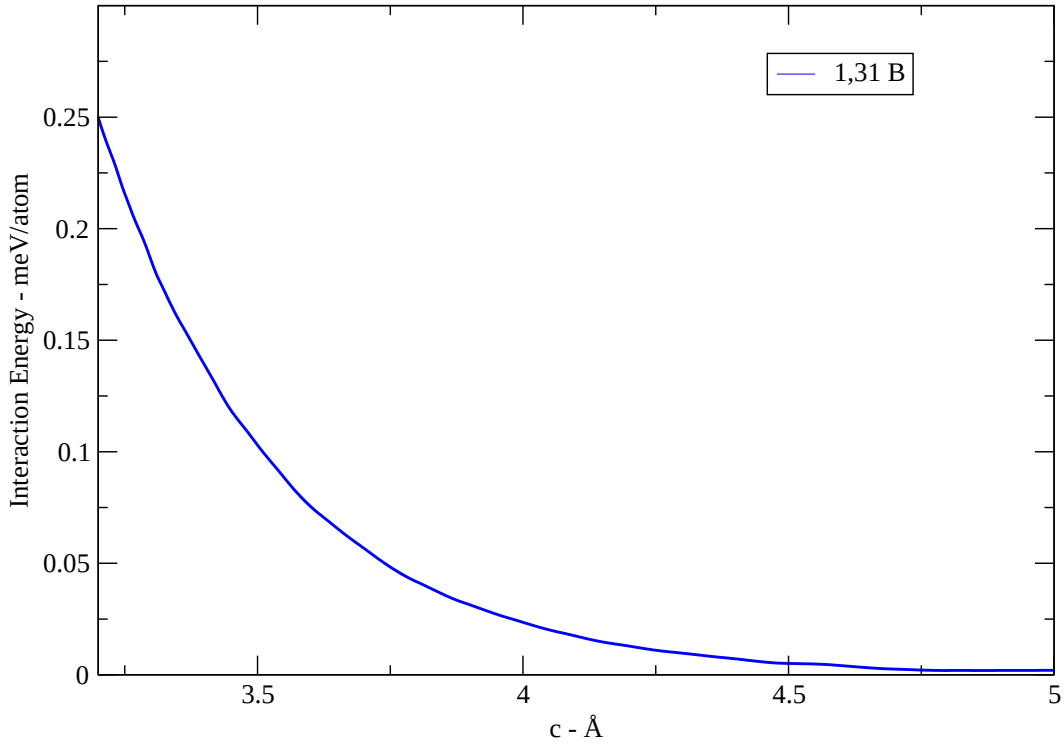

Figure A.1: Quadrupole-quadrupole interaction between two AB-stacked graphene layers for $Q_0 = 1,31B = 1,31 \cdot 10^{-26}$esu.

A.2 Convergence tests for graphene

In the in-house code FHI-AIMS[19] basis set are compiled according to their convergence with respect to the calculations of PW-LDA total energies. This NAOs are named as "tier", followed but progressive numbers indicating their size, or, in a more compact form, as "t" basis sets.
In the following sections the basis set labels refer to: "t1+f"= C[min+2s2p3d4f] H[min+2s 2p], "sb"= C[min+2s2p3s3p3d4f] H[min+1s2s2p], "t2"= C[min+2s2p3s3p3d4f5g] H[min+ 1s2s2p3d], "t3"= C[t2+2s2p3d4f] H[min+1s2s2p3s3p4d4f], "t4C"=[min+2s2p3s3p3d4d 4f5g] H[min+1s2s2p3s3p4d4f], "t4Cp"=[t4C+3s3p4d] H[min+1s2s2p3s3p4d4f].

A.2.1 PW-LDA and GGA-PBE

To evaluate the convergence of the computed cohesive energy* as a function of the basis set size we focus on a fixed in-plane lattice constant of $2,466$ Å, which roughly corresponds to the PW-LDA lattice constant. In the periodic calculations the distance between the periodic images of the graphene sheets is 15 Å and we first employ a (12x12x1) k-point mesh containing 144 k-points in the full Brillouin zone. As apparent from Fig. (A.2), already for a C[min+2s2p3s3p3d4f] basis set, convergence is almost achieved (~ 1 meV/atom for PW-LDA and for GGA-PBE with respect to the fully converged "t3" basis set).

*For simplicity in all the tables of this work the sign of cohesive energies is reversed.

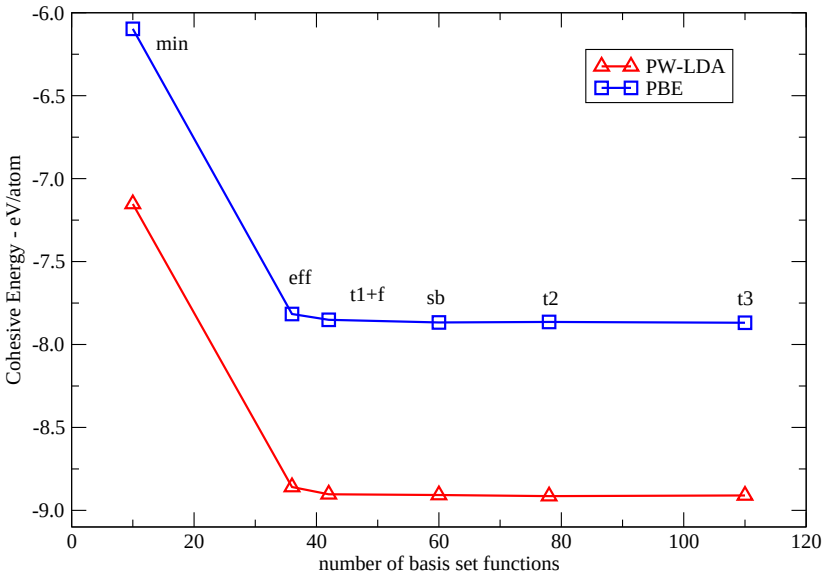

Figure A.2: Convergence of the graphene cohesive energy as a function of the basis set size per unit cell. Shown are data for a fixed in-plane lattice constant of $a = 2,466$ Å, a (12x12x1) k-mesh and using LDA and GGA-PBE.

With the thus determined basis set, we study the dependence on the employed k-mesh by systematically increasing the k-mesh from a (2x2x1) grid with 4 k-points in the full Brillouin zone to a (18x18x1) k-mesh with 324 k-points in the full Brillouin zone. The corresponding data is summarized in Fig. (A.3) and shows a rapid convergence of the cohesive energy to within $\sim$ 10 meV/atom already for a (8x8x1) k-mesh. Additionally we have tested the convergence of the k-sampling in the direction perpendicular to the periodic graphene sheets. However, due to the large extent of the supercell in this direction, we find that already a single k-point along the perpendicular direction to the surface is sufficient.
The rapid convergence of the cohesive energy with k-point sampling is rather surprising in view of the semi-metallic nature of the system. In fact, in metallic systems[128,176], due to the fact that bands are generally partially filled, typically a rather large number of k-points is required to sample the Fermi surface correctly. However, graphene is a particular semi-metal, where bands cross in only one point, the K point, so that the Fermi surface is zero dimensional. In ref.[166] a Monkhorst-Pack (8x8x4) mesh with 256 k-points is reported to be converged at an accuracy of 11 meV/atom for a plane waves basis set, while energies are converged within 30 meV/atom with respect to the number of k-points.

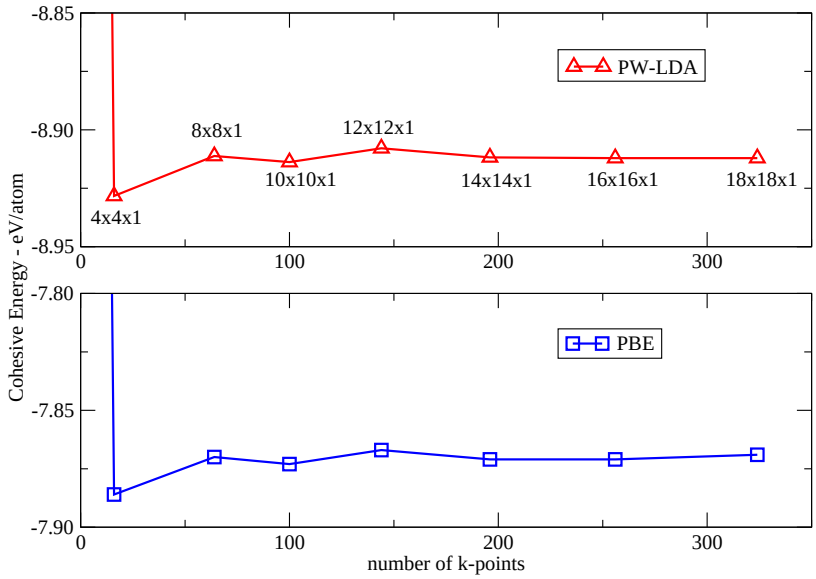

Figure A.3: Convergence of the graphene cohesive energy as a function of the k-point sampling. Shown are data at a fixed in-plane lattice constant of a = 2,466 Å, the "sb" basis set, and using LDA and GGA-PBE.

After determining the converged basis set and k-point sampling, we have also checked the influence of the vacuum separation of the repeating graphene sheets. For distances in the range $10 - 25$ Å we have found a vanishing influence on the cohesive energy in the sub-meV/atom range. Of similarly negligible influence is the truncation of the multipole expansion of the Hartree potential. With the standard setting $l_{\text{hartree}} = 4$ employed in all previous calculations a convergence of the cohesive energy with respect to this computational parameter is again already achieved within ~ 1 meV/atom. As optimized settings for the calculation of the cohesive energy we thus determine the C[min+2s2p3s3p3d] basis set, i.e. "sb", an (18x18x1) k-mesh, $l_{\text{hartree}} = 4$ and an interplane distance of 20 Å. For these settings, Fig. (3.1) shows the variation of the computed cohesive energy as a function of the in-plane lattice constant. To test how well our converged settings perform at different in-plane distances, we have recalculated this curve with a larger basis set (called "t3" in Figure (A.2)), $l_{\text{hartree}} = 6$ and (20x20x1) k-points. The obtained results differ by only 1 meV/atom with respect to the previous results.

A.2.2 PBEsol

To evaluate the cohesive energy we apply the same scheme used in the previous section, i.e. we focus first on an in-plane lattice constant of $2,466$ Å and then we study the convergence with respect to k-points mesh, basis set size and additional parameters. The behavior is very similar for all DFT functionals. In Figure (A.4) we show the convergence of the cohesive energy with respect to the basis set size for a (12x12x1) k-point mesh containing 144 k-points in the full Brillouin zone. At the "sb" basis set level the convergence is essentially achieved at the meV/atom level, as for the local and semi-local functionals PW-LDA and GGA-PBE.

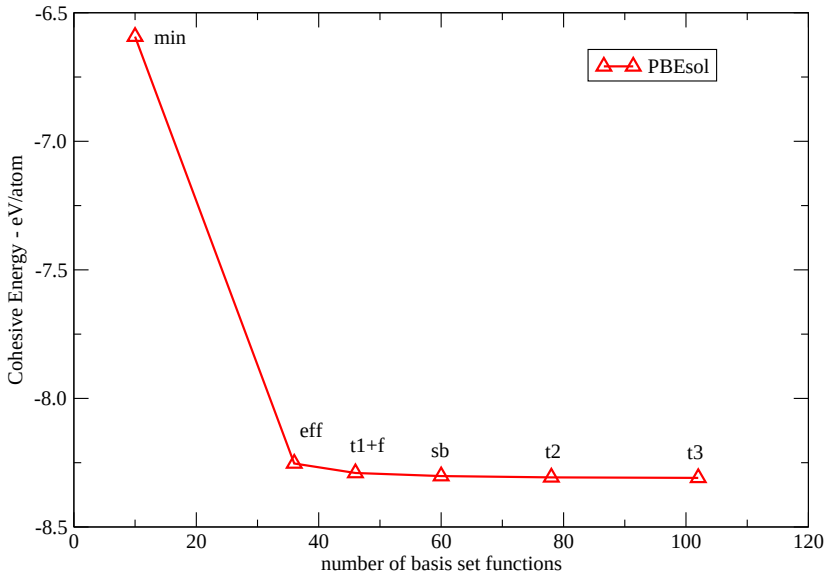

Figure A.4: Convergence of the graphene cohesive energy as a function of the basis set size per unit cell. Shown are data for a fixed in-plane lattice constant of $a = 2,466$ Å, a (12x12x1) k-mesh and using the PBEsol functional.

Subsequently we study the dependence at the "sb" basis set level with respect to the k-point mesh, starting from a (2x2x1) grid with 4 k-points in the full Brillouin zone to a (18x18x1) grid with 324 k-points in the full Brillouin zone. As shown in Fig. (A.5) the convergence is already achieved within few meV/atom for a (8x8x1) k-point mesh. As for the other parameters, namely $l_{hartree}$ and vacuum size, they behave like for the previously employed functionals, and they are therefore set to 4 and 20 Å, respectively.

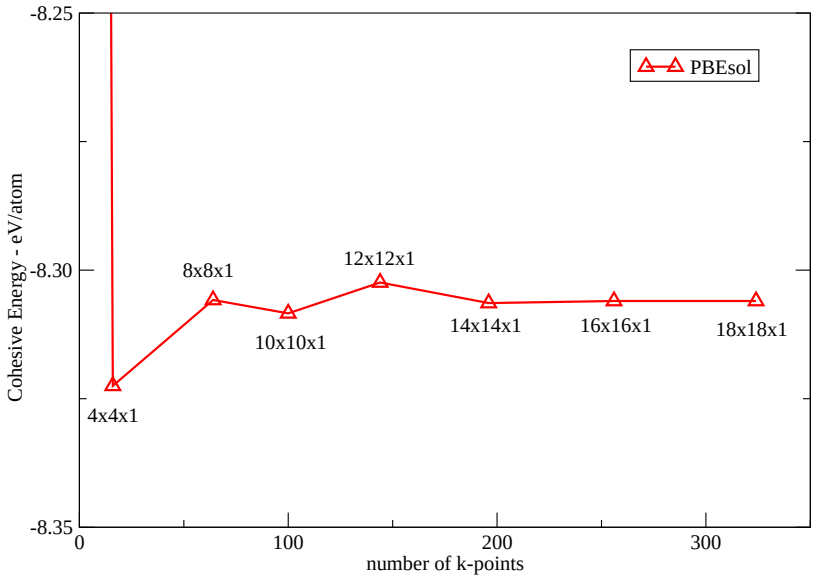

Figure A.5: Convergence of the graphene cohesive energy as a function of the k-point sampling. Shown are data at a fixed in-plane lattice constant of a = 2,466 Å, the "sb" basis set, and using LDA and GGA-PBE.

To test the convergence we performed also in this case calculations with the much larger "t3" basis set with $l_{hartree} = 6$ and a (24x24x1) k-points mesh. The results agree at the meV/atom level.

A.2.3 PBE+vdW

The atomic reference contributions are exactly like in GGA-PBE ground state spin collinear calculations, and geometries are kept as in the previous sections, i.e. we focus first on an in-plane lattice constant of 2, 466 Å. We study the convergence with respect to k-points mesh, basis set size and additional parameters. In Figure (A.6) we show the convergence of the cohesive energy with respect to the basis set size for a (12x12x1) k-point mesh containing 144 k-points in the full Brillouin zone, $l_{hartree} = 4$ and 15 Å vacuum. At the "sb" basis set level the convergence is essentially achieved at the

order of $\sim$ 1 meV/atom. In periodic calculations the convergence with the number of k-points is done with respect to the usual k-points as for the other DFT methods, and additionally the van der Waals cells parameter *vdw_cells*, i.e. the number of cells to include in the pairwise summations over atoms for van der Waals interactions. The latter converges relatively rapidly with the number of cells at already (5x5x0) cells, so that a (10x10x0) grid is considered to be safe. The former converges similarly as for the other DFT functionals, as we can see from Fig. (A.7).

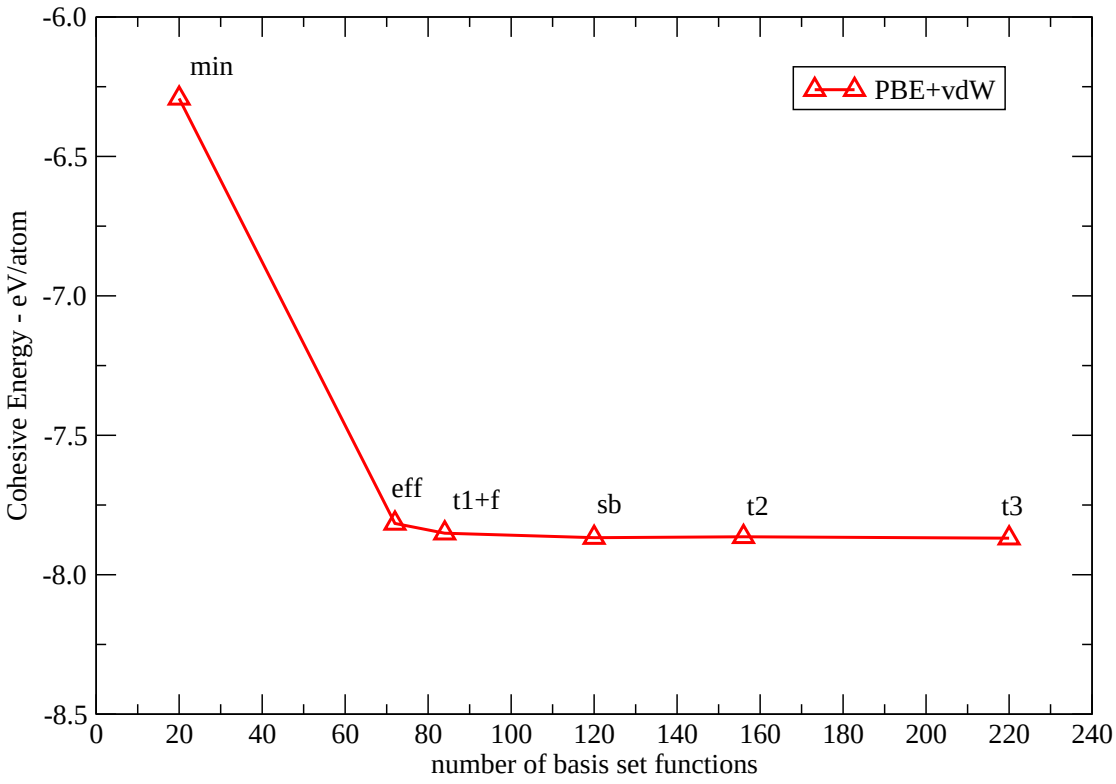

Figure A.6: Convergence of the graphene cohesive energy as a function of the basis set size per unit cell. Shown are data for a fixed in-plane lattice constant of $a = 2,466$ Å, a (12x12x1) k-mesh and using the PBE+vdW functional.

Again, to test the convergence with respect to the parameters we repeated the calculations using a highly converged basis set "t3" and $l_{\mathrm{hartree}} = 6$, using a (24x24x1) grid with 576 k-points, and the results agree at the meV level.

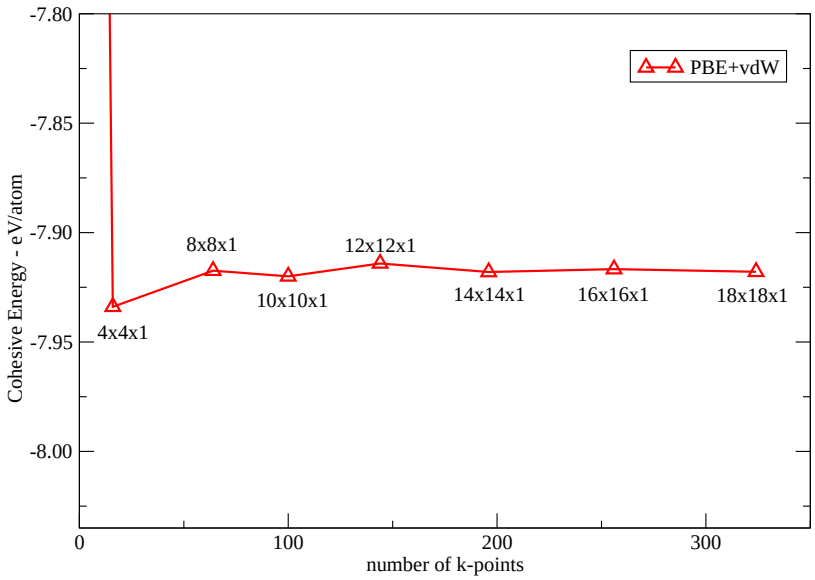

Figure A.7: Convergence of the graphene cohesive energy as a function of the k-point sampling. Shown are data at a fixed in-plane lattice constant of a = 2,466 Å, the "sb" basis set, and using PBE+vdW functional.

A.3 Clusters Extrapolations for Graphene

A.3.1 PW-LDA and GGA-PBE

Table A.1: Cohesive energy (eV/atom) extrapolation compared to the result of the periodic calculations. Shown are the values obtained when using the indicated cluster ranges in the fit (see Fig. (3.5)) at $a = 2,446$ Å.

	t1+f	sb	t2	t3	Carbon atoms	method
E_{coh}	8,86	8,87	8,87	8,87	6-96	PW-LDA
	8,86	8,87	8,87	8,87	6-54	””
	8,84	8,86	8,86	8,85	6-32	””
	8,83	8,84	8,84	8,84	6-24	””
	8,88	8,89	8,89	8,89	10-96	””
	8,88	8,90	8,90	8,90	10-54	””
	8,88	8,89	8,89	8,89	10-32	””
	8,88	8,89	8,89	8,89	10-24	””
	8,89	8,90	8,90	8,90	14-96	””
	8,90	8,91	8,91	8,91	14-54	””
	8,92	8,93	8,93	8,93	14-32	””
	8,93	8,94	8,94	8,94	14-24	””
	8,89	8,90	8,90	8,90	16-96	””
	8,90	8,91	8,91	8,92	bulk	PW-LDA
	7,80	7,82	7,82	7,82	6-96	GGA-PBE
	7,79	7,81	7,81	7,81	6-54	””
	7,78	7,79	7,79	7,79	6-32	””
	7,76	7,77	7,77	7,77	6-24	””
	7,83	7,84	7,84	7,84	10-96	””
	7,83	7,84	7,84	7,84	10-54	””
	7,82	7,83	7,84	7,84	10-32	””
	7,81	7,82	7,82	7,82	10-24	””
	7,84	7,85	7,85	7,85	14-96	””
	7,85	7,86	7,86	7,86	14-54	””
	7,86	7,87	7,87	7,87	14-32	””
	7,87	7,88	7,89	7,89	14-24	””
	7,84	7,85	7,85	7,85	16-96	””
	7,85	7,86	7,86	7,86	bulk	GGA-PBE

Table A.1 (*continued*)

	t1+f	sb	t2	t3	Carbon atoms	method
ΔE_{coh}	1,06	1,06	1,06	1,05	6-96	PW-LDA - GGA-PBE
	1,06	1,06	1,06	1,06	6-54	””
	1,07	1,07	1,06	1,07	6-32	””
	1,07	1,07	1,07	1,07	6-24	””
	1,06	1,05	1,05	1,06	10-96	””
	1,06	1,06	1,06	1,06	10-54	””
	1,06	1,06	1,06	1,05	10-32	””
	1,06	1,07	1,06	1,07	10-24	””
	1,06	1,05	1,05	1,05	14-96	””
	1,06	1,05	1,05	1,05	14-54	””
	1,06	1,06	1,05	1,06	14-32	””
	1,06	1,06	1,06	1,06	14-24	””
	1,05	1,05	1,05	1,05	16-96	””
	1,05	1,05	1,05	1,05	bulk	PW-LDA - GGA-PBE

A.3.2 PBEsol

Table A.2: Cohesive energy (eV/atom) extrapolation compared to the result of the periodic calculations. Shown are the values obtained when using the indicated cluster ranges in the fit (see Fig. (3.5)) at $a = 2,446$ Å.

	t1+f	sb	t2	t3	Carbon atoms	method
E_{coh}	8,25	8,26	8,26	8,26	6-96	PBEsol
	8,24	8,25	8,25	8,26	6-54	””
	8,22	8,24	8,24	8,24	6-32	””
	8,21	8,22	8,22	8,22	6-24	””
	8,27	8,28	8,28	8,29	10-96	””
	8,27	8,28	8,28	8,29	10-54	””
	8,27	8,28	8,28	8,28	10-32	””
	8,26	8,27	8,27	8,27	12-24	””
	8,28	8,29	8,30	8,30	14-96	””
	8,29	8,30	8,31	8,31	14-54	””
	8,30	8,31	8,32	8,32	14-32	””
	8,32	8,33	8,33	8,34	14-24	””
	8,28	8,29	8,29	8,29	16-96	””
	8,28	8,30	8,30	8,30	bulk	PBEsol
ΔE_{coh}	0,62	0,62	0,61	0,61	6-96	PW-LDA - PBEsol
	0,62	0,62	0,61	0,61	6-54	””
	0,62	0,62	0,62	0,61	6-32	””
	0,62	0,62	0,62	0,62	6-24	””
	0,61	0,62	0,61	0,61	10-96	””
	0,61	0,62	0,61	0,61	10-54	””
	0,62	0,62	0,61	0,61	10-32	””
	0,62	0,62	0,61	0,61	10-24	””
	0,61	0,61	0,61	0,61	14-96	””
	0,61	0,61	0,61	0,61	14-54	””
	0,61	0,61	0,61	0,61	14-32	””
	0,61	0,61	0,61	0,61	14-24	””
	0,61	0,61	0,61	0,60	16-96	””
	0,62	0,61	0,61	0,62	bulk	PW-LDA - PBEsol

Table A.2 (*continued*)

	t1+f	sb	t2	t3	Carbon atoms	method
ΔE_{coh}	0,45	0,44	0,46	0,45	6-96	PBEsol - GGA-PBE
	0,45	0,44	0,43	0,46	6-54	””
	0,45	0,44	0,45	0,46	6-32	””
	0,45	0,45	0,45	0,45	6-24	””
	0,45	0,44	0,46	0,45	10-96	””
	0,45	0,44	0,45	0,45	10-54	””
	0,45	0,44	0,46	0,46	10-32	””
	0,45	0,45	0,45	0,45	12-24	””
	0,45	0,44	0,46	0,45	14-96	””
	0,45	0,44	0,45	0,45	14-54	””
	0,45	0,44	0,45	0,45	14-32	””
	0,45	0,45	0,45	0,45	14-24	””
	0,45	0,44	0,46	0,45	16-96	””
	0,43	0,45	0,44	0,44	bulk	PBEsol - GGA-PBE

A.3.3 PBE+vdW

Table A.3: Cohesive energy (eV/atom) extrapolation compared to the result of the periodic calculations presented in the previous sections. Shown are the values obtained when using the indicated cluster ranges in the fit (see Fig. (3.5)) at $a = 2,446$ Å.

	t1+f	sb	t2	t3	Carbon atoms	method
E_{coh}	7,85	7,86	7,86	7,86	6-96	PBE+vdW
	7,84	7,85	7,85	7,85	6-54	””
	7,83	7,83	7,84	7,83	6-32	””
	7,80	7,81	7,82	7,81	6-24	””
	7,88	7,89	7,89	7,89	10-96	””
	7,88	7,88	7,89	7,88	10-54	””
	7,87	7,88	7,88	7,87	10-32	””
	7,85	7,86	7,87	7,86	10-24	””
	7,89	7,90	7,90	7,90	14-96	””
	7,90	7,91	7,91	7,90	14-54	””
	7,91	7,92	7,92	7,91	14-32	””
	7,91	7,93	7,93	7,92	14-24	””
	7,89	7,91	7,90	7,90	16-96	””
	7,89	7,91	7,91	7,91	bulk	PBE+vdW
ΔE_{coh}	1,01	1,01	1,01	1,01	6-96	PW-LDA - PBE+vdW
	1,01	1,02	1,01	1,02	6-54	””
	1,02	1,02	1,02	1,02	6-32	””
	1,03	1,03	1,02	1,03	6-24	””
	1,01	1,01	1,00	1,01	10-96	””
	1,01	1,01	1,01	1,01	10-54	””
	1,01	1,02	1,01	1,02	10-32	””
	1,03	1,02	1,02	1,02	10-24	””
	1,01	1,00	1,00	1,00	14-96	””
	1,01	1,01	1,01	1,01	14-54	””
	1,01	1,01	1,01	1,02	14-32	””
	1,02	1,02	1,01	1,02	14-24	””
	1,00	1,00	1,00	1,00	16-96	””
	1,01	1,00	1,00	1,01	bulk	PW-LDA - PBE+vdW

Table A.3 (*continued*)

t1+f	sb	t2	t3	Carbon atoms	method
-0,05	-0,05	-0,05	-0,05	6-96	GGA-PBE - PBE+vdW
-0,05	-0,04	-0,05	-0,04	6-54	””
-0,05	-0,04	-0,05	-0,04	6-32	””
-0,04	-0,04	-0,05	-0,04	6-24	””
-0,05	-0,05	-0,05	-0,05	10-96	””
-0,05	-0,05	-0,05	-0,04	10-54	””
-0,05	-0,04	-0,05	-0,04	10-32	””
-0,04	-0,04	-0,05	-0,04	10-24	””
-0,05	-0,05	-0,05	-0,05	14-96	””
-0,05	-0,05	-0,05	-0,04	14-54	””
-0,05	-0,05	-0,05	-0,04	14-32	””
-0,04	-0,04	-0,05	-0,04	14-24	””
-0,05	-0,06	-0,05	-0,05	16-96	””
-0,04	-0,05	-0,05	-0,05	bulk	GGA-PBE - PBE+vdW

A.3.4 MP2

The MP2 approximation parameters, i.e. the number of basis set products and the basis set product cut-off threshold, have been tested at the "sb" basis set level for the smallest molecule, i.e. benzene, and provide an extrapolated cohesive energy rapidly converged at the sub-meV/atom level, and they are therefore set to 4 (3 for hydrogens) and 10^{-4} respectively. Further tests on the basis set product cut-off threshold have been also made for larger clusters, in particular using the "t4C" and "t4Cp" basis sets, and they do not provide any substantial change. However, because of the numerical noise for the two biggest clusters calculated with the "t4C" and "t4Cp" basis set, i.e. "32 C" and "24 C" clusters, the cut-off threshold has been increased to 10^{-3}.

Table A.4: Cohesive energy (eV/atom) extrapolation as a function of the number of carbon atoms in the clusters considered in the linear regression and for the "t1+f", "sb", "t2", "t3", "t4C" and "t4Cp" basis sets and at $a = 2,446$Å. Some values for the "t3", "t4C" and "t4Cp" basis sets are missing, since the computational requirements are yet too demanding.

	t1+f	sb	t2	t3	t4C	t4Cp	Carbon atoms	method
E_{coh}	7,47	7,60	7,73				6-54	MP2
	7,44	7,58	7,71	7,75	7,79	7,79	6-32	""
	7,42	7,56	7,68	7,73	7,76	7,77	6-24	""
	7,51	7,65	7,77				10-54	""
	7,50	7,64	7,76	7,81	7,84	7,84	10-32	""
	7,49	7,62	7,75	7,79	7,83	7,83	10-24	""
	7,54	7,67	7,79				14-54	""
	7,55	7,68	7,81	7,85	7,89	7,89	14-32	""
	7,56	7,70	7,82	7,87	7,90	7,90	14-24	""
ΔE_{coh}	1,39	1,26	1,14				6-54	PW-LDA - MP2
	1,40	1,27	1,15	1,10	1,07	1,07	6-32	""
	1,41	1,28	1,16	1,11	1,08	1,07	6-24	""
	1,38	1,25	1,13				10-54	""
	1,38	1,26	1,13	1,08	1,05	1,05	10-32	""
	1,39	1,26	1,14	1,09	1,06	1,06	10-24	""
	1,37	1,24	1,12				14-54	""
	1,37	1,24	1,12	1,07	1,04	1,04	14-32	""
	1,37	1,25	1,12	1,08	1,04	1,04	14-24	""
	0,33	0,20	0,08				6-54	GGA-PBE - MP2
	0,33	0,21	0,09	0,04	0,00	0,00	6-32	""
	0,34	0,21	0,09	0,04	0,01	0,00	6-24	""
	0,32	0,19	0,07				10-54	""
	0,32	0,20	0,07	0,02	-0,01	-0,01	10-32	""
	0,33	0,20	0,08	0,03	-0,01	-0,01	10-24	""
	0,31	0,19	0,07				14-54	""
	0,31	0,19	0,07	0,02	-0,01	-0,01	14-32	""
	0,31	0,19	0,07	0,02	-0,02	-0,02	14-24	""

Table A.4 (*continued*)

t1+f	sb	t2	t3	t4C	t4Cp	Carbon atoms	method
0,38	0,25	0,13				6-54	MP2 - PBE+vdW
0,38	0,25	0,13	0,08	0,06	0,06	6-32	””
0,25	0,25	0,14	0,08	0,07	0,07	6-24	””
0,37	0,24	0,12				10-54	””
0,37	0,24	0,12	0,07	0,04	0,04	10-32	””
0,22	0,24	0,12	0,07	0,05	0,05	10-24	””
0,36	0,24	0,11				14-54	””
0,36	0,24	0,11	0,06	0,01	0,02	14-32	””
0,24	0,23	0,11	0,05	0,01	0,01	14-24	””

A.3.5 RPA

As for the MP2 method the convergence parameters have been thoroughly tested. The computational framework of the RPA method is essentially the same used for MP2. The convergence parameters behave in the same way and are therefore set to 4 (3 for hydrogens) for the number of basis set products. An additional parameter coming from the integration over the frequencies, is represented by the number of frequency intervals to integrate, i.e. the *frequency_points* parameter, which is converged rapidly at the sub-meV/atom level and therefore set by default to 80. The recent implementation of a multi-step integration procedure allows to calculate RPA total energies at the same level of accuracy using a cut-off threshold of 10^{-4} for all basis sets and all clusters sizes.

Table A.5: Cohesive energy (eV/atom) extrapolation as a function of the number of carbon atoms in the clusters considered in the linear regression and for the "t1+f", "sb", "t2", "t3", "t4C" and "t4Cp" basis sets and at $a = 2,446$Å. Some values for the "t3", "t4C" and "t4Cp" basis sets are missing, since the computational requirements are yet too demanding.

	t1+f	sb	t2	t3	t4C	t4Cp	Carbon atoms	method
E_{coh}	6.37	6.72	7,02				6-54	RPA
	6.35	6.74	7,07	7,07	7,09	7,08	6-32	""
	6.32	6.71	7,06	7,06	7,08	7,08	6-24	""
	6.45	6.79	7,06				10-54	""
	6.48	6.89	7,17	7,09	7,08	7,08	10-32	""
	6.50	6.92	7,23	7,09	7,05	7,05	10-24	""
	6.44	6.71	6.98				14-54	""
	6.49	6.79	7,09	7,14	7,14	7,13	14-32	""
	6.51	6.74	7,11	7,18	7,16	7,16	14-24	""
ΔE_{coh}	2,49	2,15	1,85				6-54	PW-LDA - RPA
	2,49	2,12	1,79	1,79	1,77	1,78	6-32	""
	2,51	2,13	1,78	1,78	1,76	1,76	6-24	""
	2,43	2,10	1,84				10-54	""
	2,40	2,00	1,72	1,80	1,81	1,82	10-32	""
	2,38	1,97	1,66	1,80	1,83	1,83	10-24	""
	2,46	2,21	1,93				14-54	""
	2,43	2,14	1,84	1,79	1,79	1,80	14-32	""
	2,42	2,20	1,83	1,77	1,78	1,78	14-24	""
	-1,43	-1,09	-0,78				6-54	RPA - GGA-PBE
	-1,42	-1,05	-0,72	-0,72	-0,70	-0,71	6-32	""
	-1,44	-1,07	-0,71	-0,71	-0,69	-0,69	6-24	""
	-1,38	-1,05	-0,78				10-54	""
	-1,34	-0,94	-0,66	-0,74	-0,75	-0,76	10-32	""
	-1,31	-0,91	-0,60	-0,73	-0,77	-0,77	10-24	""
	-1,40	-1,15	-0,88				14-54	""
	-1,37	-1,09	-0,78	-0,73	-0,73	-0,74	14-32	""
	-1,36	-1,14	-0,78	-0,71	-0,72	-0,72	14-24	""

Table A.5 (*continued*)

t1+f	sb	t2	t3	t4C	t4Cp	Carbon atoms	method
-1,48	-1,13	-0,83				6-54	RPA - PBE+vdW
-1,47	-1,09	-0,77	-0,76	-0,75	-0,75	6-32	""
-1,48	-1,10	-0,75	-0,75	-0,74	-0,74	6-24	""
-1,43	-1,09	-0,83				10-54	""
-1,39	-0,99	-0,71	-0,78	-0,80	-0,80	10-32	""
-1,35	-0,95	-0,64	-0,77	-0,81	-0,81	10-24	""
-1,45	-1,20	-0,93				14-54	""
-1,42	-1,13	-0,83	-0,77	-0,77	-0,78	14-32	""
-1,40	-1,18	-0,82	-0,75	-0,76	-0,76	14-24	""

A.3.6 RPA+

For the RPA+ method exactly the same conclusions are valid as for RPA.

Table A.6: Cohesive energy (eV/atom) extrapolation as a function of the number of carbon atoms in the clusters considered in the linear regression and for the "t1+f", "sb", "t2", "t3", "t4C" and "t4Cp" basis sets and at $a = 2,446$Å. Some values for the "t3", "t4C" and "t4Cp" basis sets are missing, since the computational requirements are yet too demanding.

	t1+f	sb	t2	t3	t4C	t4Cp	Carbon atoms	method
E_{coh}	6.30	6.65	6.98				6-54	RPA+
	6.29	6.67	7,03	7,00	7,02	7,02	6-32	""
	6.26	6.64	7,04	6.99	7,01	7,01	6-24	""
	6.36	6.72	6.99				10-54	""
	6.39	6.82	7,10	7,02	7,01	7,01	10-32	""
	6.40	6.85	7,16	7,02	6.99	7,00	10-24	""
	6.33	6.64	6.91				14-54	""
	6.33	6.72	7,02	7,07	7,07	7,07	14-32	""
	6.31	6.67	7,04	7,11	7,09	7,10	14-24	""
ΔE_{coh}	2,56	2,22	1,89				6-54	PW-LDA - RPA+
	2,56	2,18	1,82	1,85	1,84	1,83	6-32	""
	2,57	2,20	1,80	1,85	1,83	1,83	6-24	""
	2,52	2,17	1,91				10-54	""
	2,49	2,07	1,79	1,87	1,88	1,88	10-32	""
	2,48	2,04	1,73	1,87	1,90	1,88	10-24	""
	2,58	2,27	2,00				14-54	""
	2,58	2,21	1,91	1,85	1,85	1,85	14-32	""
	2,63	2,27	1,90	1,84	1,85	1,84	14-24	""
	-1,50	-1,16	-0,83				6-54	RPA+ - GGA-PBE
	-1,49	-1,12	-0,76	-0,79	-0,77	-0,77	6-32	""
	-1,50	-1,13	-0,74	-0,78	-0,76	-0,76	6-24	""
	-1,46	-1,12	-0,85				10-54	""
	-1,43	-1,01	-0,73	-0,81	-0,82	-0,82	10-32	""
	-1,41	-0,97	-0,67	-0,80	-0,84	-0,82	10-24	""
	-1,52	-1,22	-0,95				14-54	""
	-1,53	-1,16	-0,85	-0,80	-0,80	-0,80	14-32	""
	-1,57	-1,21	-0,84	-0,78	-0,80	-0,79	14-24	""

Table A.6 (*continued*)

t1+f	sb	t2	t3	t4C	t4Cp	Carbon atoms	method
-1,55	-1,20	-0,88				6-54	RPA+ - PBE+vdW
-1,54	-1,16	-0,80	-0,83	-0,81	-0,81	6-32	””
-1,54	-1,17	-0,78	-0,82	-0,81	-0,80	6-24	””
-1,51	-1,16	-0,90				10-54	””
-1,48	-1,06	-0,78	-0,85	-0,86	-0,86	10-32	””
-1,45	-1,01	-0,71	-0,84	-0,88	-0,86	10-24	””
-1,57	-1,27	-0,99				14-54	””
-1,58	-1,20	-0,90	-0,84	-0,84	-0,84	14-32	””
-1,60	-1,25	-0,89	-0,81	-0,83	-0,82	14-24	””

A.4 Convergence tests for bilayer graphene

A.4.1 PW-LDA and GGA-PBE

To evaluate the convergence in the DFT methods we focus first on a geometry with an in-plane constant of $a = 2,446$ Å and an experimental interlayer constant of $c = 3,35$ Å[133]. We start investigating the basis set convergence at a (12x12x1) grid with 144 k-points in the full Brillouin zone and 25 Å vacuum size. We thus precede to the convergence with respect to the number of k-points and in the end to the convergence with respect to vacuum size and further convergence parameters (l_{hartree}).
Figures (A.8) and (A.9) display the results for the cohesive energy, from which a similar convergence behavior with respect to basis set and k-points as in the case of graphene can be discerned. The cohesive energy is converged for a C[min+2s2p3s3p3d4f] basis set, called "sb", already at the order of $\sim$ 1 meV/atom for PW-LDA and GGA-PBE with respect to the fully converged "t3" basis set (corresponding to 220 basis functions per unit cell, compared to 120 basis functions per unit cell of the "sb" basis set). For this optimized "sb" basis set the cohesive energy is also converged to $\sim$ 1 meV/atom already for a (8x8x1) k-mesh. At the large supercell size considered, a single k-point along the direction perpendicular to the surface is found to be sufficient. As for $l_{hartree}$ paramater and the vacuum size an analogous behavior is observed for PW-LDA and PBE functionals and they are set to 4, and 20 Å, respectively.

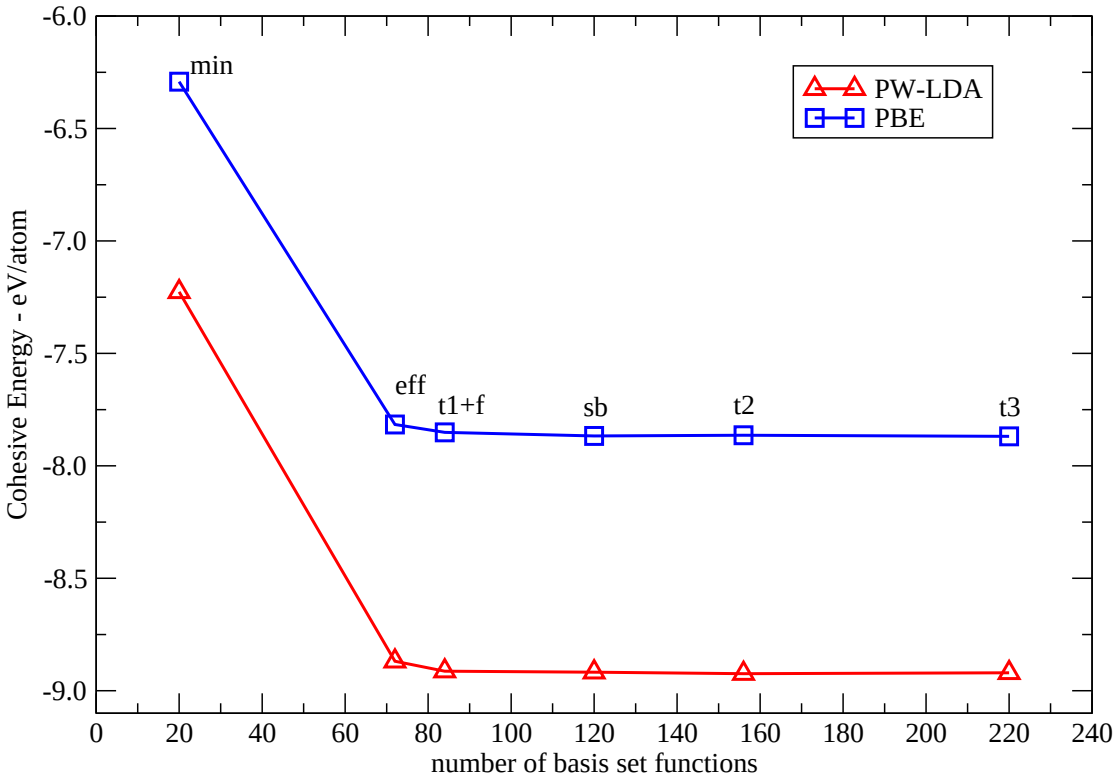

Figure A.8: Convergence of the cohesive energy with basis set size per unit cell. Shown are data for PW-LDA and GGA-PBE at a fixed in-plane distance of $a = 2,446$ Å and interlayer distance of $c = 3,35$ Å.

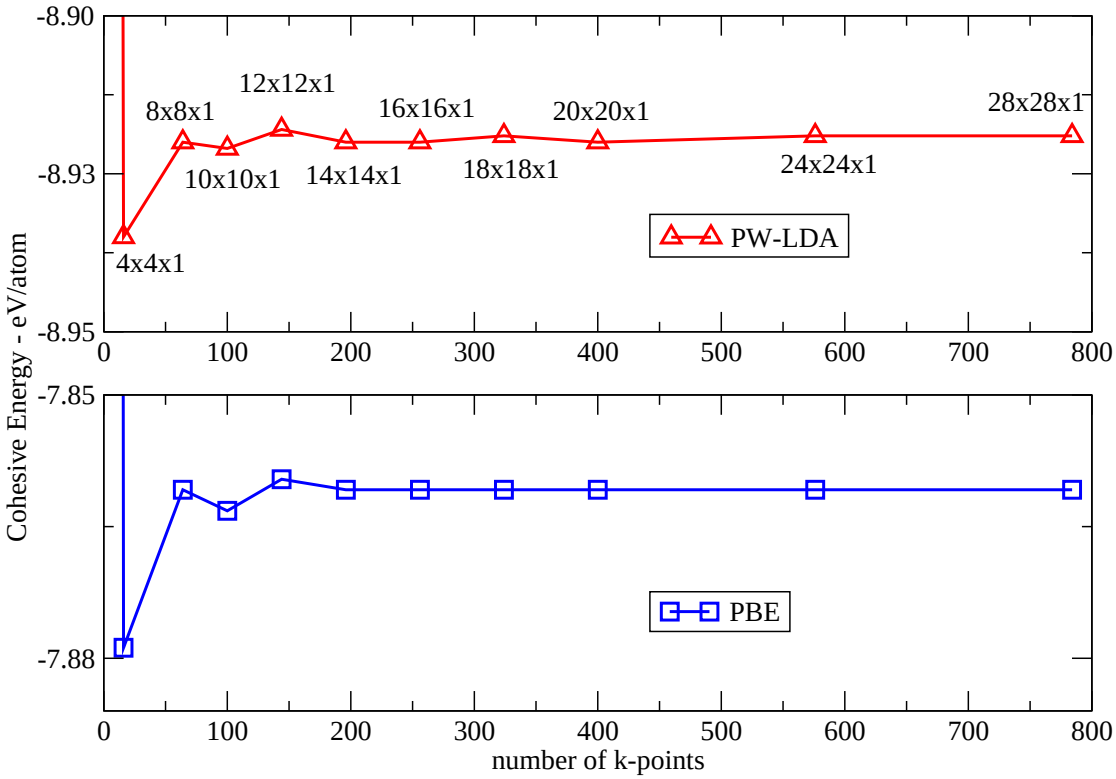

Figure A.9: Convergence of the cohesive energy as a function of the number of k-points. Shown are data for PW-LDA and GGA-PBE at fixed in-plane distance of $a = 2,446$ Å and interlayer distance of $c = 3,35$ Å, as a function of number of k-points and the "sb" basis set is used.

For what concerns the binding energy, the convergence behavior with respect to basis set and k-points is again similar to the one of the cohesive energy. In Figs. (A.10) and (A.11) we show the binding energy as a function of the basis set size and of the number of k-points. The binding energy is converged at the sub-meV/atom level for the "sb" basis set, with respect to the "t3 basis set. In Fig. (A.11) the binding energy is plotted as a function of the number of k-points for the "sb" basis set, and again the convergence is reached within ~ 1 meV/atom. The effects of the vacuum size and l_{hartree} parameter are very similar to the graphene case. Correspondingly we use as converged parameters the "sb" basis set, i.e. C[min+2s2p3s3p3d4f], a (18x18x1) grid of 326 k-points in the full Brillouin zone, 25 Å vacuum and $l_{\mathrm{hartree}} = 4$. Sample points on the curve were also calculated with much higher converged parameters ($l_{\mathrm{hartree}} = 6$, (24x24x1) mesh with 576 k-points in the full Brillouin zone) and the results agree at the order of the 1 meV/atom for the cohesive and at the sub-meV/atom level for the binding energy.

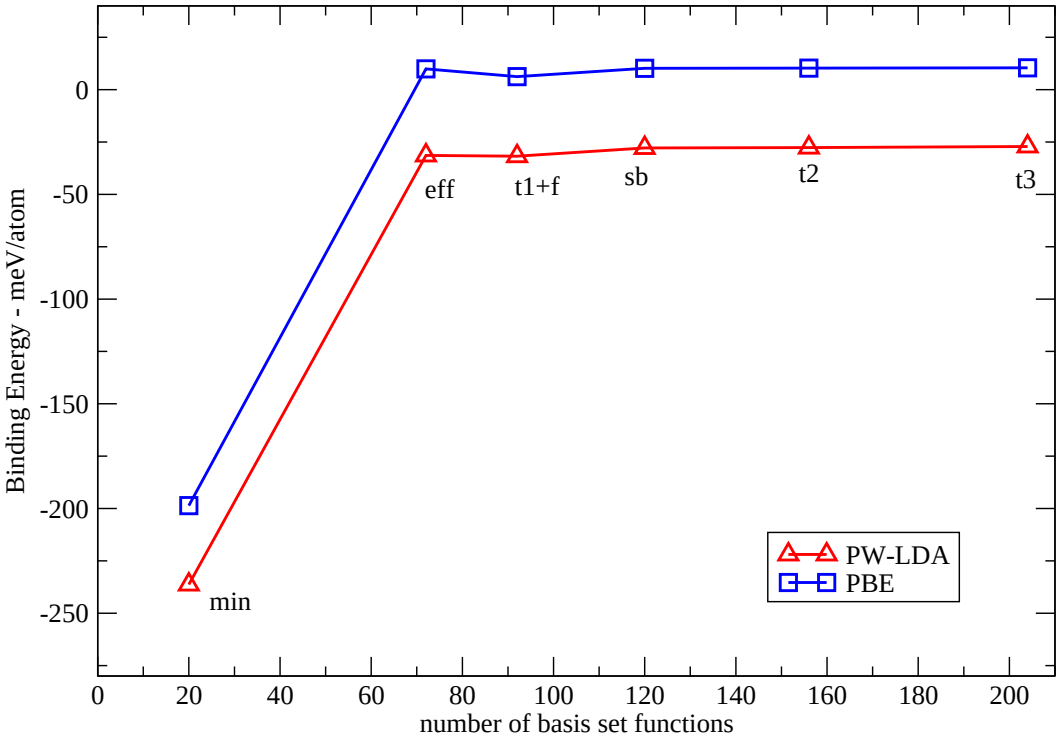

Figure A.10: Convergence of binding energies for PW-LDA and GGA-PBE at a fixed in-plane distance of $a = 2,446$ Å and interlayer distance of $c = 3,35$ Å, as a function of basis set size per unit cell.

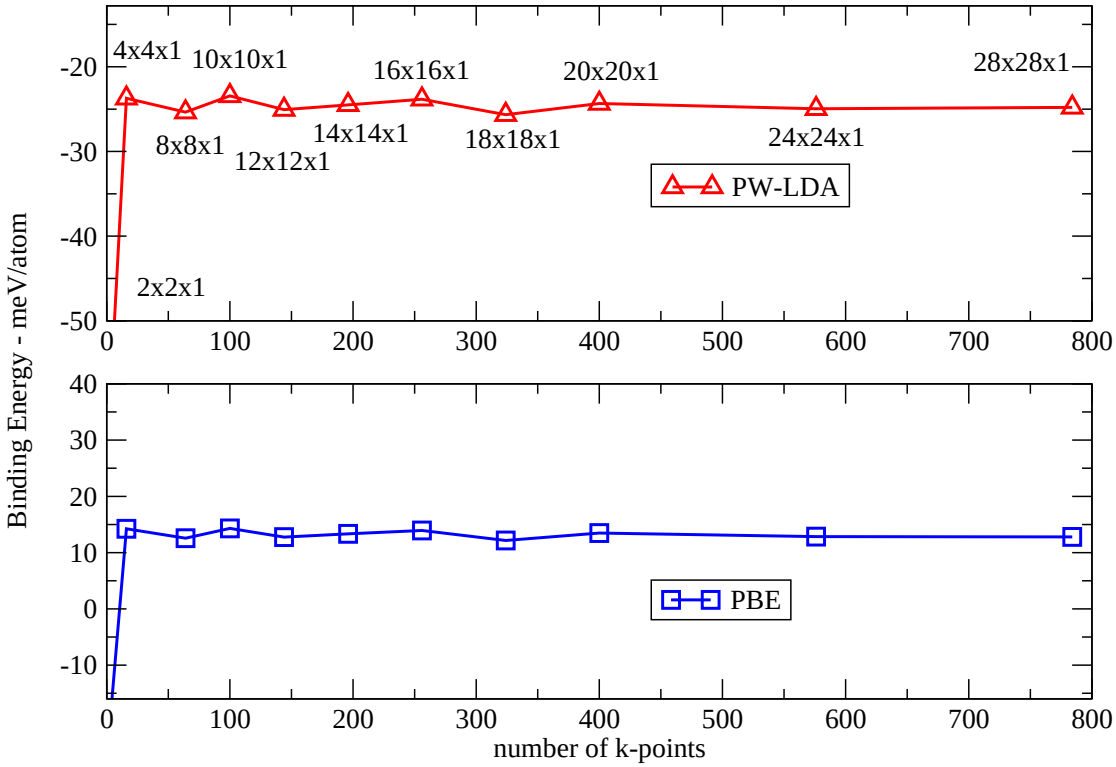

Figure A.11: Convergence of the binding energy between two stacked sheets as a function of the number of k-points. Shown are data for PW-LDA and GGA-PBE at a fixed in-plane distance of $a = 2,446$ Å and interlayer distance of $c = 3,35$ Å, as a function of number of k-points and using the "sb" basis set.

A.4.2 PBEsol

We proceed to the evaluation of the convergence of parameters at the fixed geometry of $a = 2,446$ Å and $c = 3,35$ Å. First we compute the cohesive energy for a (12x12x1) grid with 144 k-points in the first Brillouin zone and 25 Å vacuum, and then we investigate the convergence with respect to the $l_{hartree}$ parameter and vacuum size. Figs. (A.12) and (A.13) show a behavior similar to the graphene case and to the other local and semi-local DFT functionals previously employed in this study (PW-LDA and GGA-PBE). The cohesive energy is again converged at the order of 1 meV/atom already for the "sb" basis set, i.e. C[min+2s2p3s3p3d4f], with respect to the fully converged basis set "t3". At the large supercell considered a single k-point along the direction normal to the surface is found to be sufficient. With respect to the binding energy, Figs. (A.14) and (A.15), the convergence with the basis set size is again similar to the cohesive energy case, and it is converged at the sub-meV/atom level already for the "sb" basis set. The same conclusions are valid for the convergence parameters as for the other DFT functionals. We therefore set $l_{hartree} = 4$ and use a (18x18x1) grid of 326 k-points in the full Brillouin zone. Sample points taken at finer parameter (24x24x1) grid with 576 k-points in the full Brillouin zone show differences of the order of sub-meV/atom.

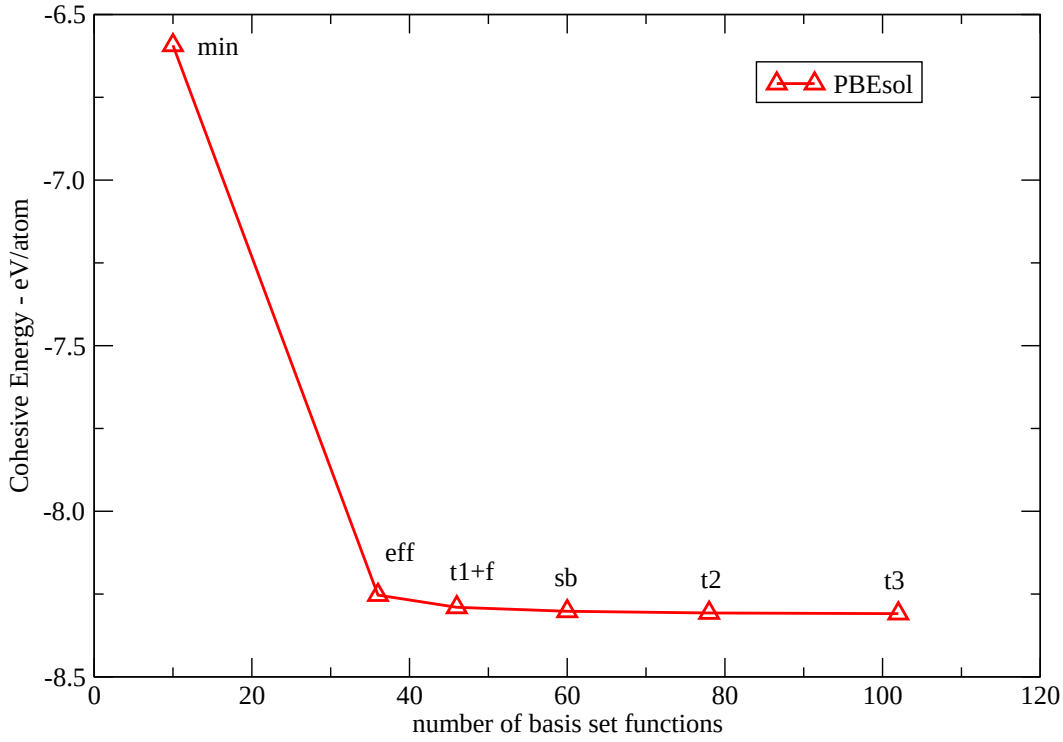

Figure A.12: Convergence of the cohesive energy with basis set size per unit cell. Shown are data for the PBEsol functional at a fixed in-plane distance of $a = 2,446$ Å and interlayer distance of $c = 3,35$ Å.

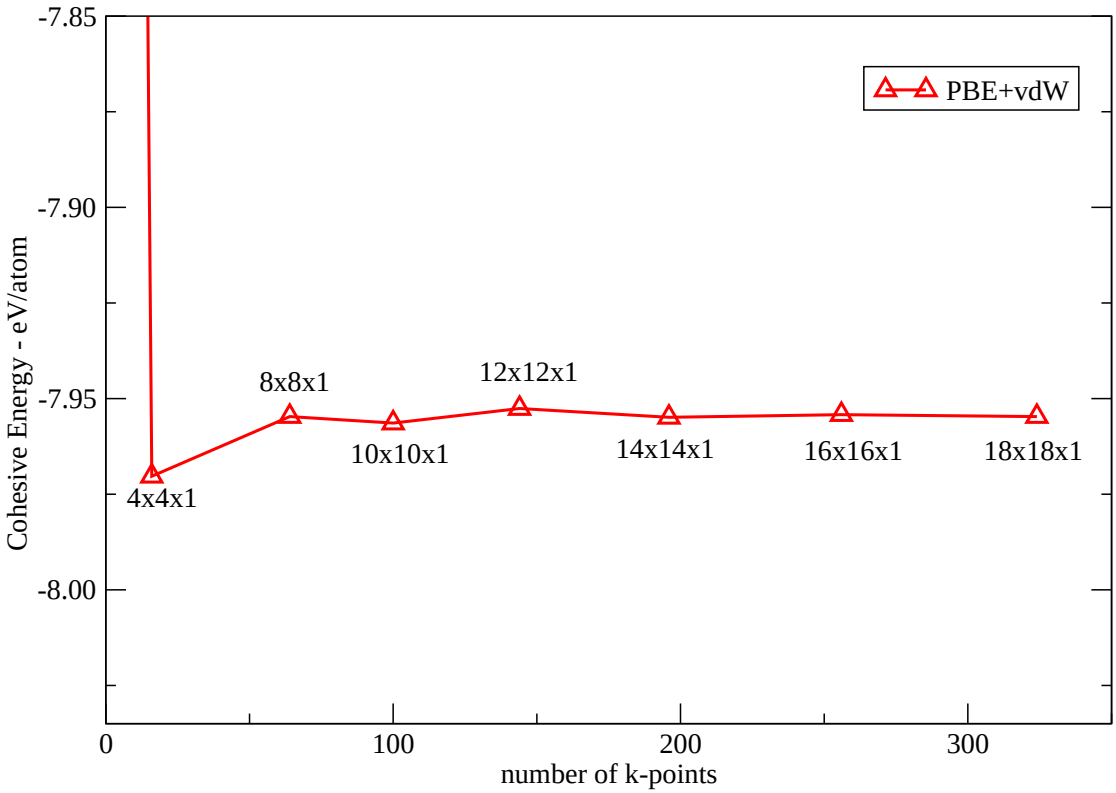

Figure A.13: Convergence of the cohesive energy as a function of the number of k-points. Shown are data for PBEsol functional at fixed in-plane distance of $a = 2,446$ Å and interlayer distance of $c = 3,35$ Å, as a function of number of k-points and the "sb" basis set is used.

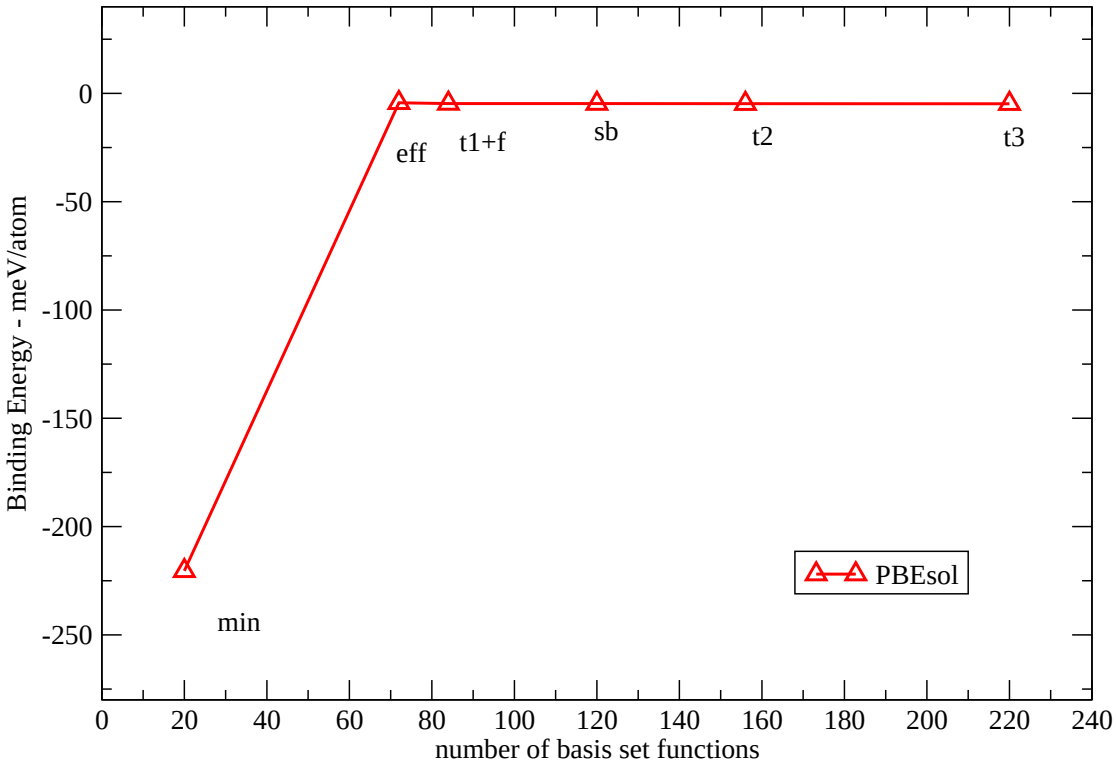

Figure A.14: Convergence of binding energies for PBEsol functional at a fixed in-plane distance of $a = 2,446$ Å and interlayer distance of $c = 3,35$ Å, as a function of basis set size per unit cell.

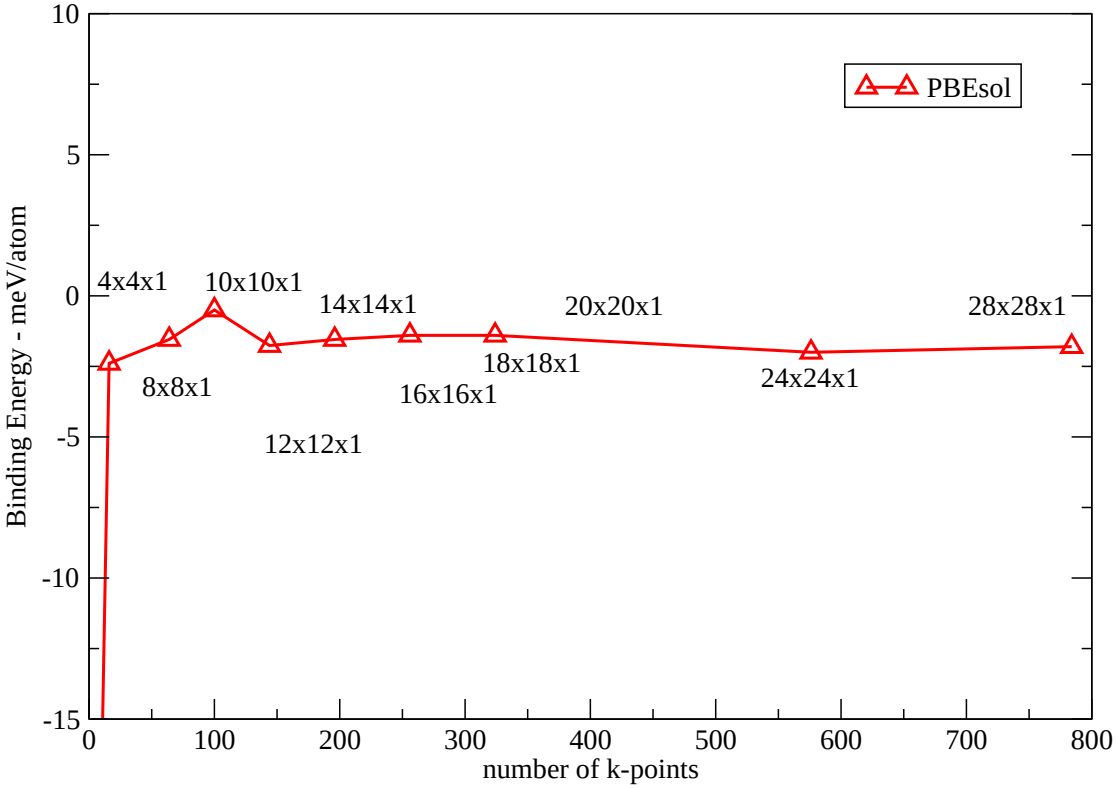

Figure A.15: Convergence of the binding energy between two stacked sheets as a function of the number of k-points. Shown are data for PBEsol functional at a fixed in-plane distance of $a = 2,446$ Å and interlayer distance of $c = 3,35$ Å, as a function of number of k-points and using the "sb" basis set.

A.4.3 PBE+vdW

We evaluate the convergence of the PBE+vdW functional at the fixed geometry of $a = 2,446$ Å and $c = 3,35$ Å as a function of k-points grid, number of van der Waals cells and vacuum size. As for the other DFT functionals the cohesive energy, Figs. (A.16) and (A.17), is converged at the meV/level already for a "sb" basis set at (12x12x1) grid with 144 k-points in the first Brillouin zone, and 25 Å vacuum and $l_{hartree} = 4$. Similarly the binding energy, Figs. (A.18) and (A.19), is converged at the sub-meV/atom level. Hence we set $l_{hartree} = 4$ and a (18x18x1) grid of 326 k-points and 25 Å vacuum in our calculations. Sample points taken with a (24x24x1) grid with 576 k-points in the full Brillouin zone show again differences of the order of sub-meV/atom.

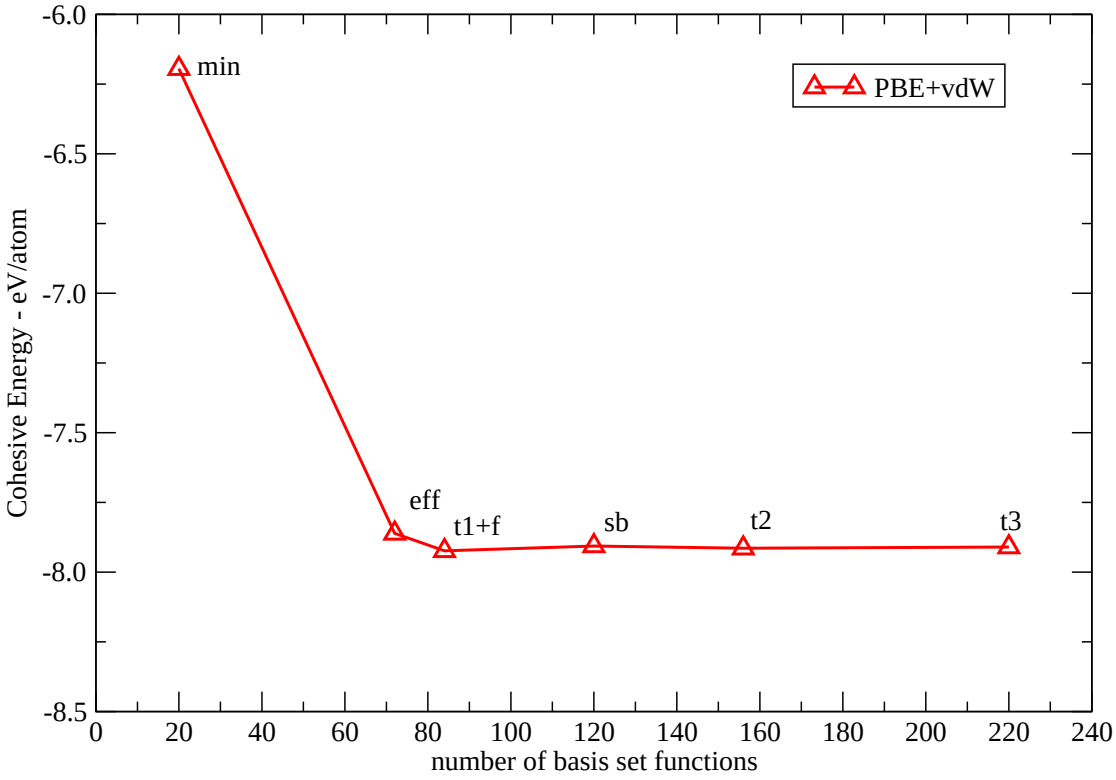

Figure A.16: Convergence of the cohesive energy with basis set size per unit cell. Shown are data for PBE+vdW at a fixed in-plane distance of $a = 2,446$ Å and interlayer distance of $c = 3,35$ Å.

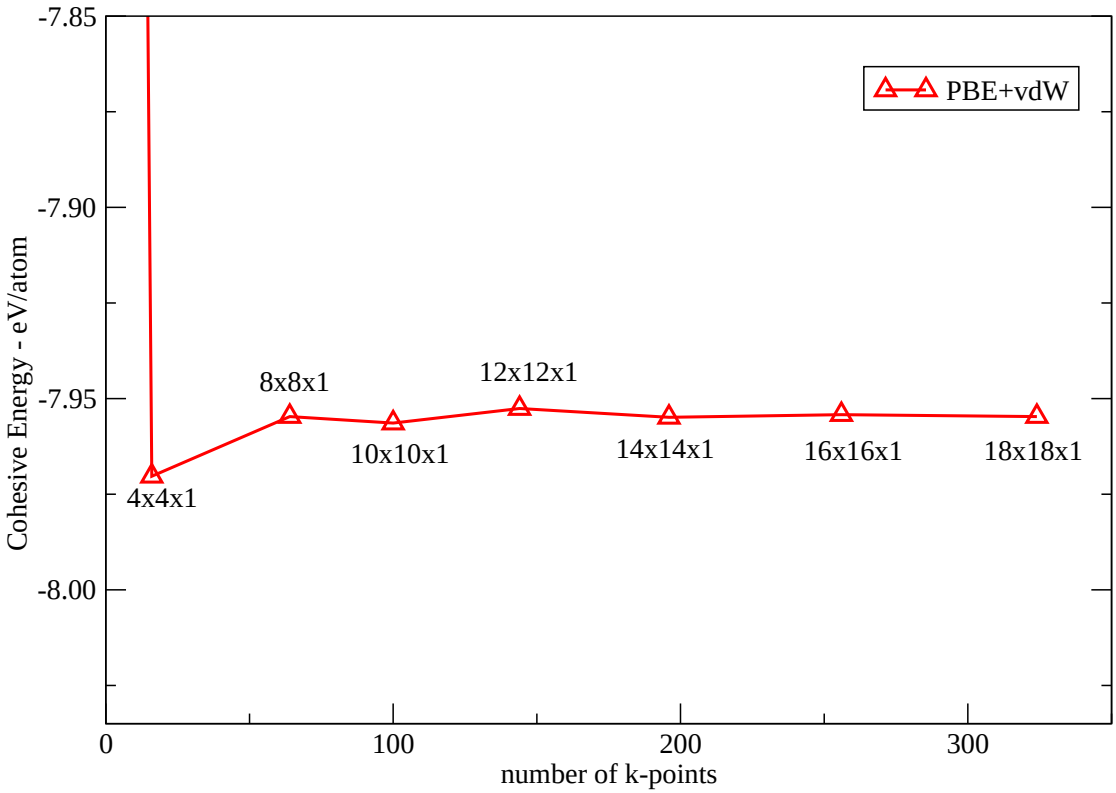

Figure A.17: Convergence of the cohesive energy as a function of the number of k-points. Shown are data for PBE+vdW at fixed in-plane distance of $a = 2,446$ Å and interlayer distance of $c = 3,35$ Å, as a function of number of k-points and the "sb" basis set is used.

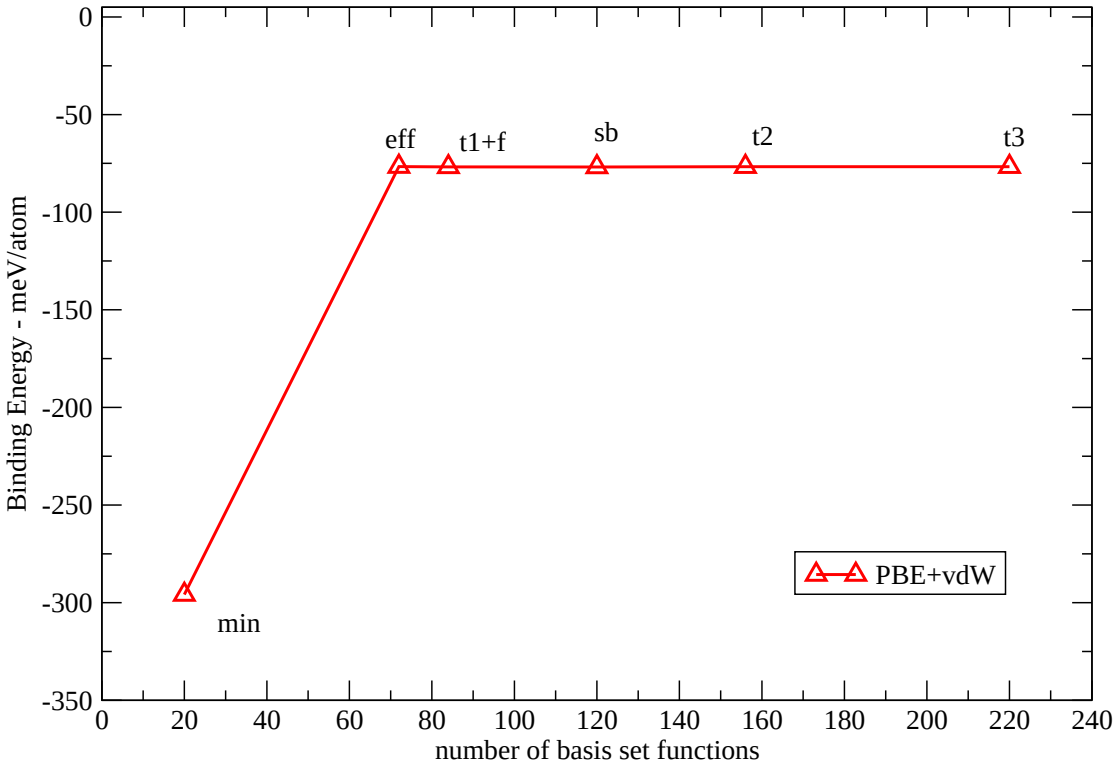

Figure A.18: Convergence of binding energies for PBE+vdW at a fixed in-plane distance of $a = 2,446$ Å and interlayer distance of $c = 3,35$ Å, as a function of basis set size per unit cell.

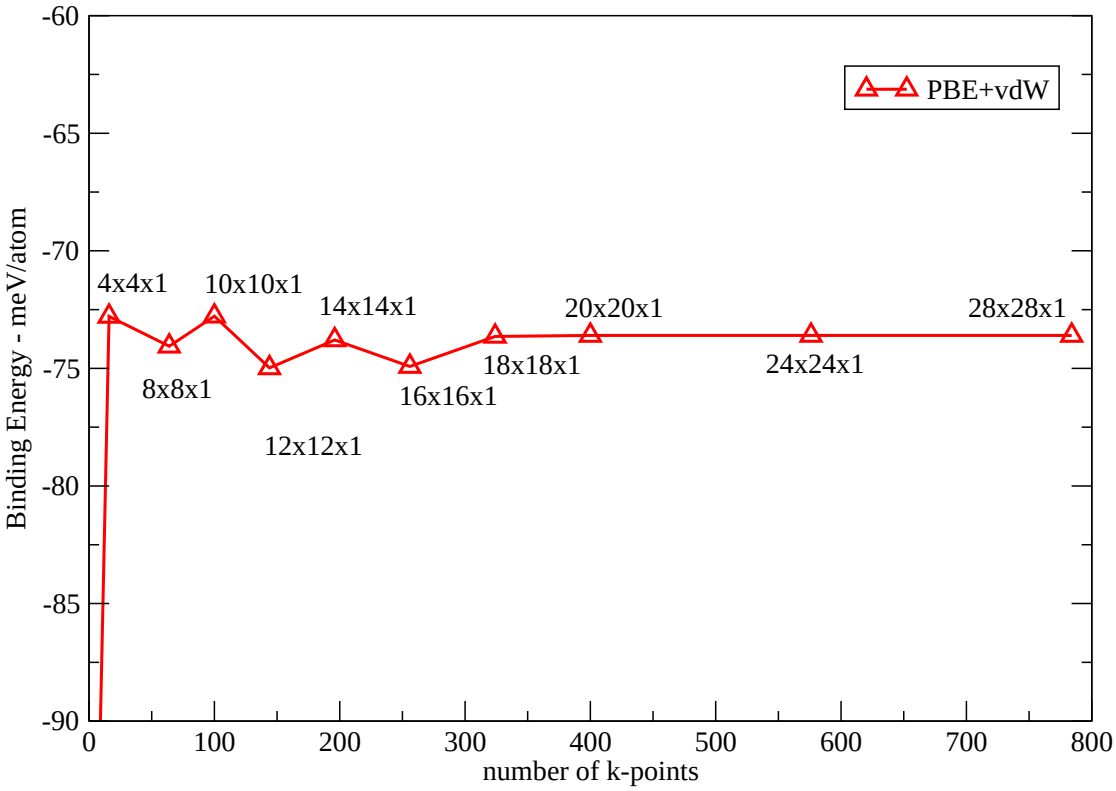

Figure A.19: Convergence of the binding energy between two stacked sheets as a function of the number of k-points. Shown are data for PBE+vdW at a fixed in-plane distance of $a = 2,446$ Å and interlayer distance of $c = 3,35$ Å, as a function of number of k-points and using the "sb" basis set.

A.5 Clusters Extrapolations for Bilayer Graphene

A.5.1 PW-LDA and GGA-PBE

Table A.7: Cohesive energy (eV/atom) extrapolation compared to the result of the periodic calculations. Shown are the values obtained when using the indicated cluster ranges in the fit (see Fig. (3.15)). Some values for the "t3" basis set are missing, since the computational requirements for the "192 C" cluster are yet too demanding.

	t1+f	sb	t2	t3	Carbon atoms	method
E_{coh}	8,88	8,89	8,89		12-192	PW-LDA
	8,87	8,88	8,88	8,88	12-108	""
	8,86	8,87	8,87	8,87	12-64	""
	8,84	8,85	8,85	8,86	12-48	""
	8,81	8,82	8,82	8,82	12-40	""
	8,90	8,91	8,91		20-192	""
	8,90	8,91	8,91	8,91	20-108	""
	8,90	8,91	8,91	8,91	20-64	""
	8,89	8,89	8,90	8,90	20-48	""
	8,83	8,83	8,84	8,84	20-40	""
	8,91	8,92	8,92		28-192	""
	8,92	8,93	8,93	8,93	28-108	""
	8,93	8,94	8,94	8,94	28-64	""
	8,95	8,96	8,96	8,96	28-48	""
	8,89	8,90	8,90	8,90	28-40	""
	8,90	8,91	8,91		32-192	""
	8,92	8,92	8,93	8,93	bulk	PW-LDA

Table A.8 (*continued*)

	t1+f	sb	t2	t3	Carbon atoms	method
	7,80	7,81	7,81		12-192	GGA-PBE
	7,80	7,80	7,80	7,80	12-108	””
	7,77	7,79	7,79	7,79	12-64	””
	7,75	7,77	7,77	7,77	12-48	””
	7,71	7,72	7,72	7,72	12-40	””
	7,82	7,83	7,82		20-192	””
	7,82	7,83	7,83	7,83	20-108	””
	7,82	7,83	7,83	7,83	20-64	””
	7,81	7,82	7,82	7,82	20-48	””
	7,73	7,74	7,74	7,74	20-40	””
	7,83	7,85	7,84		28-192	””
	7,84	7,85	7,85	7,85	28-108	””
	7,86	7,87	7,87	7,87	28-64	””
	7,87	7,88	7,88	7,88	28-48	””
	7,79	7,80	7,80	7,80	28-40	””
	7,83	7,84	7,83		32-192	””
	7,85	7,85	7,86	7,86	bulk	GGA-PBE
ΔE_{coh}	1,08	1,08	1,08		12-192	PW-LDA - GGA-PBE
	1,07	1,08	1,08	1,08	12-108	””
	1,09	1,08	1,08	1,09	12-64	””
	1,09	1,09	1,09	1,09	12-48	””
	1,10	1,10	1,09	1,10	12-40	””
	1,08	1,07	1,08		20-192	””
	1,08	1,08	1,08	1,08	20-108	””
	1,08	1,08	1,08	1,08	20-64	””
	1,08	1,07	1,08	1,08	20-48	””
	1,10	1,09	1,10	1,10	20-40	””
	1,07	1,07	1,08		28-192	””
	1,07	1,07	1,07	1,07	28-108	””
	1,08	1,07	1,07	1,07	28-64	””
	1,08	1,08	1,08	1,08	28-48	””
	1,10	1,10	1,10	1,10	28-40	””
	1,07	1,07	1,08		32-192	””
	1,07	1,07	1,07	1,07		PW-LDA - GGA-PBE

Table A.8: Binding energy (meV/atom) extrapolation compared to the result of the periodic calculations. Shown are the values obtained when using the indicated cluster ranges in the fit (see Fig. (3.15)). Some values for the "t3" basis set are missing, since the computational requirements for the "192 C" cluster are yet too demanding.

	t1+f	sb	t2	t3	Carbon atoms	method
$E_{\text{bind - AB}}$	-26	-26	-26		12-192	PW-LDA
	-26	-26	-26	-26	12-108	""
	-28	-26	-26	-26	12-64	""
	-28	-26	-26	-26	12-48	""
	-28	-26	-24	-26	12-40	""
	-26	-24	-24		20-192	""
	-26	-24	-24	-24	20-108	""
	-26	-24	-24	-24	20-64	""
	-24	-22	-22	-22	20-48	""
	-22	-22	-22	-20	20-40	""
	-26	-24	-24		28-192	""
	-26	-24	-24	-24	28-108	""
	-24	-24	-24	-24	28-64	""
	-22	-22	-22	-22	28-48	""
	-16	-14	-14	-14	28-40	""
	-26	-24	-24		32-192	""
	-26	-26	-26	-26	bulk	PW-LDA

Table A.8 (*continued*)

	t1+f	sb	t2	t3	Carbon atoms	method
	12	14	14		12-192	GGA-PBE
	12	14	14	14	12-108	””
	12	14	14	14	12-64	””
	14	14	14	14	12-48	””
	14	14	14	14	12-40	””
	12	14	14		20-192	””
	12	14	14	14	20-108	””
	14	14	14	14	20-64	””
	14	16	16	14	20-48	””
	18	18	18	18	20-40	””
	12	14	14		28-192	””
	12	14	14	14	28-108	””
	12	14	14	14	28-64	””
	14	14	14	14	28-48	””
	22	22	22	22	28-40	””
	12	12	12		32-192	””
	12	12	12	12	bulk	GGA-PBE
ΔE_{bind}	-40	-38	-38		12-192	PW-LDA - GGA-PBE
	-40	-38	-40	-38	12-108	””
	-40	-40	-40	-40	12-64	””
	-40	-40	-40	-40	12-48	””
	-42	-42	-40	-40	12-40	””
	-38	-38	-38		20-192	””
	-38	-38	-38	-38	20-108	””
	-38	-38	-38	-38	20-64	””
	-38	-38	-38	-38	20-48	””
	-40	-40	-40	-38	20-40	””
	-38	-38	-38		28-192	””
	-38	-38	-38	-38	28-108	””
	-38	-36	-38	-36	28-64	””
	-36	-36	-36	-36	28-48	””
	-38	-36	-36	-36	28-40	””
	-38	-38	-38		32-192	””
	-38	-38	-38	-38	bulk	PW-LDA - GGA-PBE

A.5.2 PBEsol

Table A.9: Cohesive energy (eV/atom) extrapolation compared to the result of the periodic calculations. Shown are the values obtained when using the indicated cluster ranges in the fit (see Fig. (3.15)). Some values for the "t3" basis set are missing, since the computational requirements for the "192 C" cluster are yet too demanding.

	t1+f	sb	t2	t3	Carbon atoms	method
E_{coh}	8,25	8,26	8,26		12-192	PBESol
	8,24	8,25	8,25	8,26	12-108	""
	8,23	8,24	8,24	8,24	12-64	""
	8,21	8,22	8,22	8,23	12-48	""
	8,17	8,18	8,18	8,18	12-40	""
	8,27	8,28	8,29		20-192	""
	8,27	8,28	8,29	8,29	20-108	""
	8,27	8,28	8,28	8,28	20-64	""
	8,26	8,27	8,27	8,27	20-48	""
	8,19	8,20	8,20	8,21	20-40	""
	8,28	8,29	8,30		28-192	""
	8,29	8,30	8,31	8,31	28-108	""
	8,31	8,31	8,32	8,32	28-64	""
	8,32	8,33	8,33	8,34	28-48	""
	8,25	8,26	8,27	8,27	28-40	""
	8,28	8,29	8,29		32-192	""
	8,31	8,32	8,32	8,32	bulk	PBESol

Table A.9 (*continued*)

	t1+f	sb	t2	t3	Carbon atoms	method
ΔE_{coh}	0,63	0,62	0,62		12-192	PW-LDA - PBEsol
	0,63	0,62	0,63	0,63	12-108	””
	0,63	0,62	0,63	0,63	12-64	””
	0,64	0,62	0,63	0,63	12-48	””
	0,64	0,63	0,63	0,64	12-40	””
	0,63	0,61	0,62		20-192	””
	0,63	0,62	0,62	0,62	20-108	””
	0,63	0,62	0,62	0,62	20-64	””
	0,63	0,62	0,63	0,63	20-48	””
	0,64	0,63	0,63	0,63	20-40	””
	0,62	0,61	0,62		28-192	””
	0,62	0,61	0,62	0,62	28-108	””
	0,63	0,61	0,62	0,62	28-64	””
	0,63	0,62	0,62	0,62	28-48	””
	0,64	0,63	0,63	0,63	28-40	””
	0,62	0,61	0,62		32-192	””
	0,61	0,60	0,61	0,61	bulk	PW-LDA - PBEsol
	0,45	0,44	0,46		12-192	GGA-PBE - PBEsol
	0,45	0,44	0,43	0,46	12-108	””
	0,45	0,44	0,46	0,46	12-64	””
	0,45	0,44	0,46	0,46	12-48	””
	0,46	0,45	0,46	0,46	12-40	””
	0,45	0,44	0,46		20-192	””
	0,45	0,44	0,45	0,45	20-108	””
	0,45	0,44	0,46	0,46	20-64	””
	0,45	0,44	0,46	0,46	20-48	””
	0,46	0,45	0,46	0,46	20-40	””
	0,45	0,44	0,46		28-192	””
	0,45	0,44	0,45	0,45	28-108	””
	0,45	0,44	0,45	0,45	28-64	””
	0,45	0,44	0,45	0,46	28-48	””
	0,46	0,45	0,47	0,47	28-40	””
	0,45	0,44	0,46		32-192	””
	0,46	0,47	0,46	0,46	bulk	GGA-PBE - PBEsol

Table A.10: Binding energy (meV/atom) extrapolation compared to the result of the periodic calculations. Shown are the values obtained when using the indicated cluster ranges in the fit (see Fig. (3.15)). Some values for the "t3" basis set are missing, since the computational requirements for the "192 C" cluster are yet too demanding.

	t1+f	sb	t2	t3	Carbon atoms	method
$E_{\text{bind - AB}}$	-4	-2	-2		12-192	PBEsol
	-4	-2	-2	-2	12-108	""
	-4	-2	-2	-2	12-64	""
	-4	-2	-2	-2	12-48	""
	-4	-1	-2	-2	12-40	""
	-4	-1	-1		20-192	""
	-3	-1	-1	-1	20-108	""
	-3	-1	-1	-1	20-64	""
	-2	0	0	0	20-48	""
	0	3	3	2	20-40	""
	-4	-1	-1		28-192	""
	-4	-1	-1	-2	28-108	""
	-3	-1	-1	-1	28-64	""
	-1	1	1	1	28-48	""
	5	8	8	7	28-40	""
	-4	-2	-2		32-192	""
	-4	-2	-2	-2	bulk	PBEsol

Table A.10 (*continued*)

	t1+f	sb	t2	t3	Carbon atoms	method
ΔE_{bind}	23	22	22		12-192	PW-LDA - PBEsol
	19	22	22	21	12-108	””
	19	22	22	22	12-64	””
	20	23	23	22	12-48	””
	20	24	21	23	12-40	””
	19	22	22		20-192	””
	19	22	22	21	20-108	””
	19	22	22	22	20-64	””
	20	23	23	23	20-48	””
	23	26	26	25	20-40	””
	18	21	21		28-192	””
	18	22	21	21	28-108	””
	19	22	22	21	28-64	””
	20	23	23	23	28-48	””
	27	30	30	29	28-40	””
	18	21	21		32-192	””
	19	21	21	21	bulk	PW-LDA - PBEsol
	17	15	15		12-192	PBEsol - GGA-PBE
	17	15	15	15	12-108	””
	17	15	15	15	12-64	””
	17	15	16	16	12-48	””
	18	16	16	16	12-40	””
	16	15	15		20-192	””
	16	15	15	15	20-108	””
	16	15	15	15	20-64	””
	16	15	15	15	20-48	””
	17	15	15	15	20-40	””
	16	15	15		28-192	””
	16	15	15	15	28-108	””
	16	14	14	14	28-64	””
	15	14	14	14	28-48	””
	9	7	7	7	28-40	””
	25	24	24	22	32-192	””
	15	15	15	15	bulk	PBEsol - GGA-PBE

A.5.3 PBE+vdW

Table A.11: Cohesive energy (eV/atom) extrapolation compared to the result of the periodic calculations. Shown are the values obtained when using the indicated cluster ranges in the fit (see Fig. (3.15)). Some values for the "t3" basis set are missing, since the computational requirements for the "192 C" cluster are yet too demanding.

	t1+f	sb	t2	t3	Carbon atoms	method
E_{coh}	7,89	7,90	7,90		12-192	PBE+vdW
	7,88	7,89	7,89	7,88	12-108	""
	7,87	7,87	7,87	7,87	12-64	""
	7,84	7,85	7,85	7,85	12-48	""
	7,81	7,80	7,81	7,81	12-40	""
	7,91	7,93	7,93		20-192	""
	7,91	7,92	7,92	7,92	20-108	""
	7,91	7,91	7,92	7,91	20-64	""
	7,89	7,90	7,90	7,90	20-48	""
	7,82	7,81	7,83	7,83	20-40	""
	7,93	7,94	7,94		28-192	""
	7,93	7,94	7,94	7,94	28-108	""
	7,95	7,95	7,95	7,95	28-64	""
	7,95	7,96	7,97	7,96	28-48	""
	7,87	7,88	7,89	7,88	28-40	""
	7,92	7,94	7,94		32-192	""
	7,93	7,94	7,94	7,95	bulk	PBE+vdW

Table A.11 (*continued*)

	t1+f	sb	t2	t3	Carbon atoms	method
ΔE_{coh}	0,99	0,98	0,99		12-192	PW-LDA - PBE+vdW
	0,99	0,98	0,99	1,00	12-108	””
	0,99	0,99	1,00	1,00	12-64	””
	1,00	1,00	1,00	1,01	12-48	””
	1,00	1,01	1,01	1,01	12-40	””
	0,98	0,97	0,98		20-192	””
	0,99	0,98	0,99	0,99	20-108	””
	0,99	0,98	0,99	1,00	20-64	””
	1,00	0,99	0,99	1,00	20-48	””
	1,01	1,02	1,00	1,01	20-40	””
	0,98	0,97	0,98		28-192	””
	0,98	0,97	0,98	0,99	28-108	””
	0,98	0,98	0,99	1,00	28-64	””
	1,00	0,99	0,99	1,00	28-48	””
	1,02	1,01	1,01	1,02	28-40	””
	0,98	0,96	0,98		32-192	””
	0,99	0,98	0,99	0,98	bulk	PW-LDA - PBE+vdW
	-0,09	-0,08	-0,10		12-192	GGA-PBE - PBE+vdW
	-0,09	-0,08	-0,06	-0,08	12-108	””
	-0,09	-0,08	-0,09	-0,08	12-64	””
	-0,09	-0,07	-0,09	-0,08	12-48	””
	-0,10	-0,07	-0,09	-0,08	12-40	””
	-0,09	-0,09	-0,10		20-192	””
	-0,09	-0,08	-0,09	-0,08	20-108	””
	-0,09	-0,08	-0,09	-0,08	20-64	””
	-0,08	-0,07	-0,09	-0,08	20-48	””
	-0,09	-0,06	-0,09	-0,08	20-40	””
	-0,09	-0,09	-0,10		28-192	””
	-0,09	-0,08	-0,09	-0,08	28-108	””
	-0,09	-0,08	-0,09	-0,08	28-64	””
	-0,08	-0,07	-0,09	-0,08	28-48	””
	-0,08	-0,07	-0,09	-0,08	28-40	””
	-0,09	-0,09	-0,11		32-192	””
	-0,08	-0,09	-0,08	-0,09	bulk	GGA-PBE - PBE+vdW

Table A.12: Binding energy (meV/atom) extrapolation compared to the result of the periodic calculations. Shown are the values obtained when using the indicated cluster ranges in the fit (see Fig. (3.15)). Some values for the "t3" basis set are missing, since the computational requirements for the "192 C" cluster are yet too demanding.

	t1+f	sb	t2	t3	Carbon atoms	method
$E_{\text{bind - AB}}$	-76	-71	-71		12-192	PBE+vdW
	-76	-70	-71	-70	12-108	""
	-75	-70	-70	-70	12-64	""
	-75	-69	-70	-70	12-48	""
	-76	-70	-71	-71	12-40	""
	-76	-72	-71		20-192	""
	-75	-71	-70	-70	20-108	""
	-74	-70	-69	-69	20-64	""
	-74	-68	-68	-68	20-48	""
	-76	-69	-69	-69	20-40	""
	-77	-72	-72		28-192	""
	-75	-71	-70	-70	28-108	""
	-74	-69	-69	-69	28-64	""
	-72	-67	-67	-67	28-48	""
	-75	-66	-66	-66	28-40	""
	-77	-73	-73		32-192	""
	-76	-72	-72	-72	bulk	PBE+vdW

Table A.12 (*continued*)

	t1+f	sb	t2	t3	Carbon atoms	method
ΔE_{bind}	50	46	46		12-192	PW-LDA - PBE+vdW
	49	45	45	45	12-108	””
	48	44	44	44	12-64	””
	48	43	44	44	12-48	””
	48	43	46	44	12-40	””
	51	48	47		20-192	””
	50	47	46	46	20-108	””
	49	46	45	45	20-64	””
	50	46	46	45	20-48	””
	53	48	48	48	20-40	””
	51	48	47		28-192	””
	50	47	46	46	28-108	””
	49	46	45	45	28-64	””
	49	46	45	45	28-48	””
	58	52	52	52	28-40	””
	51	48	48		32-192	””
	49	47	47	47	bulk	PW-LDA - PBE+vdW
	89	85	85		12-192	GGA-PBE - PBE+vdW
	88	84	84	84	12-108	””
	88	83	84	83	12-64	””
	88	83	84	83	12-48	””
	91	84	86	85	12-40	””
	89	85	85		20-192	””
	88	84	84	84	20-108	””
	87	84	83	83	20-64	””
	88	84	83	83	20-48	””
	93	87	87	87	20-40	””
	89	85	85		28-192	””
	88	84	84	83	28-108	””
	86	83	82	82	28-64	””
	86	82	82	82	28-48	””
	89	81	81	80	28-40	””
	98	95	95		32-192	””
	87	85	85	85	bulk	GGA-PBE - PBE+vdW

A.5.4 MP2

Also for what concerns the bilayer graphene case, the MP2 approximation parameters, i.e. the number of basis set products and the basis set product cut-off threshold, have been tested at the "sb" basis set level for the smallest cluster, i.e. the benzene dimer. They provide extrapolated cohesive and binding energies rapidly converged at the sub-meV/atom level, and therefore they are set as for the graphene case. Also for the graphitic case further tests on the basis set product cut-off threshold for larger clusters using the "t4C" and "t4Cp" basis sets do not show any substantial change. Because of the numerical noise for the biggest clusters, i.e. "28 C" and "32 C" clusters, calculated with the "t4C" and "t4Cp" basis set, the cut-off threshold has been increased to 10^{-3}.

Table A.13: Cohesive energy (eV/atom) extrapolation as a function of the number of carbon atoms in the clusters considered in the linear regression and different basis sets.Some values for the "t3" and "t4C" basis sets are missing, since the computational requirements are yet too demanding.

	t1+f	sb	t2	t3	t4C	Carbon atoms	method
E_{coh}	7,49	7,64	7,76			12-64	MP2
	7,47	7,62	7,74	7,79		12-48	""
	7,42	7,56	7,69	7,74	7,77	12-40	""
	7,55	7,70	7,82			20-64	""
	7,54	7,68	7,80	7,85		20-48	""
	7,45	7,60	7,72	7,77	7,80	20-40	""
	7,60	7,74	7,86			28-64	""
	7,61	7,75	7,87	7,92		28-48	""
	7,52	7,67	7,80	7,84	7,88	28-40	""
ΔE_{coh}	1,36	1,23	1,11			12-64	PW-LDA - MP2
	1,37	1,24	1,12	1,07		12-48	""
	1,39	1,25	1,13	1,08	1,05	12-40	""
	1,35	1,21	1,09			20-64	""
	1,35	1,21	1,10	1,05		20-48	""
	1,38	1,23	1,12	1,07	1,04	20-40	""
	1,33	1,20	1,08			28-64	""
	1,34	1,21	1,08	1,03		28-48	""
	1,37	1,23	1,10	1,06	1,02	28-40	""
	0,28	0,15	0,02			12-64	GGA-PBE - MP2
	0,29	0,15	0,03	-0,02		12-48	""
	0,29	0,16	0,04	-0,02	-0,05	12-40	""
	0,27	0,12	0,04			20-64	""
	0,27	0,14	0,02	-0,04		20-48	""
	0,28	0,14	0,02	-0,03	-0,06	20-40	""
	0,26	0,13	0,01			28-64	""
	0,26	0,13	0,01	-0,04		28-48	""
	0,27	0,13	0,01	-0,04	-0,08	28-40	""

Table A.13 (*continued*)

t1+f	sb	t2	t3	t4C	Carbon atoms	method
0,36	0,22	0,10			12-64	PBE+$_{vd}$W - MP2
0,37	0,23	0,11	0,05		12-48	""
0,39	0,26	0,14	0,08	0,04	12-40	""
0,33	0,20	0,08			20-64	""
0,34	0,21	0,09	0,03		20-48	""
0,41	0,27	0,16	0,10	0,05	20-40	""
0,31	0,18	0,05			28-64	""
0,31	0,18	0,06	0,00		28-48	""
0,40	0,26	0,15	0,09	0,04	28-40	""

Table A.14: Binding energy (meV/atom) extrapolation as a function of the number of carbon atoms in the clusters considered in the linear regression and different basis sets.Some values for the "t3" and "t4C" basis sets are missing, since the computational requirements are yet too demanding.

	t1+f	sb	t2	t3	t4C	Carbon atoms	method
$E_{\text{bind - AB}}$	-102	-112	-114			12-64	MP2
	-100	-110	-112	-118		12-48	""
	-100	-112	-114	-120	-120	12-40	""
	-102	-112	-114			20-64	""
	-100	-108	-110	-118		20-48	""
	-100	-110	-112	-119	-118	20-40	""
	-102	-110	-112			28-64	""
	-96	-104	-106	-114		28-48	""
	-92	-102	-104	-110	-110	28-40	""
$\Delta E_{\text{bind - AB}}$	74	86	88			12-64	PW-LDA - MP2
	72	84	86	92		12-48	""
	72	84	88	92	92	12-40	""
	78	88	90			20-64	""
	76	86	88	96		20-48	""
	78	90	92	98	98	20-40	""
	76	88	90			28-64	""
	74	84	86	94		28-48	""
	76	88	88	96	96	28-40	""
	114	126	128			12-64	GGA-PBE - MP2
	114	124	126	132		12-48	""
	114	126	128	134	134	12-40	""
	116	126	128			20-64	""
	114	124	126	132		20-48	""
	118	128	130	136	136	20-40	""
	114	124	126			28-64	""
	110	120	122	130		28-48	""
	114	124	126	132	132	28-40	""

Table A.14 (*continued*)

t1+f	sb	t2	t3	t4C	Carbon atoms	method
-27	-42	-43			12-64	MP2 - PBE+vdW
-25	-41	-42	-49		12-48	""
-24	-42	-42	-49	-49	12-40	""
-28	-42	-44			20-64	""
-26	-40	-42	-50		20-48	""
-24	-41	-43	-50	-49	20-40	""
-28	-42	-44			28-64	""
-24	-38	-40	-48		28-48	""
-18	-35	-37	-45	-45	28-40	""

A.5.5 RPA

Since the computational framework of the current RPA implementation is the same as MP2, such a method present similar demands with respect to the convergence of the parameters. The recent implementation of multi-step integration[159] allows to put safely for all cluster ranges a cut-off threshold of 10^{-4}, while the number of basis set products for the carbon and hydrogen atoms are set to 4 and 3, respectively.

Table A.15: Cohesive energy (eV/atom) extrapolation as a function of the number of carbon atoms in the clusters considered in the linear regression and different basis sets.Some values for the "t3" and "t4C" basis sets are missing, since the computational requirements are yet too demanding.

	t1+f	sb	t2	t3	t4C	Carbon atoms	method
$E_{\text{bind - AB}}$	6,37	6,75	7,09			12-64	RPA
	6,33	6,73	7,09	7,09		12-48	""
	6,27	6,68	7,08	7,06	7,08	12-40	""
	6,54	6,90	7,20			20-64	""
	6,55	6,94	7,25	7,12		20-48	""
	6,61	7,00	7,38	7,07	7,08	20-40	""
	6,60	6,78	7,11			28-64	""
	6,69	6,76	7,13	7,21		28-48	""
	6,71	6,60	7,25	7,23	7,25	28-40	""
ΔE_{coh}	2,49	2,14	1,78			12-64	PW-LDA - RPA
	2,51	2,11	1,77	1,77		12-48	""
	2,53	2,12	1,74	1,76	1,74	12-40	""
	2,36	2,03	1,71			20-64	""
	2,33	1,95	1,65	1,78		20-48	""
	2,21	1,83	1,46	1,77	1,76	20-40	""
	2,33	2,15	1,83			28-64	""
	2,26	2,18	1,82	1,75		28-48	""
	2,18	2,29	1,65	1,67	1,65	28-40	""
	-1,40	-1,04	-0,69			12-64	RPA - GGA-PBE
	-1,43	-1,04	-0,68	-0,68		12-48	""
	-1,44	-1,05	-0,65	-0,66	-0,65	12-40	""
	-1,28	-0,94	-0,66			20-64	""
	-1,25	-0,88	-0,57	-0,70		20-48	""
	-1,12	-0,75	-0,37	-0,68	-0,66	20-40	""
	-1,25	-1,09	-0,75			28-64	""
	-1,18	-1,12	-0,75	-0,67		28-48	""
	-1,08	-1,21	-0,55	-0,57	-0,55	28-40	""

Table A.15 (*continued*)

t1+f	sb	t2	t3	t4C	Carbon atoms	method
-1,48	-1,10	-0,77			12-64	RPA - PBE+vdW
-1,51	-1,11	-0,76	-0,75		12-48	””
-1,54	-1,14	-0,75	-0,76	-0,73	12-40	””
-1,35	-1,00	-0,70			20-64	””
-1,33	-0,95	-0,64	-0,76		20-48	””
-1,24	-0,87	-0,50	-0,80	-0,77	20-40	””
-1,30	-1,13	-0,80			28-64	””
-1,23	-1,16	-0,79	-0,71		28-48	””
-1,21	-1,33	-0,69	-0,70	-0,66	28-40	””

Table A.16: Binding energy (meV/atom) extrapolation as a function of the number of carbon atoms in the clusters considered in the linear regression and different basis sets. Some values for the "t3" and "t4C" basis sets are missing, since the computational requirements are yet too demanding.

	t1+f	sb	t2	t3	t4C	Carbon atoms	method
$E_{\text{bind - AB}}$	-42	-47	-48			12-64	RPA
	-42	-47	-48	-61		12-48	""
	-43	-48	-49	-61	-60	12-40	""
	-41	-45	-47			20-64	""
	-41	-45	-46	-61		20-48	""
	-40	-45	-46	-61	-61	20-40	""
	-41	-45	-46			28-64	""
	-39	-43	-44	-60		28-48	""
	-36	-40	-41	-59	-59	28-40	""
	15	21	22			12-64	PW-LDA - RPA
	15	21	22	35		12-48	""
	15	21	24	34	34	12-40	""
	16	22	23			20-64	""
	17	22	23	38		20-48	""
	18	24	25	41	40	20-40	""
	16	21	22			28-64	""
	16	22	22	38		28-48	""
	19	25	26	45	45	28-40	""
	-55	-60	-61			12-64	RPA - GGA-PBE
	-56	-61	-62	-74	-74	12-48	""
	-57	-62	-63	-75	-74	12-40	""
	-55	-60	-61			20-64	""
	-55	-60	-61	-76	-77	20-48	""
	-58	-63	-64	-79	-78	20-40	""
	-54	-58	-59			28-64	""
	-53	-58	-59	-74	-76	28-48	""
	-57	-62	-63	-81	-80	28-40	""

Table A.16 (*continued*)

t1+f	sb	t2	t3	t4C	Carbon atoms	method
34	24	23			12-64	RPA - PBE+vdW
33	22	22	9		12-48	””
34	22	22	10	11	12-40	””
34	25	24			20-64	””
33	24	22	7		20-48	””
36	24	23	8	8	20-40	””
34	26	25			28-64	””
33	24	23	7		28-48	””
39	27	25	7	7	28-40	””

A.5.6 RPA+

For the RPA+ convergence tests, the same conclusions as for RPA are valid.

Table A.17: Cohesive energy (eV/atom) extrapolation as a function of the number of carbon atoms in the clusters considered in the linear regression and different basis sets.Some values for the "t3" and "t4C" basis sets are missing, since the computational requirements are yet too demanding.

t1+f	sb	t2	t3	t4C	Carbon atoms	method
6,30	6,69	7,06			12-64	RPA+
6,26	6,66	7,06	7,02		12-48	""
6,20	6,61	7,06	6,99	7,00	12-40	""
6,47	6,84	7,13			20-64	""
6,49	6,87	7,18	7,05		20-48	""
6,54	6,92	7,30	7,00	7,01	20-40	""
6,53	6,74	7,04			28-64	""
6,62	6,70	7,06	7,14		28-48	""
6,68	6,52	7,18	7,16	7,17	28-40	""
2,56	2,20	1,81			12-64	PW-LDA - RPA+
2,58	2,18	1,79	1,84		12-48	""
2,60	2,20	1,75	1,83	1,82	12-40	""
2,43	2,09	1,78			20-64	""
2,40	2,02	1,72	1,85		20-48	""
2,28	1,91	1,53	1,84	1,83	20-40	""
2,40	2,19	1,90			28-64	""
2,33	2,25	1,89	1,82		28-48	""
2,21	2,37	1,72	1,74	1,73	28-40	""
-1,47	-1,10	-0,73			12-64	RPA+ - GGA-PBE
-1,49	-1,11	-0,71	-0,75		12-48	""
-1,51	-1,12	-0,66	-0,73	-0,72	12-40	""
-1,35	-0,99	-0,73			20-64	""
-1,32	-0,96	-0,64	-0,77		20-48	""
-1,19	-0,83	-0,44	-0,75	-0,73	20-40	""
-1,32	-1,14	-0,82			28-64	""
-1,25	-1,19	-0,82	-0,74		28-48	""
-1,11	-1,29	-0,62	-0,64	-0,63	28-40	""

Table A.17 (*continued*)

t1+f	sb	t2	t3	t4C	Carbon atoms	method
-1,55	-1,16	-0,80			12-64	RPA+ - PBE+vdW
-1,58	-1,18	-0,79	-0,82		12-48	""
-1,61	-1,21	-0,76	-0,83	-0,81	12-40	""
-1,42	-1,05	-0,77			20-64	""
-1,40	-1,02	-0,71	-0,83		20-48	""
-1,31	-0,95	-0,57	-0,87	-0,84	20-40	""
-1,37	-1,18	-0,87			28-64	""
-1,30	-1,23	-0,86	-0,78		28-48	""
-1,24	-1,41	-0,76	-0,77	-0,74	28-40	""

Table A.18: Binding energy (meV/atom) extrapolation as a function of the number of carbon atoms in the clusters considered in the linear regression and different basis sets.Some values for the "t3" and "t4C" basis sets are missing, since the computational requirements are yet too demanding.

	t1+f	sb	t2	t3	t4C	Carbon atoms	method
$E_{\text{bind - AB}}$	-40	-45	-46			12-64	RPA+
	-40	-45	-46	-59		12-48	""
	-41	-46	-47	-59	-58	12-40	""
	-40	-44	-45			20-64	""
	-39	-43	-44	-59		20-48	""
	-39	-43	-44	-60	-60	20-40	""
	-39	-43	-44			28-64	""
	-38	-41	-42	-58		28-48	""
	-34	-38	-39	-57	-58	28-40	""
	13	19	20			12-64	PW-LDA - RPA+
	13	19	20	33		12-48	""
	13	19	22	33	32	12-40	""
	14	20	21			20-64	""
	15	20	21	36		20-48	""
	16	22	23	39	39	20-40	""
	14	20	21			28-64	""
	15	20	21	37		28-48	""
	18	23	24	43	44	28-40	""
	-53	-59	-60			12-64	RPA+ - GGA-PBE
	-54	-59	-60	-73	-73	12-48	""
	-55	-60	-61	-73	-72	12-40	""
	-53	-58	-59			20-64	""
	-53	-58	-59	-74	-74	20-48	""
	-56	-61	-62	-77	-78	20-40	""
	-52	-57	-58			28-64	""
	-51	-56	-57	-73	-73	28-48	""
	-55	-60	-61	-79	-80	28-40	""

Table A.18 (*continued*)

t1+f	sb	t2	t3	t4C	Carbon atoms	method
35	25	24			12-64	RPA+ - PBE+vdW
35	24	24	11		12-48	""
36	24	24	11	12	12-40	""
35	26	24			20-64	""
35	25	24	9		20-48	""
37	26	25	9	9	20-40	""
34	26	25			28-64	""
35	26	25	9		28-48	""
41	28	27	8	8	28-40	""

Acknowledgements

I wish to thank first of all the FHI der Max-Planck Gesellschaft to have me allowed to do my PhD, in particular my supervisor prof. K. Reuter, and the people of the Marie-Curie Early Stage Researchers *MONET* network for funding. I thank also prof. E.K.U. Gross for his availability as a second supervisor.

Un grazie ai vecchi amici, Alessandro, Daniele, Fabio, Francesco e Pietro, per le vacanze trascorse insieme negli ultimi anni, per lo svago, il divertimento e lo *sciallo*. Un grazie a Davide e Fabio Pietrucci per gli incoraggiamenti, la stima e i saggi consigli. Un grazie anche a Cinzia, Dani, Marta, Silvia e Valeria; le donne hanno la gran qualità di farti apprezzare certe cose e di addolcirne altre, o a volte tingerle un pò di amaro. Ringrazio Fabio Caruso, Lauro, Marco, Mariana, Matteo, Mathis e Viktor per le infinite idiozie sparate a pranzo e il periodo a Berlino al di fuori dalle mura dell'istituto. Ringrazio Enrico e Gabo per gli allenamenti e il tempo passato a Berlino o altrove. Ringrazio gli amici che ho rivisto purtroppo raramente, in particolare, Aitor, Anne-Laure, Bernard e Amelie, Chee, Elinor, Elvis, Giacomo e Diana, Jaisiel, il Marcone, Manu, Panos, Philippe, Tosio, Valentina Isetta e Valentina Vitali. Ringrazio i colleghi disperati o *da ricovero*, perché ti motivano a resistere o a farti sentire migliore... triste, ma vero.

Un pensiero anche alla Germania e al popolo tedesco, che mi ha generosamente ospitato questi anni:
Quis porro, praeter periculum horridi et ignoti maris, Asia aut Africa aut Italia relicta Germaniam peteret, informem terris, asperam caelo, tristem cultu aspectuque, nisi si patria sit?

De Origine et situ Germanorum, *Tacitus, 98 A.D.*

Bibliography

[1] The *NIST* reference on constants, units, and uncertainty. `http://physics.nist.gov/cuu/Constants/index.html`.

[2] Mathematica, version 7.0, 2008.

[3] M. Abramowitz and I.A. Stegun. *Handbook of Mathematical Functions: with Formulas, Graphs, and Mathematical Tables*. Dover Publications, 1965.

[4] A.A. Abrikosov. *Methods of Quantum Field Theory in Statistical Physics*. Dover Publications, 1975.

[5] C. Adamo and V. Barone. *J. Chem. Phys.*, 110:6158, 1999.

[6] N. I. Akhiezer and I. M. Glazman. *Theory of Linear Operators in Hilbert Space*. Dover Publications, 1993.

[7] R. Al-Jishi and G. Dresselhaus. *Phys. Rev. B*, 26:4514, 1982.

[8] W. Andreoni. *The Physics of Fullerene-based and Fullerene-related Materials*. Springer, 2000.

[9] G. Arfken and H. Weber. *Mathematical Methods for Physicists*. Academic Press, 2001.

[10] B. Arnaud, S. Lebègue, P. Rabiller, and M. Alouani. *Phy. Rev. Lett.*, 96:026402, 2006.

[11] D. Arnett. *Supernovae and Nucleosynthesis*. Princeton University Press, 1996.

[12] A.Szabo and N.S. Ostlund. *Modern Quantum Chemistry*. Dover Publications, 1982.

[13] P. Atkins and R. Friedman. *Molecular Quantum Mechanics*. Oxford University Press, 2005.

[14] B.M. Axilrod and E. Teller. *J. Chem. Phys.*, 11:299, 1943.

[15] P.Y. Ayala and G.E. Scuseria. *J. Chem. Phys.*, 110:3660, 1999.

[16] R.J. Bartlett and M. Musial. *Rev. Mod. Phys.*, 79:291, 2007.

[17] L. Benedict, N. Chopra, M. Cohen, and A. Zettl. *Chem. Phys. Lett.*, 286:490, 1998.

[18] G. Binnig and H. Rohrer. *Rev. Mod. Phys.*, 59(3):615, 1987.

[19] V. Blum, R. Gehrke, F. Hanke, P. Havu, V. Havu, X. Ren, K. Reuter, and M. Scheffler. *Comp. Phys. Commun.*, 180:2175, 2009.

[20] H.P. Boehm. *Carbon*, 1997:581, 35.

[21] S.F. Boys. *Proc. R. Soc. (London) A*, 200:542, 1950.

[22] S.F. Boys and F. Bernardi. *Mol. Phys.*, 19:553, 1970.

[23] A.D. Buckingham, P.W. Fohler, and J.M. Hutsen. *Chem. Rev.*, 88:963, 1988.

[24] J.L. Calais. *Int. J. Quant. Chem.*, 56:541, 1998.

[25] T.Y. Chang. *Rev. Mod. Phys.*, 39:911, 1967.

[26] A. Charlier, E. McRae, M.F. Charlier, A. Spire, and S. Forster. *Phys. Rev. B*, 57:6689, 1998.

[27] J.C. Charlier, X. Gonze, and J.P. Michenaud. *Europhys. Lett.*, 28:403, 1994.

[28] X. Chu and A. Dalgarno. *J. Chem. Phys.*, 121:4083, 2004.

[29] M. Cini. *Topics and Methods in Condensed Matter Theory.* Springer, 2007.

[30] J.F. Cornwell. *Group Theory in Physics: An Introduction (vol. 1&2).* Academic Press, 1997.

[31] T. Cwiok, B. Jeziorski, W. Kolos, R. Moszynski, and K. Szalewicz. *J. Mol. Struct. (Theochem)*, 307:135, 1994.

[32] S.M. Cybulski. *J. Chem. Phys.*, 97:7545, 1992.

[33] R.O. Dillon, I. L. Spain, and J. W. McClure. *J. Phys. Chem. Solids*, 38:635, 1977.

[34] M. Dion, H. Rydberg, E. Schröder, D. C. Langreth, and B.I. Lundqvist. *Phys. Rev. Lett*, 95:246401, 2004.

[35] M. Dion, H. Rydberg, E. Schröder, D. C. Langreth, and B.I. Lundqvist. *Phys.Rev.Lett.*, 95:109902, 2005.

[36] P.A.M. Dirac. *Proc. Cambridge Phil. Roy. Soc.*, 26:376, 1930.

[37] P.A.M. Dirac. *The Principles of Quantum Mechanics.* Clarendon Press, 1930.

[38] J.F. Dobson. *Surface Science*, 601:5667, 2007.

[39] J.F. Dobson, A. White, and A. Rubio. *Phys. Rev. Lett.*, 96:073201, 2006.

[40] J. Donohue. *Structures of the Elements.* Krieger Pub. Co., 1982.

[41] I.E. Dzyaloshinskii, E.M. Lifshitz, and L.P. Pitaevskii. *Soviet Physics Uspekhi*, 73:381, 1961.

[42] H. Ehrenreich and M. H. Cohen. *Phys. Rev.*, 715:786, 1959.

[43] W.H.A. Ernst and M. Däne. *Computational Materials Science: From Basic Principles to Material Properties (Lecture Notes in Physics)*. Springer, 2004.

[44] M. Erzernhof and G.E. Scuseria. *J. Chem. Phys.*, 110:5029, 1999.

[45] A. Fasolino, J. H. Los, and M. I. Katsnelson. *Nature Materials*, 6:857, 2007.

[46] E. Fermi. *Rend. Accad. Naz. Lincei*, 6:602, 1927.

[47] A.L. Fetter and J.D. Walecka. *Quantum Theory of Many-Particle Systems*. Dover Publications, 2003.

[48] M. Feyereisen, G. Fitzgerald, and A. Komornicki. *Chem. Phys. Lett.*, 208:359, 1993.

[49] M. Feyereisen and R.A. Kendall. *Theor. Chem. Acc.*, 84:289, 1993.

[50] F. Furche. *Phys. Rev. B*, 64:195120, 2001.

[51] F. Furche. *J. Chem. Phys.*, 129:114105, 2008.

[52] A.K. Geim and K.S. Novoselov. *Nature Materials*, 6:183, 2007.

[53] H. Goldstein, C.P. Poole, and J.L. Safko. *Classical Mechanics*. Addison Wesley, 2001.

[54] A. Görling. *Phys. Rev. A*, 59:3359, 1999.

[55] T. Gould, K. Simpkins, and F. Dobson. *Phys. Rev. B*, 77:165134, 2008.

[56] S. Gowtham, R.H. Scheicher, R. Ahuja, R. Pandey, and S.P. Karna. *Phys. Rev. B*, 76:033401, 2007.

[57] S. Grimme. *J. Phys. Chem. C*, 111:11199, 2007.

[58] E.K.U. Gross and R.M. Dreizler. *Density Functional Theory*. Springer, 1995.

[59] G. Grosso and G.P. Parravicini. *Solid State Physics*. Academic Press, 2000.

[60] A. Grüneis, C. Attaccalite, L. Wirtz H. Shiozawa, Saito, T. Pichler, and A. Rubio. *Phys. Rev. B*, 78:205425, 2008.

[61] M. Gutowski and L. Piela. *Mol. Phys.*, 64:337, 1988.

[62] M. Hanfland, H. Berister, and K. Syassen. *Phys. Rev. B*, 39:12598, 1989.

[63] J. Harl and G. Kresse. *Phys. Rev. B*, 77:045136, 2008.

[64] M. Hasegawa and K. Nishidate. *Phys. Rev. B*, 70:205431, 2004.

[65] W.H. Hehre, R. Ditchfield, and J.A. Pople. *J. Chem. Phys.*, 56:2257, 1972.

[66] W.H. Hehre, J.F. Stewart, and J.A. Pople. *J. Chem. Phys.*, 51:2657, 1969.

[67] T. Helgaker, P. Jorgensen, and J. Olsen. *Molecular Electronic-Structure Theory.* Wiley, 2000.

[68] S. Hembacher, F.J. Giessibl, J. Mannhart, and C.F. Quate. *PNAS*, 100:12539, 2003.

[69] J. Heyd and G. Scuseria. *J. Chem. Phys.*, 121:1187, 2004.

[70] F.L. Hirshfeld. *Theoret. Claim. Acta (Berl.)*, 44:129, 1977.

[71] P. Hohenberg and W. Kohn. *Phys. Rev. B*, 136:864, 1964.

[72] A.W. Hull. *Phys. Rev.*, 10:661, 1917.

[73] E.A. Hylleraas. *Z. Phys.*, 54:347, 1929.

[74] S. Ijima and T. Ichihashi. *Nature*, 363:603, 1993.

[75] C. Itzykson and J.B. Zuber. *Quantum Field Theory.* Dover Publications, 2006.

[76] J.D. Jackson. *Classical Electrodynamics.* Wiley, 1998.

[77] B.G. Janesko, T.M. Henderson, and G.E. Scuseria. *J. Chem. Phys.*, 130:081105, 2009.

[78] A. Janotti, S.H. Wei, and D.J. Singh. *Phys. Rev. B*, 64:174107, 2001.

[79] T. Janowski and P. Pulay. *Chem. Phys. Lett.*, 447:27, 2007.

[80] F. Jensen. *Introduction to Computational Chemistry.* Wiley, 1998.

[81] E.R. Johnson and A.D. Becke. *J. Chem. Phys.*, 123:024101, 2005.

[82] R.O. Jones and O. Gunnarsson. *Rev. Mod. Phys.*, 61:689, 1989.

[83] J. Junquera, O. Paz, D. Sanchez-Portal, and E. Artacho. *Phys. Rev. B*, 64:235111, 2001.

[84] P. Jurecka, J. Poner, J. Erný, and P. Hobza. *Phys. Chem. Chem. Phys.*, 8:1985, 2006.

[85] C.L. Kane and E.J. Mele. *Phys. Rev. B*, 59:R12 759, 1999.

[86] I.G. Kaplan. *Intermolecular Interactions: Physical Picture, Computational Methods and Model Potentials.* Wiley, 2006.

[87] T. Kato. *Pure Appl. Math.*, 10:151, 1957.

[88] M.I. Katsnelson, K.S. Novoselov, and A.K. Geim. *Nature Physics*, 2:620, 2006.

[89] R.A. Kendall and H.A. Früchtl. *Theor. Chem. Acc.*, 1:158, 1997.

[90] W. Kohn and L.J. Sham. *Phys. Rev. A*, 140:1133, 1965.

[91] H.W. Kroto, J.R. Heath, S.C. O'Brien, R.F. Curl, and R.E. Smalley. *Nature*, 318:362, 1985.

[92] K.N. Kudin and G.E. Scuseria. *Phys. Rev. B*, 61:16440, 2000.

[93] S. Kümmel and L. Kronik. *Rev. Mod. Phys.*, 80:3, 2008.

[94] S. Kurth and J.P. Perdew. *Phys. Rev. B*, 59:10461, 1999.

[95] W. Kutzelnigg. *Theor. Chem. Acc.*, 68:445, 1985.

[96] L.D. Landau and E.M. Lifshitz. *Mechanics: Volume 1.* Butterworth-Heinemann, 1976.

[97] L.D. Landau and E.M. Lifshitz. *The Classical Theory of Fields: Volume 2.* Butterworth-Heinemann, 1980.

[98] L.D. Landau and E.M. Lifshitz. *Statistical Physics: Volume 5.* Butterworth-Heinemann, 1980.

[99] L.D. Landau and E.M. Lifshitz. *Quantum Mechanics Non-Relativistic Theory: Volume 3.* Butterworth-Heinemann, 1981.

[100] L.D. Landau and E.M. Lifshitz. *Quantum Electrodynamics: Volume 4.* Butterworth-Heinemann, 1982.

[101] D.C. Langreth and J.P. Perdew. *Solid State Commun.*, 17:1425, 1975.

[102] D.C. Langreth and J.P. Perdew. *Phys. Rev. B*, 15(6):2884, 1977.

[103] N.N. Lebedev and R.R. Silverman. *Special Functions and Their Applications.* Dover Publications, 1972.

[104] C. Lee, W. Yang, and R.G. Parr. *Phys. Rev. B*, 37:785, 1988.

[105] S.G. Lemay, J.W. Janssen, M. van den Hout, M. Mooij, M. J. Bronikowski, P.A. Willis, R.E. Smalley, L.P. Kouwenhoven, and C. Dekker. *Nature*, 412:617, 2001.

[106] N. Levy. *Proc. N.A.S.*, 76:6062, 1979.

[107] N. Levy. *Phys. Rev. A*, 26:1200, 1982.

[108] W. Liang and M. Head-Gordon. *J. Phys. Chem. A*, 108:3206, 2004.

[109] E. Lieb. *Int. J. Quant. Chem.*, 24:243, 1983.

[110] H. Lipson and A.R. Stokes. *Proc. R. Soc. London A*, 181:101, 1942.

[111] J. Liu, M.W. Feyereisen, J. Almöff, C.M. Rohlfing, and Sæbo. *Chem. Phys. Lett.*, 183:478, 1991.

[112] C. Møller and M.S. Plesset. *Phys. Rev.*, 46:618, 1934.

[113] F. London. *Trans. Faraday Soc.*, 33:8, 1937.

[114] H.C. Longuet-Higgins. *Discussions of the Faraday Society*, 40:7, 1965.

[115] A. Ludsteck. *Acta Crystallographica Section A: Crystal Physics*, 28:59, 1972.

[116] F.R. Manby. *J. Chem. Phys.*, 119:1607, 2003.

[117] S. Marchini, S. Günther, and J. Wintterlin. *Phys. Rev. B*, 76:075429, 2007.

[118] H. Margenau. *Rev. Mod. Phys.*, 11:1, 1939.

[119] M.A.L. Marque, C.A. Ullrich, F. Nogueira, A. Rubio, K. Burke, and E.K.U. Gross, editors. *Time-Dependent Density Functional Theory*. Springer, 2006.

[120] J. Martini, N. Akermani, G. Ulbricht, T. Lohmann, J.H. Smeth, K. von Klitizng, and A.Yacoby. *Nature Physics*, 4:144, 2008.

[121] R.M. Martins. *Electronic Structure: Basic Theory and Practical Methods*. Cambridge University Press, 2008.

[122] R.D. Mattuck. *A Guide to Feynman Diagrams in the Many-Body Problem*. Dover Publications., 1976.

[123] E. McCann and V.I. Fal'ko. *Phys.Rev.Lett.*, 96:086805, 2006.

[124] J.W. McClure. *Phys. Rev.*, 104:666, 1956.

[125] J.W. McClure. *Phys. Rev.*, 108:612, 1957.

[126] N.D. Mermin. *Phys. Rev.*, 176:250, 1968.

[127] A. Messiah. *Quantum Mechanics*. Dover Publications, 1999.

[128] M. Methfessel and A.T. Paxton. *Phys. Rev. B*, 6:40, 1989.

[129] J.C. Meyer, A.K. Geim, M.I. Katsnelson, K.S. Novoselov, T.J. Booth, and S. Roth. *Nature*, 446:60, 2007.

[130] T. Miyake, F. Aryasetiawan, T. Kotani, M. van Schilfgaarde, M. Usuda, and K. Terakura. *Phys. Rev. B*, 66(24):245103, 2002.

[131] M. Mohr, J. Maultzsch, E. Dobard, S. Reich, I. Milo, M. Damnjanovi, A. Bosak, M. Krisch, and C. Thomsen. *Phys. Rev. B*, 76(3):035439, 2007.

[132] P.J. Mohr, B.N. Taylor, and D.B. Newell. *Rev. Mod. Phys.*, 80:633, 2008.

[133] N. Mounet and M. Marzari. *Phys. Rev. B*, 71:205214, 2005.

[134] S. Mouras, A. Hamm, D. Djurado, and J.C. Cousseins. Synthesis of first stage graphite intercalation compounds with fluorides. *Revue de Chimie Minerale*, page 572, 24.

[135] J. Munday, F. Capasso, and V. Parsegian. *Nature*, 457:170, Jan 2009.

[136] J.N. Munday, F. Capasso, and V.A. Parsegian. *Nature*, 457:170, 2009.

[137] Y. Muto. *J. Phys.-Math. Soc. Japan*, 17:629, 1943.

[138] T. Nakanishi and T. Ando. *physica status solidi (b)*, 245:2173, 2008.

[139] J.W. Negele and H. Orland. *Quantum Many-particle Systems*. Westview Press, 1998.

[140] A.H. Castro Neto, F. Guinea, N.M. Peres, K.S. Novoselov, and A.K. Geim. *Rev. Mod. Phys.*, 81:109, 2009.

[141] Y. M. Niquet, M. Fuchs, and X. Gonze. *Phys. Rev. A*, 68(3):032507, 2003.

[142] K. S. Novoselov, S. V. Morozov 1 A. K. Geim, D. Jiang, Y. Zhang, S. V. Dubonos, I.V. Grigorieva, and A.A. Firsov. *Science*, 306:666, 2004.

[143] A. Olasz, K. Vanommeslaeghe, A. Krishtal, T. Veszpremi, C.V. Alsenoy, and P. Geerlings. *J. Chem. Phys.*, 127:224105, 2007.

[144] P. Ordejon. *Phys, Stat. Sol. B*, 217:335, 2000.

[145] F. Ortmann, F. Bechstedt, and W.G. Schmidt. *Phys. Rev. B*, 73:205101, 2006.

[146] R.G. Parr and W. Yan. *Density-Functional Theory of Atoms and Molecules*. Oxford University Press, 1989.

[147] D.C. Patton and M.R. Pederson. *Int. J. Quant. Chem.*, 69:619, 1998.

[148] L. Pauling. *Proc. N.A.S.*, 56:1646, 1966.

[149] B. Paulus. *Physics Reports*, 428:1, 2006.

[150] J.P. Perdew, K. Burke, and M. Ernzerhof. *Phys. Rev. Lett.*, 77:3865, 1996.

[151] J.P. Perdew, A. Ruzsinszky, O.A. Vydrov G.I. Csonka, G.E. Scuseria, L.A. Constantin, X. Zhou, and K. Burke. *Phys. Rev. Lett.*, 100:136406, 2008.

[152] J.P. Perdew and Y. Wang. *Phys. Rev. B*, 45:113244, 1992.

[153] J.P. Perdew and A. Zunger. *Phys. Rev. B*, 23:5048, 1981.

[154] A. Peres. *Quantum Theory: Concepts and Methods (Mathematics and Its Applications)*. 1995.

[155] V. Peuckert. *J. Phys. C*, 11:4945, 1978.

[156] S. Pisana, M. Lazzeri, and C. Casiraghi. *Nature*, 6:998, 2007.

[157] C. Pisani, M. Busso, G. Capecchi, S. Casassa, R. Dovesi, L. Maschio, C. Zicovich-Wilson, and M. Schütz. *J. Chem. Phys.*, 122:094113, 2005.

[158] S.L. Price and M. Alderton A.J. Stone. *Molecular Physics*, 52:987, 1984.

[159] A. Quarteroni, R. Sacco, and F. Saleri. *Numerical Mathematics*. Springer, 2006.

[160] A. K. Rajagopal and John C. Kimball. Correlations in a two-dimensional electron system. *Phys. Rev. B*, 15:2819, 1977.

[161] X. Ren, A. Sanfilippo, A. Tkatchenko, P. Rinke, V. Blum, K. Reuter, and M. Scheffler. *(to be published)*.

[162] W. Rudin. *Functional Analysis*. McGraw-Hill, 1991.

[163] E. Runge and E. K. U. Gross. *Phys. Rev. Lett.*, 52:997, 1984.

[164] S. Rybak, B. Jeziorski, and K. Szalewicz. *J. Chem. Phys.*, 95:6576, 1991.

[165] J.J. Sakurai. *Modern Quantum Mechanics*. Addison Wesley, 1993.

[166] M.C. Schabel and J.L. Martins. *Phys. Rev. B*, 46:7185, 2004.

[167] M. Schütz, G. Hetzer, and H.J. Werner. *J. Chem. Phys.*, 111:5691, 1999.

[168] G.E. Scuseria, T.M. Henderson, and D.C. Sorensen. *J. Chem. Phys.*, 129:231101, 2008.

[169] T.. Seyller, A. Bostwick, K. V. Emtsev, K. Horn, L. Ley, J. L. McChesney, T. Ohta, J.D. Riley, E. Rotenberg, and F. Speck. *physica status solidi (b)*, 245:1436, 2008.

[170] L.J. Sham and M. Schlüter. *Phys. Rev. Lett.*, 51:1888, 1983.

[171] P.L. Silvestrelli. *Phys. Rev. Lett.*, 100:053002, 2008.

[172] J.C. Slater. *Phys. Rev.*, 31:333, 1928.

[173] J.C. Slater. *Phys. Rev.*, 36:57, 1930.

[174] D. Spanjaard and M.C. Desjonqueres. *Interactions of Atoms and Solids with Molecules*. Plenum, New York, 1990.

[175] L. Spanu, S. Sorella, and G. Galli. Nature and strength of interlayer binding in graphite. *Phys. Rev. Lett.*, 103(19):196401, 2009.

[176] V.N. Staroverov and G.E. Scuseria. *Phys. Rev. B*, 69:075102, 2004.

[177] H. Stoll. *J. Chem. Phys*, 97:8449, 1992.

[178] P.W. Sutter, J.I. Flege, and E.A. Sutter. *Nature Materials*, page 1, 2008.

[179] M. Swart, P.T. van Duijnen, and J.G. Snijders. *J. Molec. Struct.*, 458:11, 1998.

[180] L. Zhechkov T. Heine and G. Seifert. *Phys. Chem. Chem. Phys.*, 6:980, 2004.

[181] J.D. Talman and W. F. Shadwick. *Phys. Rev. A*, 14:36, 1976.

[182] J. M. Tao, J. P. Perdew, V. N. Staroverov, and G. E. Scuseria. *Phys. Rev. Lett.*, 91:146401, 2003.

[183] L.H. Thomas. *Proc. Cambridge Phil. Roy. Soc.*, 23:542, 1927.

[184] A. Tkatchenko and M. Scheffler. *Phys. Rev. Lett.*, 102:073005, 2009.

[185] A. Tkatchenko, R. A. Di Stasio, M. Head-Gordon, and M. Scheffler. *J. Chem. Phys.*, 131:094106, 2009.

[186] S.B. Trickey, G.H.F. Diercksen, and F. Mueller-Plathe. *Astrophys. J.*, 336:L37, 1989.

[187] S.B. Trickey, F. Mueller-Plathe, G.H.F. Diercksen, and J.C. Boettger. *Phys. Rev. B*, 45:4460, 1992.

[188] O. Vahtras, J. Almöff, and M.W. Feyereisen. *Chem. Phys. Lett.*, 213:514, 1993.

[189] F. Varchon, P. Mallet, J.Y. Veuillen, and L. Magaud. *Phys. Rev. B*, 77:235412, 2008.

[190] A. Vernov and W.A. Steele. *Langmuir*, 8:155, 1992.

[191] O.A. von Lilienfeld and A. Tkatchenko. *J. Chem. Phys.*, 2010 (submitted).

[192] P.R. Wallace. *Phys. Rev.*, 71:622, 1947.

[193] H.J. Werner, F.R. Manby, and P.J. Knowles. *J. Chem. Phys.*, 118:8149, 2003.

[194] D.B. Whitehouse and A.D. Buckingham. *J. Chem. Faraday Trans.*, 89(12):1909, 1993.

[195] H.L. Williams, K. Szalewicz, B.l Jeziorski, R. Moszynski, and S. Rybak. *J. Chem. Phys.*, 98:1279, 1993.

[196] P. Wind, W. Klopper, and T. Helgaker. *Theor. Chem. Acc.*, 107:173, 2002.

[197] R. Zacharia, H. Ulbricht, and T. Hertel. *Phys. Rev. B*, 69:155406, 2004.

[198] A. Zangwill and P. Soven. *Phys. Rev. A*, 21:1561, 1980.

[199] C. Zeinalipour-Yazdi and D. Pullman. *Chem. Phys.*, 348:233, 2008.

[200] Y. Zhang and W. Yang. *Phys. Rev. Lett.*, 1998:890, 80.